NUCLEAR REACTIONS INDUCED IN YTTRIUM-89 BY 5-85 MEV PROTONS

G.B. Saha, 1965

NUCLEAR REACTIONS INDUCED IN YTTRIUM-89 BY 5-85 MEV PROTONS

by

Gopal Bandhu Saha, M.Sc. (Dacca)

A thesis submitted to the Faculty of Graduate
Studies and Research in partial fulfilment of
the requirements for the degree of
Doctor of Philosophy

Department of Chemistry
McGill University
Montreal.

January, 1965

Ph.D. CHEMISTRY

GOPAL BANDHU SAHA

NUCLEAR REACTIONS INDUCED IN YTTRIUM-89 BY 5-85 MEV PROTONS

ABSTRACT

Excitation functions for the (p,xn) (x = 1-4) and (p,pxn) (x = 1-5) reactions induced in Y^{89} by 5-85 Mev protons have been measured by radiochemical techniques. The measured excitation functions have been compared with the statistical theory and cascade-evaporation calculations. Comparison shows that compound nucleus formation is the principal reaction mechanism at energies up to 25-30 Mev. At higher energies the probability of compound nucleus formation decreases and direct interactions predominate.

Isomer ratios have been measured for the products of the (p,p2n), (p,p3n) and (p,p4n) reactions. The ratios indicate a compound nucleus mechanism at energies between the threshold and peak energies and a direct interaction mechanism at higher energies. This conclusion has been further confirmed by an approximate calculation based on the sharp cut-off approximation.

ACKNOWLEDGEMENTS

I am glad to have the opportunity to express my gratitude and thanks to Professor L. Yaffe for suggesting the problem, and his help and encouragement in the early phase of this work.

It is a great pleasure for me to extend my gratitude and thanks to Dr. N.T. Porile whose constant advice, invaluable discussions and encouragement added greatly to my thesis and made it presentable.

Cordial advice, help and inspiration of Dr. D.A. Marsden made work a pleasure. I am ever grateful and thankful to him for all he did for me.

I wish to thank Dr. C.L. Rao and Dr. S.K. Mukherji for their help and suggestions which were invaluable in the early period of this work. I am indebted to Dr. B.B. Paul for his sincere help and encouragement in many respects. I wish to thank my friend Mr. J.H. Forster for his help and various discussions during this work. Help from all other colleagues in this laboratory in many respects is highly appreciated.

I wish to thank Professor R.E. Bell, Director of the Foster Radiation Laboratory, for permission to use the cyclotron and Mr. R. Mills, the cyclotron operator, for his co-operation and assistance in carrying out the bombardments.

Special thanks are offered to Miss Ann Mylchreest for her excellent typing of this thesis.

I am indebted to the National Research Council for an award of a Studentship (1964-1965), to McGill University for an award of a Graduate Fellowship (1963-1964) and to the Chemistry Department for Demonstratorships throughout the period of this work.

TABLE OF CONTENTS

I. INTRODUCTION

Since the discovery of nuclear reactions, a number of theories and nuclear models have been postulated in order to explain their mechanism. None of them is however comprehensive enough to explain all the features of nuclear reactions. Every theory and every model has its own merits and demerits and certain limits of applicability. The following is a brief outline of the current theories which are relevant to the present study.

I-1. The Statistical Theory

In order to explain the mechanism of nuclear reactions at low energy, Bohr (1) first introduced the concept of compound nucleus formation. Basic in this theory is the assumption of the nucleus as a system of nucleons with strong and short-range interactions. When a projectile with certain kinetic energy impinges upon such a nuclear system along a particular entrance channel, it shares its energy and momentum with all other nucleons through multiple collisions. Finally an equilibrium system, the so-called compound nucleus, is formed, whose excitation energy equals the kinetic energy plus the binding energy of the projectile. This compound nucleus has a mean life-time of the order of 10^{-14} to 10^{-17} sec., long compared to the nuclear time, defined by the time required by a particle to traverse the nuclear diameter ($\sim 10^{-22}$ sec.).

The decay of the compound nucleus into reaction products proceeds independently of the mode of formation, but certainly depends

on its excitation energy, momentum and parity. A nucleon will be emitted along a particular exit channel when sufficient energy is accidentally concentrated on it by random collisions among the nucleons. The emission of a neutron requires, in addition to its binding energy, an extra energy to surmount the centrifugal barrier. Similarly in the case of a charged particle emission an additional amount of energy is needed to overcome the Coulomb barrier.

At very low incident energy (< 1 Mev) the compound nucleus is formed only in certain discrete energy states, as demanded by quantum mechanics. Such well-defined quantum states can be treated with the well-known principle of detailed balance. The transition probability from an initial state $|\alpha\rangle$ to a final state $|\beta\rangle$, $P_{\alpha\beta}$, is related to the transition probability from the state $|\beta\rangle$ to the state $|\alpha\rangle$, $P_{\beta\alpha}$, by

$$\rho_\alpha P_{\alpha\beta} = \rho_\beta P^*_{\beta\alpha} \qquad \ldots\ldots (I\text{-}1)$$

where ρ_α and ρ_β are the densities of states $|\alpha\rangle$ and $|\beta\rangle$, and the star on $P_{\beta\alpha}$ indicates a time-reversed transition i.e. a transition in which all velocities and momenta have changed sign.

With increasing excitation energy the life-time of the compound nucleus, τ, decreases and the corresponding uncertainty in the energy of the compound nucleus, $\Gamma = \frac{\hbar}{\tau}$, will thus increase. A large number of broad but closely spaced compound states are formed, which overlap one another leading to what is called the "continuum". Due to availability of many levels both in the initial and the final nuclei, the decay of the compound nucleus can be treated statistically.

Eqn. I-1 can be suitably applied to the discrete energy states

of the compound nucleus. As many levels are present within the width Γ, the application of Eqn. I-1 to the highly excited nucleus is in general complicated due to interference effects between matrix elements related to the transition probabilities. It is however assumed that the matrix elements possess randomly distributed phases due to the randomized internal motion of the compound nucleus. When the cross-sections are averaged over an incident energy spread ΔE that is much larger than the width Γ, (cross-sections are proportional to the absolute square of the relevant matrix elements), cross terms due to interference effects will disappear. The principle of detailed balance, when applied to such cases, gives only an average transition probability. A fruitful implication of the random phase assumption is that the compound nucleus can be considered as a classical system in the absence of interference effects, as these are typical of wave mechanics. These are the basic aspects of the statistical theory. Weisskopf (2) made use of Eqn. I-1 in calculating the probability of decay of a compound nucleus in a particular channel.

When the compound nucleus is highly excited, it decays by emission of particles as long as energy is available for their emission. The multiple decay of the compound nuclei proceeds by the evaporation of a first particle, thereby leaving the residual nuclei with a broad distribution of excitations determined by the energy of the evaporated particles. These residual nuclei can then emit more particles successively until no further emission of particles is energetically possible. Of course, energy and angular momentum have to be conserved in each step of the decay. The angular distribution of the emitted particles is symmetrical about 90 degrees in the centre of mass system and the energy

distribution of the emitted particles is Maxwellian in character.

Experimental verification of compound nucleus formation has been made by several authors. The classical experiment of Ghoshal (3) involved the formation of Zn^{64} compound nuclei of the same excitation energy by alpha particle bombardment of Ni^{60} and proton bombardment of Cu^{63}. The measured relative yields of different reaction products were found to be the same within experimental uncertainty indicating that a compound nucleus is formed and its decay is independent of the mode of formation. This experiment was further verified by John (4). However, the difficulty with this type of comparison is that even though the compound nuclei are formed with the same excitation energy by proton and alpha particle bombardments, there will be a difference in angular momenta of the two systems. Grover (5) mentioned that excitation functions are affected by the competition between particle and gamma ray emission. This competition depends largely on the excitation energies and the relative spin difference of the residual nuclei before and after final de-excitation. It is known that the final residual nuclei are generally formed in low spin states and also that the emitted particles do not carry away large angular momentum. Now if the residual nucleus before the final de-excitation step possesses high spin, then particle emission cannot lead to the available states of the final nucleus and hence photon emission competes. Thus the rotational energy associated with the angular momentum of the residual nucleus before final de-excitation is not available for particle emission and is dissipated by photon emission. Consequently the effective threshold of a reaction will be increased and hence the excitation function will be shifted. Porile et al (6) compared the excitation functions from

Ge^{70} compound nuclei produced by proton and alpha particle bombardments. They observed qualitatively that the relative yields of different reaction products were the same if the alpha particle excitation functions were shifted by about 3 Mev. Recently Grover and Nagle (7) measured the cross-sections of the (α,n), (α,2n), and (p,n) and (p,2n) reactions involving the same compound nucleus Po^{210}. They could interpret their results in terms of compound nucleus mechanism by taking into account the effect of angular momentum difference between the two compound nuclei.

The verification of symmetry of the angular distribution of the emitted particles about 90 degrees provides a convenient experimental test of the compound nucleus mechanism. Wolfenstein (8) first found that the angular distributions of the emitted particles are symmetrical about 90 degrees. Recent measurements of the angular distributions of emitted protons have been made by Glover and Purser (9), and Armstrong and Rosen (10) using 14 Mev neutron bombardments of different elements. They found the angular distribution to be symmetric about 90 degrees.

Sherr and Brady (11) found that their alpha particle spectra due to $Co^{59}(p,\alpha)Fe^{56}$ reaction were similar in shape to those of $Fe^{56}(\alpha,\alpha')Fe^{56}$ reaction obtained by Lassen et al (12) at similar energies. This gives ample proof that the energy spectra of the particles which are emitted from the same compound nucleus formed in different ways should have the same shape, as implied by the independence hypothesis.

Compound nucleus formation can also be verified by recoil-range measurements. Maximum values of recoil ranges are obtained when complete momentum transfer occurs, leading to compound nucleus formation. Porile et al (13) measured the recoil ranges for reactions induced in In^{115} and

In^{113} with protons of 5-10 Mev and alpha particles of 20-40 Mev. Most of their results agreed reasonably well with the values expected from compound nucleus formation. Recently Blann et al (14) measured the recoil ranges of different reaction products obtained by alpha particle bombardment of Ni^{58} in the energy range 46-68 Mev. In most of the reactions they found a complete momentum transfer indicating that the reaction proceeds through compound nucleus formation. Deviations observed in some cases were attributed to the low momentum transfer resulting from non-compound nuclear processes.

The validity of compound nucleus formation can also be tested from an agreement between the experimental results and the calculations according to the statistical theory. Porile (15) measured excitation functions for alpha-induced reactions on Zn^{64} for incident energies up to 41 Mev. The measured results were compared with the calculations according to the statistical theory. Agreement was not consistent for all reactions indicating that the statistical theory is not completely applicable. Houck and Miller (16), and Hahn and Miller (17) measured excitation functions of different reactions induced by alpha bombardment of Sn^{124}, Fe^{54} and Ni^{58} in the energy range 10-40 Mev. They compared their measured values with statistical theory calculations. Good agreement was found in the energy range of 20-30 Mev indicating that compound nucleus formation is valid in this energy range. Comparisons between experiments and Monte Carlo calculations using the statistical theory are discussed later.

I-2. The Direct Interaction Mechanism

Experimental proofs of the compound nucleus theory, as mentioned in the preceding section, however, do not imply that compound nucleus formation is the only mechanism. Angular distributions of inelastically scattered protons from proton bombardments of various elements were measured by Eisberg and Igo (18) at 31 Mev, by Gugelot (19) at 18 Mev and by Cohen (20) at 23 Mev. They observed asymmetry in the angular distributions of the emitted protons and attributed it to the direct interaction processes. From an analysis of the inelastic proton and alpha particle scattering data obtained by 15-19 Mev proton bombardment of V, Ni etc., Sherr and Brady (11) showed that a fraction of the reactions results from direct processes. This process can be envisaged in the light of Weisskopf's idea (21) that, in contrast to Bohr's assumption of strong coupling, weak coupling prevails among the nucleons in a nucleus. Hence direct interaction can take place even at low energies. The occurrence of direct interaction at low energies is also conceivable in terms of the optical model. In the optical model description the nucleus is considered as an opaque sphere partly absorbing and partly refracting the incoming particle. The absorbing part of the potential is small at low energies and increases with increasing energy of the incident particle, whereas the refracting part exhibits the opposite behaviour. Moreover, the absorbing part is inversely proportional to the mean free path of the incident particle. As mentioned by Peaslee (22) and Hodgson (23), the mean free path of the incident particle is large at low energies, passes through a flat minimum and then increases with incident energy. The mean free path Λ is given by

$$\Lambda = \frac{1}{\rho \bar{\sigma}} \qquad \ldots\ldots (I\text{-}2)$$

where ρ is the nucleon density and $\bar{\sigma}$ is the effective nucleon-nucleon collision cross-section. At low energies the effective cross-section is small, because most of the collisions are forbidden by Pauli exclusion principle. The latter makes a collision with small momentum transfer impossible unless the struck nucleons lie near the top of the Fermi energy. Therefore, the mean free path will be long. As the incident energy is increased, the effective collision cross-section will be increased resulting in a decrease of the mean free path. However at very high energies the total collision cross-section decreases thereby reducing the effective cross-section as a result of which the mean free path will again increase. Thus due to its long mean free path at both low and high energies the incident particle may traverse the nucleus, while making only a few collisions.

As first suggested by Serber (24), high energy nuclear reactions are considered to proceed by a two-step process: knock-on or cascade process and evaporation process. In the cascade process the reaction proceeds through successive two-body collisions between the incident particle and the individual nucleons in the target nucleus. Since the wavelength of the very high energy particle (effective size) is very small compared to the internucleon distance, it can obviously be visualised that such a two-body collision is not affected by the presence of other nucleons in the nucleus. Therefore, these collisions can be considered as collisions between free nucleons (Impulse Approximation). After the first collision both or either of the collision partners may be emitted or collide with other nucleons depending on the kinematics and energetics

of the process. An intranuclear cascade is thus generated, in which a few prompt nucleons with varying kinetic energy are emitted leaving behind a residual nucleus with a wide distribution of energies. Each cascade step is, however, governed by the Pauli exclusion principle, the momentum distribution of the nucleons in the nucleus and reflection and refraction by the real part of the potential. A characteristic feature of high energy nuclear reactions is that the incident particle, having a long mean free path, may traverse through the target nucleus without suffering any collisions. This phenomenon leads to what is called "nuclear transparency".

The cascade process continues until the energy of the collision partners decreases to such an extent that one can no longer neglect the influence of the nucleus as a whole on the two-body collisions, and consequently no more prompt particles can be emitted. Ultimately, an equilibrium is established in the residual nucleus through multiple collisions among the nucleons. The residual nuclei will then evaporate off a few more particles until the excitation energy is not sufficient to emit any more particles. This evaporation process is very slow and stochastic in nature. This phenomenon bears a complete analogy with the statistical theory, and is, therefore, described in terms of the statistical model.

Although the cascade-evaporation model was formulated to explain high energy reactions, it also appears to be valid below 100 Mev. The evidence comes from the experimental observations made by several authors. From a study of photographic emulsion bombarded with 50-125 Mev protons, Hodgson (25) found that about 30% of the emitted particles are due to the nuclear cascade initiated by the primary particle. In another experiment

involving (p,α) reactions in nuclear emulsion at a proton energy of 45 Mev he (26) observed similar evidence of the knock-on process. Eisberg and Igo (18) concluded from their 31 Mev proton scattering results that the cascade process is a part of the reaction mechanism. Moreover, from a consideration of the mean free path in terms of the optical model as described previously it is understood that the cascade-evaporation model is applicable at lower energies. It should however be pointed out that at energies below 100 Mev the nuclear reactions are expected to proceed through a combination of both compound nucleus formation and cascade-evaporation process. At low energies the former will be predominant and at high energies the latter will be prominent.

The random nature of both cascade and evaporation processes suggests the use of the Monte Carlo method in calculating the formation cross-section of a reaction product. A Monte Carlo calculation of the cascade process was first performed by Goldberger (27). Several authors (28) (29) (30) (31) (32), among others, followed the same technique using various values for the different nuclear parameters such as nuclear radius, potential well depth, and cut-off energy. In all of these calculations the nucleus is envisaged as a degenerate Fermi gas in a square potential well with a uniform density distribution. Among all these calculations, that of Metropolis et al (31) (32) is the most comprehensive giving results for a number of target nuclei and different energies. In this calculation a large number of cascades was followed for each set of initial conditions resulting in better statistical accuracy than that of the previous calculations. The output of the computation gives the type, number, energy and angular distribution of the emitted particles, and the distribution in atomic number Z, mass number A and excitation

energy of the residual nuclei.

Rudstam (30) and Dostrovsky et al (33) (34), among others, have used Weisskopf's (2) evaporation formalism in the Monte Carlo calculation of the evaporation process. The calculation of Dostrovsky et al (34) is the most comprehensive one. For a starting nucleus the calculation gives Z and A of the residual nucleus and also the energies and multiplicities of the evaporated particles.

The results of the Monte Carlo calculation of both cascade and evaporation processes are coupled together to give the resultant probability of the formation of a nuclear reaction product. Experimental results have been compared with both types of calculations. Dostrovsky et al (34) compared their calculated cross-sections for proton-induced reactions with the results of Meadows (35) for Cu^{63} and Cu^{65} targets, and those of Sharp et al (36) for Co^{59}. Reasonable agreement was achieved at energies up to 50 Mev, although the calculated values were too low for the simple (p,n) and (p,pn) reactions. Porile et al (6) found fair agreement at energies up to about 30 Mev between the statistical theory calculation and their experimental excitation functions for reactions of Ga^{69} and Ga^{71} with protons. The high energy tails of the excitation functions for the (p,n) and (p,pn) reactions could not be accounted for by the statistical theory calculation.

Metropolis et al (31) compared their cascade calculation for 82 Mev protons with the inelastic proton scattering results measured by Strauch and Titus (37) at 96 Mev. A slight interpolation was made to make the calculated values correspond to 96 Mev protons. Good agreement was found. The energy distribution of the emitted protons measured by Hadley and York (38) from 90 Mev neutron bombardment of copper was

compared with cascade calculation of Metropolis et al (31). Fair agreement was found within statistical errors. The cascade-evaporation calculation was performed by Porile et al (6) for 46.5 Mev proton-induced excitation functions for Ga^{69} and Ga^{71} target nuclei. The calculation was in good agreement with their experimental values.

The discrepancy between the calculation and the experimental results was attributed in several cases to the use of a uniform density distribution and to the neglect of reflection and refraction of the cascade particles by the real part of the potential. Bertini (39) used a three-step-function potential for the nucleus considering a non-uniform nucleon density distribution, but did not take into account the effect of reflection and refraction of the particles in the cascade calculation. Recently Chen et al (40) performed a Monte Carlo calculation of the cascade process using a seven-step-function potential for the nucleus. They considered the reflection and refraction of the cascade particles at the surfaces of changing potential. This cascade calculation has been adopted for the present study.

I-3. Formation of Isomers and Isomer Ratios

A nuclear isomer is a metastable excited state of a nucleus. An isomeric state normally owes its existence to a large spin and small energy difference between the nuclear ground state and the state in question. In terms of the Shell Model, this situation is met by odd-A nuclides having outer shells that are nearly filled.

When a nuclear reaction occurs, a residual nucleus is formed in a large number of excited levels after the emission of particles. All

these excited states de-excite to the ground state by the emission of a cascade of photons. Usually the transition of an upper state to a lower one is very rapid and the half-lives of the highly excited states are very short. If, however, the difference in spins of two low-lying states is large, then the transition from the upper state to the lower state is forbidden. The upper state will then have a comparatively long half-life. This will be an isomeric state of the nuclide in question.

The relative probability of formation of each state of an isomeric pair has been so far interpreted in terms of the compound nucleus mechanism. The total angular momentum of a compound nucleus is the vector sum of the target spin, the projectile spin and the orbital angular momentum brought in by the projectile. The vectorial addition of these quantities gives rise to a spin distribution of the compound states. Following the emission of particles and photons carrying away angular momenta from the compound nucleus, different spin distributions of the residual states are obtained. The probability of formation of an isomer with a specific spin is dependent on these spin distributions of the compound and residual nuclei.

As the energy of the projectile is increased, the angular momentum brought in by the particle will increase thereby leading to a large angular momentum of the compound nucleus. Moreover, if the target spin or the projectile spin is large, the angular momentum of the compound nucleus can be large even at low energies. As the emitted particles do not usually carry away large angular momentum and also the photon cascade is composed of dipole and quadrupole radiations, the decay of a compound nucleus with high angular momentum will favour the formation of a high spin isomer and vice-versa. Furthermore, nuclear reactions involving

low angular momentum transfer give a larger yield of the isomer with spin closer to that of the target nucleus.

An important quantity in the description of isomers is the ratio of the formation cross-section of the high-spin state, σ_H, to that of the low-spin state, σ_L. This quantity, σ_H/σ_L, is called the isomer ratio. It is sometimes convenient to refer instead to the formation cross-sections of the ground and metastable states. These are denoted by σ_g and σ_m respectively. For the reasons mentioned above, the isomer ratio for a particular reaction should increase with an increase in projectile energy. However, at higher energies, where a direct interaction is operative and hence low angular momentum transfer occurs, the isomer ratio decreases.

Isomer ratios for various reactions have been measured by a number of authors, and Wing (41) has recently compiled a large body of isomer ratio data. Porile et al (6) measured the isomer ratios for the $Ga^{71}(p,2pn)Zn^{69m,g}$ reaction in the energy range of 13-56 Mev. They found that the isomer ratio increases with bombarding energy up to about 42 Mev and then decreases. The initial increase is due to the increase of the average angular momentum of the compound nucleus with bombarding energy, and the decrease at higher energies is a result of the low angular momentum transfer in the direct process. Meadows et al (42) measured the isomeric ratios for different (p,pn) reactions at various energies up to 100 Mev. They calculated qualitatively the isomer ratios for these reactions from an initial spin distribution of the compound nucleus. Reasonable agreement between the calculation and the experimental results was found within a factor of 2-3. They explained the variation of the isomer ratio with bombarding energy in terms of the compound nucleus and direct processes.

A more accurate theoretical calculation of isomer ratios has been performed by Vandenbosch and Huizenga (43). Fair agreement was obtained between the calculated values and their experimental isomer ratios of $Hg^{197m,g}$ produced by different reactions. Need et al (44) and Need (45) measured the isomer ratios of $Sn^{120}(p,\alpha)In^{117m,g}$ reactions at different energies up to 22 Mev. On comparison of these results with the Vandenbosch and Huizenga type of calculations reasonable agreement was achieved.

The effect of angular momentum on the isomer ratios can be suitably studied by heavy-ion-induced nuclear reactions because of the large angular momentum brought in by the projectile. Seegmiller (46) and Kiefer (47) investigated the effects of angular momentum on the isomer ratios of $Te^{119m,g}$ and $Ce^{137m,g}$ respectively using various heavy-ion-induced reactions. They found that the isomer ratios increase with increasing angular momentum carried in by the projectile.

I-4 Previous Work of Interest

A number of excitation function studies involving inelastic reactions of medium energy particles with medium weight elements have been previously made. Experiments involving proton bombardment in the medium energy range are however very few compared to those of alpha particle and heavy-ion bombardments. Only the proton-induced excitation function studies relevant to the present study are outlined below.

Meadows (35) measured the excitation functions for the (p,xn) and (p,pxn) reactions of copper with protons up to 100 Mev. His experimental results showed a fair agreement with the predictions of the

statistical model at low energies and also qualitative agreement with those of Serber's transparency model at high energies.

Sharp et al (36) determined the formation cross-sections of various nuclides produced by proton bombardments of cobalt at various energies up to 100 Mev. Their results were interpreted in terms of the compound nucleus mechanism at low energy and a mixture of compound nucleus and Serber mechanisms at higher energy.

Caretto and Wiig (48) reported absolute cross-sections for a number of nuclides produced from yttrium by 60-240 Mev proton bombardments. They explained their results qualitatively in the light of the cascade-evaporation theory.

Kavanagh and Bell (49) measured the excitation functions of the (p,pn), (p,p2n) and (p,p3n) reactions in gold in the proton energy range 18-86 Mev. Their results were much larger than those predicted by the statistical and cascade-evaporation theories, and they were interpreted in terms of two-body collisions in the diffuse surface of the target nucleus.

In the study of spallation of medium weight elements, Rudstam (30) irradiated arsenic with protons of energies 49 Mev, 103 Mev and 170 Mev. A comparison of the experimental results with a Monte Carlo cascade-evaporation calculation yielded good agreement. Rudstam also developed an empirical formula with four parameters and found a fit to the experimental results with the formula within a factor of about 2.

Hontzeas and Yaffe (50) measured the cross-sections of different spallation products produced by 5-85 Mev proton bombardment of V^{51}. They found a fit to the experimental values with the Rudstam's empirical formula (30) with four parameters.

Porile et al (6) performed excitation function measurements for various reactions induced in Ga^{69} and Ga^{71} with 13-56 Mev protons. From a comparison with the evaporation calculation as well as the cascade-evaporation calculation, their results provided evidence that compound nucleus formation is the principal mechanism for proton energies up to 30 Mev, although the simple (p,n) (p,pn) reactions involve a direct interaction even at this low energy. Also they concluded that as the incident energy is increased, the compound nuclear process decreases and direct interaction predominates.

I-5. Purpose of the Present Study

The present investigation involves a study of the nuclear reactions induced by 5-85 Mev protons in yttrium. The following are the reasons for choosing such a system:

(a) Yttrium is monoisotopic and thus the interference of extraneous reactions on a particular excitation function, arising from the use of polyisotopic target materials, can be avoided.

(b) Proton bombardment of yttrium yields a range of radiochemically observable products. The reactions are not complicated by fission. Moreover, yttrium provides a nucleus of sufficient complexity and the energy range is sufficiently large to permit a meaningful comparison to the statistical and the cascade-evaporation model calculations.

(c) Three pairs of isomers are formed in (p,pxn) reactions. The theoretical prediction of the formation cross-sections of these isomers is complicated by non-compound nuclear processes entailed in

such reactions. However, qualitative information about the reaction mechanism could be obtained from these isomer ratios.

The following presentation, however, is not claimed to be a complete analysis of the subject; it will give some information about the validity of the current theories of nuclear reactions.

II. EXPERIMENTAL PROCEDURES

II-1. Preparation of Targets

The target material was a mixture of 'spec-pure' Yttrium Oxide*, Y_2O_3 (99.99% yttrium) and 'spec-pure' Copper Oxide*, CuO (99.99% copper). The copper oxide was used to monitor the intensity of the proton beam.

Exact amounts of yttrium oxide and copper oxide, both in powder form, were weighed in the atomic ratio of 1:1 and mixed intimately in a mortar. The mixture was analysed for copper by a spectrophotometric method using sodium diethyldithiocarbamate reagent (51). The mixture was found to be homogeneous as expected from the similar densities of these oxides (Y_2O_3 - 4.84 and CuO - 6.4).

About 50 milligrams of the mixture were used for each bombardment. The mixture was loaded into an aluminum tube (.0625" outside diameter and .0015" wall thickness) which was closed flat at one end. After loading, the other end was also pinched shut and the two ends of the tube were bent diagonally. Finally the aluminum tube was rolled flat with a glass rod to make it a comparatively thin target so that energy degradation of the beam could be neglected. All targets were prepared using the same mixture.

The target was fastened to a target holder which was then fixed to the end of the cyclotron probe. The probe was set at a fixed radial distance corresponding to the desired bombarding energy. A representative diagram of the target and the target holder is shown in Fig. 1.

---

* Available from Johnson, Mathey and Company.

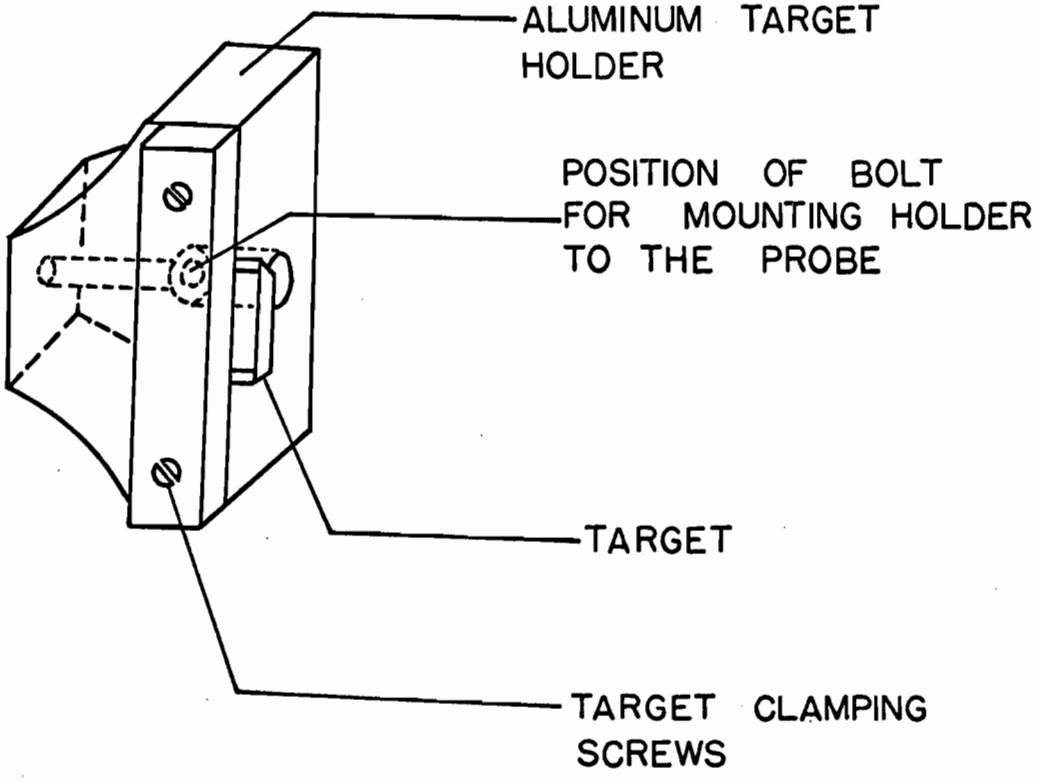

FIG. 1. Assembly of Target and Target Holder.

II-2. Irradiations

All irradiations were carried out in the internal proton beam of the McGill Synchrocyclotron. Bombardments were made in the energy range of 5 Mev to 85 Mev at 3 Mev intervals up to 48 Mev and then at 6 Mev intervals up to 85 Mev. Irradiation periods ranged from 30 minutes to 70 minutes depending on the activity desired and also the day-to-day variation of the proton beam intensity. The intensity of the proton beam varied between 0.5 and 1.0 microampere.

II-3. Chemical Procedures

At high bombarding energy, the nuclides expected to be formed include zirconium, yttrium, strontium, rubidium, bromine (from spallation of yttrium) and zinc, copper, nickel, cobalt, iron, manganese (from spallation of copper). Since we were interested in the nuclides of zirconium and yttrium, as well as copper above 15 Mev, and zinc up to 15 Mev, our attention was focussed on the chemistry of these elements only.

The general schemes of separation were mainly based on those reported in "Collected Radiochemical Procedures" - LA-1721, 2nd edition (1958) for zirconium and yttrium, and those given by Kraus and Moore (52) for copper and zinc. However, at some stages, slight modifications were made to suit the present problem.

After irradiation, the target was detached from the target holder and transferred to a 40 ml centrifuge tube containing 10 mg of zirconium carrier (exactly known). It was then dissolved by heating in

a few millilitres of conc. HCl and a few drops of hydrogen peroxide. The target solution was then evaporated to dryness and taken up in 2 ml of 6M HCl solution. This solution, cooled to room temperature, was passed through an ion-exchange column of Dowex-1 x 8 (mesh size 100-200) 6 cm long and 1 cm in diameter, already equilibrated with 6M HCl. It was then eluted with 15 ml of 6M HCl. In this step, yttrium, zirconium, strontium, rubidium, manganese, nickel and sodium (spallation product of aluminum) were eluted and collected in a lusteroid tube for further chemistry of zirconium and yttrium. Only copper, zinc, cobalt and iron remained adsorbed on the column. Copper was eluted with 2M HCl. Cobalt also passed through in this step. This eluate was saved for copper purification.

A few millilitres of conc. HCl were added to the solution (6M HCl) obtained in the first elution to increase its molarity up to 8-10. Inactive carriers of nickel, manganese, cobalt, strontium, rubidium ($\sim$5 mg each) were added. Zirconium phosphate, $ZrH_2(PO_4)_2$, was precipitated with 3.5% solution of sodium phosphate, Na_2HPO_4, while the rest of the elements remained in solution. It was then centrifuged and the supernate was decanted in a lusteroid tube. The precipitate was processed as described below for the purification of zirconium.

The supernate was scavenged twice more with zirconium phosphate precipitation on adding zirconium carrier and sodium phosphate solution so that the last trace of zirconium activity was removed. Yttrium fluoride, YF_3, was precipitated from the solution by adding 2 ml conc. HF. This precipitate was centrifuged and kept for further chemistry of yttrium. The supernate was discarded.

Zirconium:- Zirconium phosphate obtained above was washed with

conc. HCl, dissolved in 2 ml of conc. HF and diluted to about 25 ml with water. One ml of saturated $Ba(NO_3)_2$ solution was then added to precipitate zirconium as barium fluorozirconate, $BaZrF_6$. After washing the $BaZrF_6$ precipitate twice with dil. HF, it was dissolved by stirring in 5 ml of saturated boric acid, H_3BO_3 and 2 ml of conc. nitric acid, HNO_3, and then diluted with 5 ml of water. Barium was precipitated as sulphate with a few drops of conc. H_2SO_4 and removed by centrifugation. Strontium carrier was added to the supernate and zirconium hydroxide was precipitated with conc. NH_4OH. The hydroxide precipitate was washed with water and redissolved in 10 ml of conc. HCl. Yttrium, rubidium, manganese, nickel and cobalt carriers were added to the solution as hold-back carriers. The cycle of precipitations of phosphate through hydroxide was repeated twice more. Finally zirconium hydroxide was washed twice with water, dissolved in 4M HCl and made up to 5 ml or 10 ml in a volumetric flask depending on the activity produced and desired.

Yttrium:- Yttrium fluoride precipitate obtained from the target solution was washed with dil. HF, dissolved in 2 ml saturated H_3BO_3 and 2 ml conc. HNO_3 and diluted to 10 ml with water. The solution was transferred to a glass centrifuge tube containing 10 mg of strontium carrier . Yttrium hydroxide, $Y(OH)_3$, was precipitated with conc. NH_4OH, washed twice with water and finally dissolved in 10 ml conc. HCl. Zirconium, rubidium, manganese, nickel and cobalt carriers were added to the solution to serve as hold-back carriers in the precipitation of YF_3 with conc. HF. The procedure from the precipitation of YF_3 through $Y(OH)_3$ was repeated twice more. Finally, after washing, yttrium hydroxide precipitate was dissolved in 20 ml conc. HNO_3.

Yttrium was then extracted by shaking for 10 minutes with 20 ml

of tributyl-phosphate (TBP) equilibrated with conc. HNO_3. The organic phase was scrubbed with 20 ml of conc. HNO_3. Yttrium was extracted back thrice with 10 ml portions of distilled water by shaking for 5 minutes. The back extracted aqueous solution was treated with conc. NH_4OH to precipitate $Y(OH)_3$. The precipitate was then washed thrice with water, dissolved in 4M HCl and made up to 5 ml or 10 ml in a volumetric flask, as desired.

The Sr^{87m} and Sr^{85m} nuclides have gamma rays similar in energies to those of Y^{87m} and Y^{86m} respectively. The growth of these strontium nuclides from yttrium nuclides in the yttrium samples made it difficult to determine the activities of Y^{87m} and Y^{86m}. In order to avoid this difficulty strontium was separated from the yttrium solution very quickly and these nuclides were counted immediately. To the above yttrium solution obtained after TBP extraction, were added about 10 mg of strontium carrier. Conc. NH_4OH was added to precipitate $Y(OH)_3$. This precipitate was centrifuged and decanted. After washing once with water, $Y(OH)_3$ was brought into solution with a few drops of conc. HCl, and diluted to nearly 20-25 ml. An aliquot was taken and counted immediately. The milking experiment usually took 7 min. to 10 min. Four separations were carried out for each bombarding energy for the nuclides of interest. The chemical yield of each of these samples was determined. Before a milking experiment was performed for Y^{87m}, the yttrium main solution was made up to a definite volume. An aliquot was taken for counting those nuclides whose activity could be determined without interference from other nuclides. At the same time a definite amount of the solution was saved for chemical yield determination. The rest of the yttrium solution was then utilised for milking experiments.

In the case of a milking experiment for Y^{86m} ($t_{1/2}$ = 48.5 min.) the separations were carried out first, and then the remaining solution was made up to a definite volume to measure other activities.

Copper:- The $Cu^{65}(p,pn)Cu^{64}$ reaction was used to monitor the proton beam above 15 Mev. The solution obtained after the ion-exchange elution in the second step was dried under an infra-red lamp and taken up in 2 ml of 6M HCl. The solution was then passed through another ion-exchange column of Dowex-1 x 8 resin (mesh size 100-200) which was about 12 cm long and 1 cm in diameter. The column was washed with 4M HCl till the coloured band of copper reached the end of the column. Copper was then removed by eluting with 1.5M HCl, and finally made up to 5 ml or 10 ml depending on the activity produced.

Zinc:- For bombardments up to 15 Mev, the $Cu^{63}(p,n)Zn^{63}$ reaction was used as the monitor reaction. After irradiation the target was dissolved in conc. HCl and a few drops of H_2O_2 in a centrifuge cone containing 10 mg each of zinc and zirconium carriers (exactly known). The solution was evaporated to dryness and then taken up in 2 ml of 2M HCl solution. It was then passed through an ion-exchange column of Dowex-1 x 8 of dimensions mentioned earlier (the one used for the target solution). The column was then washed with about 15 ml of 2M HCl. Zirconium and yttrium were separated from the eluate according to the procedure described above. The column was then washed with 0.5M HCl several times to remove copper completely. Zinc was then eluted with distilled water. Zinc carbonate was precipitated from the solution with saturated sodium carbonate. After centrifugation and decantation zinc carbonate was finally dissolved in 2M HCl and made up to 10 ml.

Sources for either gamma counting or beta counting were

prepared by taking an aliquot from the main solution made above in a small screw-cap glass vial (size - 15.5 mm x 50 mm). Each sample was made up to 2 ml to make the geometry of the source subtended at the detector reproducible. The rest of the solution was used for the determination of the chemical yields. Some of the copper samples were counted using the total volume and the chemical yields were determined later by diluting the whole sample to a definite volume.

II-4. Determination of Chemical Yields

Spectrophotometric methods were adopted to measure the chemical yields of zirconium and yttrium, whereas those of copper and zinc were determined by titration.

Zirconium:- The spectrophotometric method recommended by Horton (53) was followed to determine the chemical yield of zirconium, using the complexing agent 2-(2-hydroxy -3,6-disulpho-1-naphthylazo)-benzenearsonic acid (commercially known as Thoron). The chemical yields varied from 50% to 90%. A standard curve is shown in Fig. 2.

Yttrium:- The chemical yields of yttrium were determined by developing its complex with sodium alizarine sulphonate, as described by Sandell (54) in the presence of ammonium acetate-acetic acid buffer, and then measuring the absorbance with the spectrophotometer. The chemical yields obtained were of the order of 50%-80%. A standard curve is shown in Fig. 3.

Copper:- The chemical yields of copper were determined by titration with the disodium salt of ethylenediamine tetra-acetic acid (55) using a murexide indicator. The measured yields were of the order of

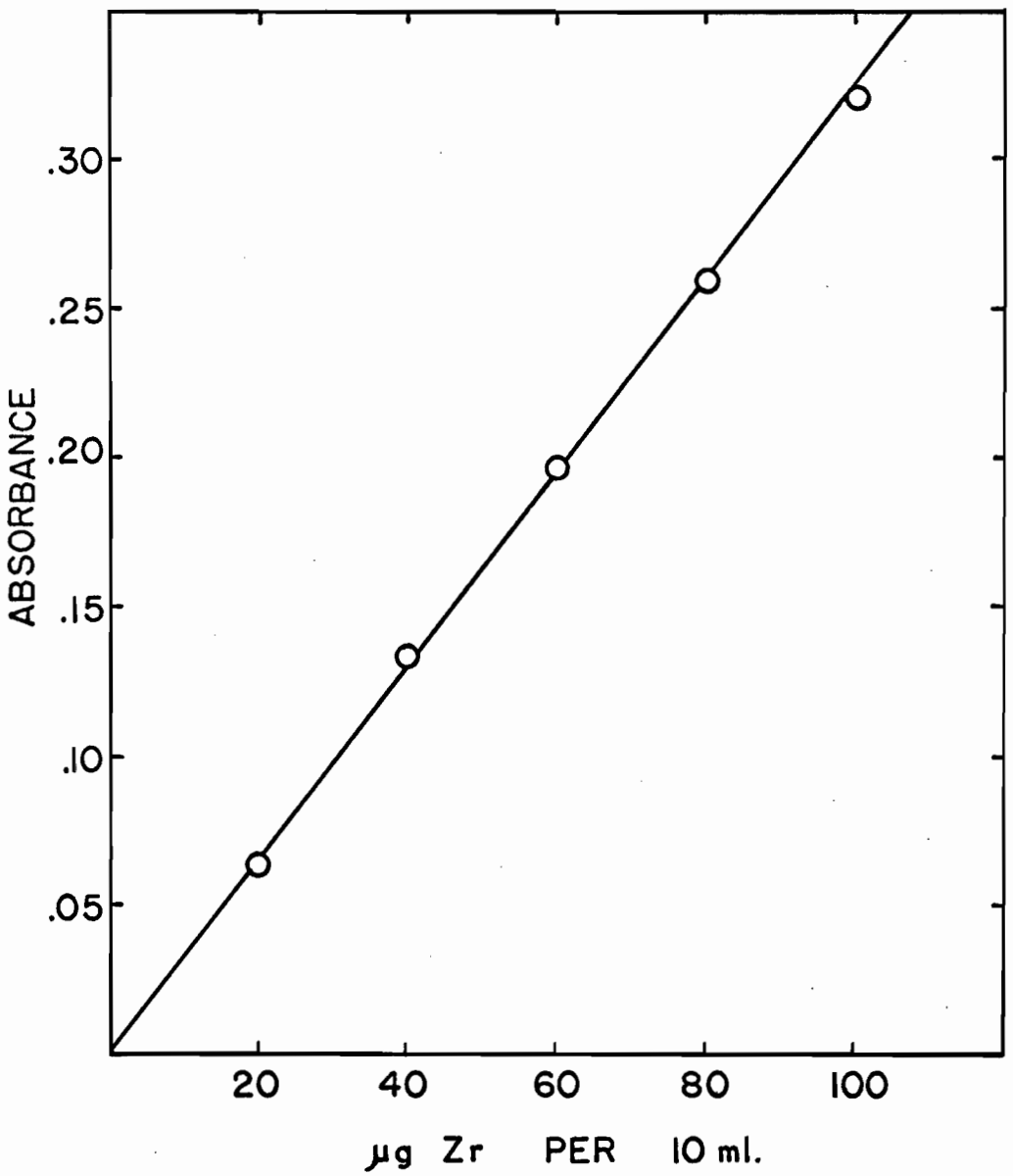

FIG. 2. Standard Absorbance Curve for Zirconium-Thoron Complex.

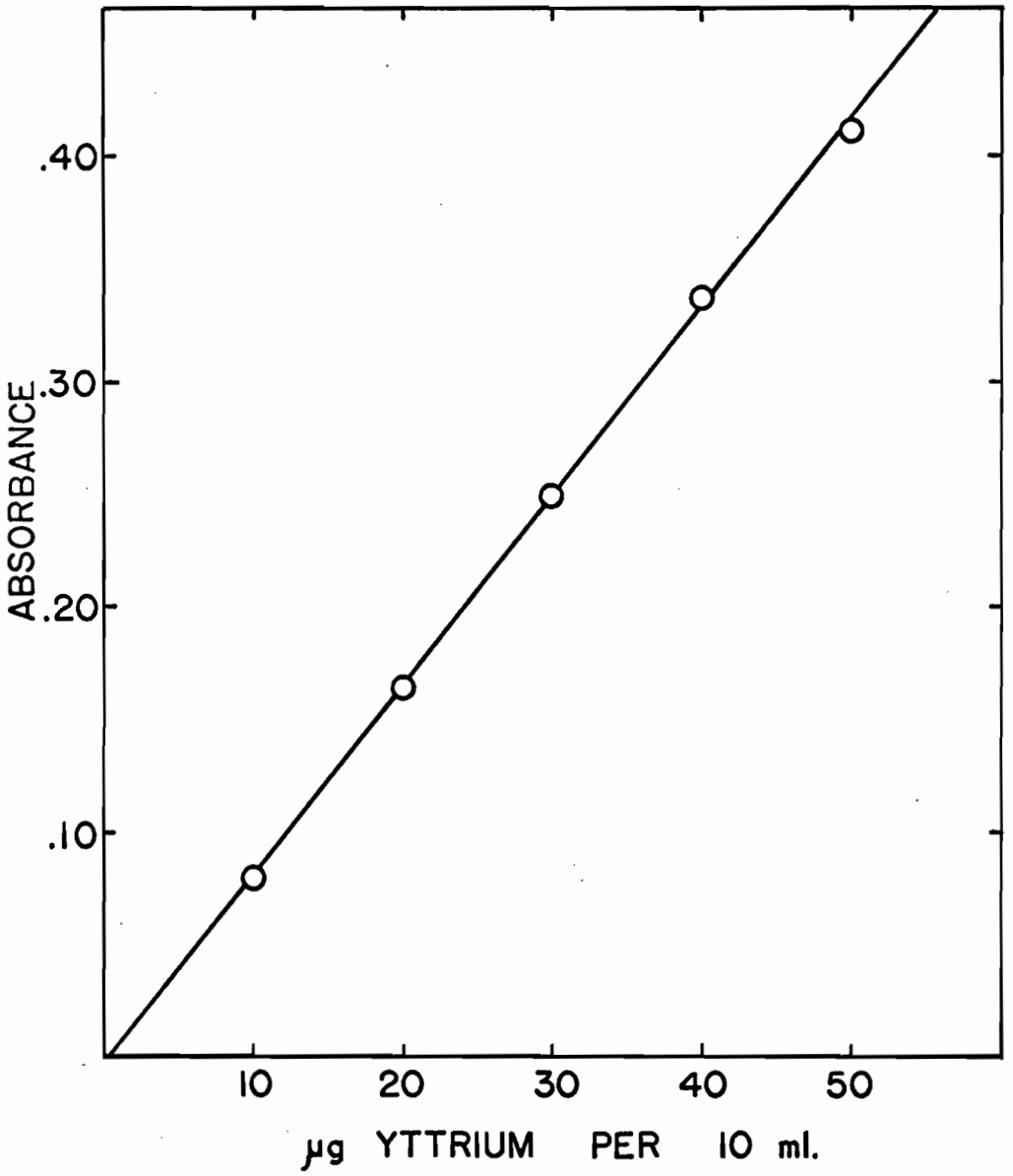

FIG. 3. Standard Absorbance Curve for Yttrium-Sodium Alizarin Sulphonate Complex.

60%-95%.

Zinc:- The chemical yields of zinc were measured by titration with disodium ethylenediamine tetra-acetate (55) using Eriochrome Black-T indicator at controlled pH 10. Chemical yields of 85%-97% were obtained.

II-5. Counting Techniques

Throughout this investigation, two kinds of counting techniques were adopted. A scintillation detector, coupled with a 100 channel pulse height analyser, was used to measure the characteristic gamma rays of particular nuclides. A coincidence counter was used to measure the 0.511 Mev annihilation gamma rays of β^+-emitters.

(a) Scintillation Method

A commercially available (Harshaw Chemical Company) 3" x 3" NaI (Tl) crystal served as the detector for gamma radiations. The crystal was coupled to a Dumont type 6364 photomultiplier tube. The crystal, hermetically sealed in an aluminum can, was shielded by lead to reduce the background pulses. Fluorescent radiations from lead were attenuated by lining with iron and lucite inside the lead.

The output pulses from the amplifier were stored in a 100 channel pulse height analyser (Computing Devices of Canada Ltd., Model AEP 2230). The stored data could be recorded on an analogue basis with a recording unit or printed out with a digital print-out system.

The dead-time of the analyser varied from 35 μsec. to 135 μsec., depending on the pulse height. Fortunately, the spectrum was not dis-

torted due to this dead-time, but its overall amplitude was reduced. However the analyser was equipped with a microammeter to measure the percentage loss due to dead-time. These dead-time losses were minimised by counting the sample at an appropriate geometry.

The detection efficiencies for gamma rays of various energies for different source positions were determined experimentally by Grant, May and Rayudu using several standard gamma sources. These values are reported in the Appendix of Reference (56). These values were used in the present calculation.

The resolution of the NaI (Tl) crystal was about 12.8 per cent for the 0.662 Mev gamma ray of Cs^{137}.

(b) Coincidence Method

A 0.511 Mev gamma-0.511 Mev gamma coincidence unit was utilised in the measurement of annihilation radiations of β^+-emitters. Two 1 1/2" x 1" NaI (Tl) crystals, coupled to photomultiplier tubes, were placed at 180 degrees with respect to the source. The base line and window width of the multiple coincidence unit (Cosmic Radiation Labs., Model 801) were adjusted so that only coincident 0.511 Mev gamma rays were detected.

In order to correct for the rare chances of accidental coincidences, one of these detectors was paired with a third 1 1/2" x 1" NaI (Tl) crystal placed at 90 degrees to the source, but with the same geometry with respect to it as the other two.

The source was mounted on a lucite block with the source-to-detector distance being 3 inches. A roll of copper foils in annular form was placed surrounding the source in order to ensure the complete

absorption and annihilation of positrons. The detection efficiency of the counter was about 0.1%.

The coincidence unit was calibrated against a 4π-counter using a Na^{22} source. It is known that the volume within which a positron annihilates increases with its energy. This will have an effect on the calibration made by using a Na^{22} source having 0.54 Mev positrons. However, this effect was checked by counting $Zn^{63}(E_{\beta^+} = 2.35$ Mev) and Na^{22} at different source-to-detector distances, and finding the ratio of the two activities. It was found that at a source-to-detector distance of about 3 inches and up, the ratio was constant. The day-to-day variation in the efficiency of the set-up was checked by a Na^{22} standard source.

II-6. Analysis of Spectra

The preliminary step in the analysis of spectra was to determine the energies of the photopeaks. This was accomplished with an energy calibration curve prepared by measuring various gamma rays of different long-lived standard sources (e.g. Na^{22}, Cs^{137}, Co^{60}, Mn^{54}).

The determination of the area of a photopeak involved difficulty in estimating background under the peak. The difficulty was due to the contribution of the Compton distribution of the high energy peaks to the photopeaks of the low energy ones. Lazar (57) and Heath (58) have suggested the "stripping method", but this procedure was too tedious to be applied to the analysis of hundreds of spectra. Therefore, a different but simpler method was adopted as described below.

Backgrounds of different photopeaks in a complex spectrum were

hand drawn in the manner consistent with that adopted in determining the photopeak efficiencies. For some peaks, backgrounds were drawn intuitively taking care of all phenomena occurring under the peak. Typical background estimations for different peaks are shown in Figs. 4-6 inclusive. The photopeak areas were then obtained by subtracting the background from the total area.

The photopeak areas were then corrected for efficiency, geometry, dead-time loss, chemical yield, and dilution factor according to the following relation, to give the absolute photon emission rates, N,

$$N = A_p \times \frac{100}{(100 - D.L.)} \times \frac{1}{E_p} \times \frac{100}{C.Y.} \times F. \quad \ldots \text{(II-1)}$$

where A_p = photopeak area,

D.L. = dead-time loss in per cent,

E_p = efficiency for a particular source position,

C.Y. = chemical yield of the nuclide of interest in per cent,

F. = dilution factor.

After determining the absolute photon emission rates of a particular nuclide at different time intervals the decay curve is plotted. Absolute photon emission rates, N_o, at the end of bombardment (for zirconium nuclides) or at the end of separation (for some yttrium nuclides) were obtained by graphical extrapolation or computer analysis.

From a knowledge of branching ratios and internal conversion coefficients, the absolute photon emission rates, N_o, at the end of bombardment or separation were converted to absolute disintegration rates,

FIG. 4. Typical gamma-ray spectra of zirconium samples.
Dotted lines indicate the estimated background.
(a) 56 days after bombardment at 27.5 Mev.
0.39 Mev peak is due to Zr^{88}.
(b) 22.3 hours after bombardment at 57 Mev.
Prominent 0.241 Mev peak is due to Zr^{86}.

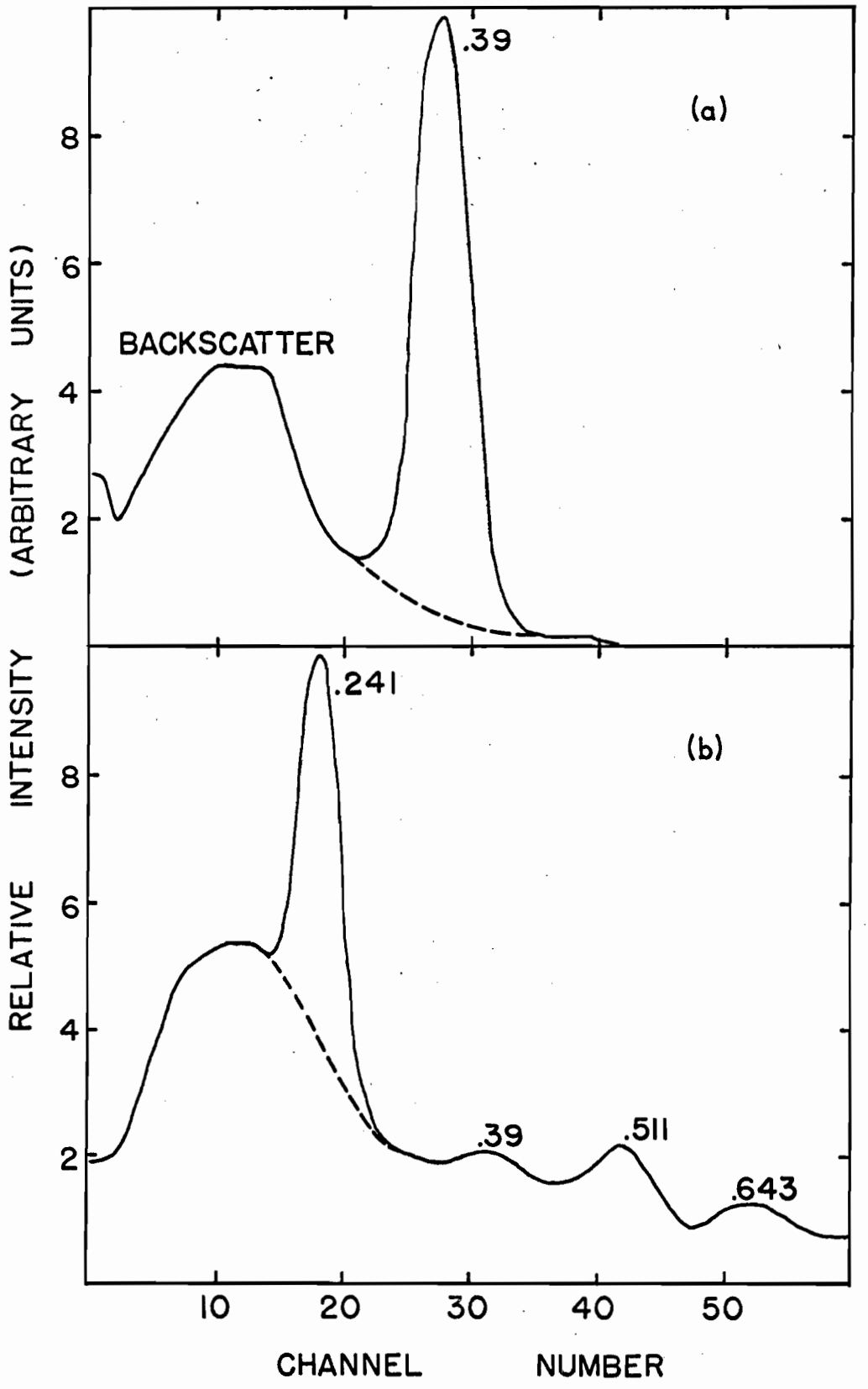
.39
(a)
BACKSCATTER
8
6
4
2
(ARBITRARY UNITS)
.241
(b)
8
6
4
2
RELATIVE INTENSITY
.39
.511
.643
10
20
30
40
50
CHANNEL NUMBER

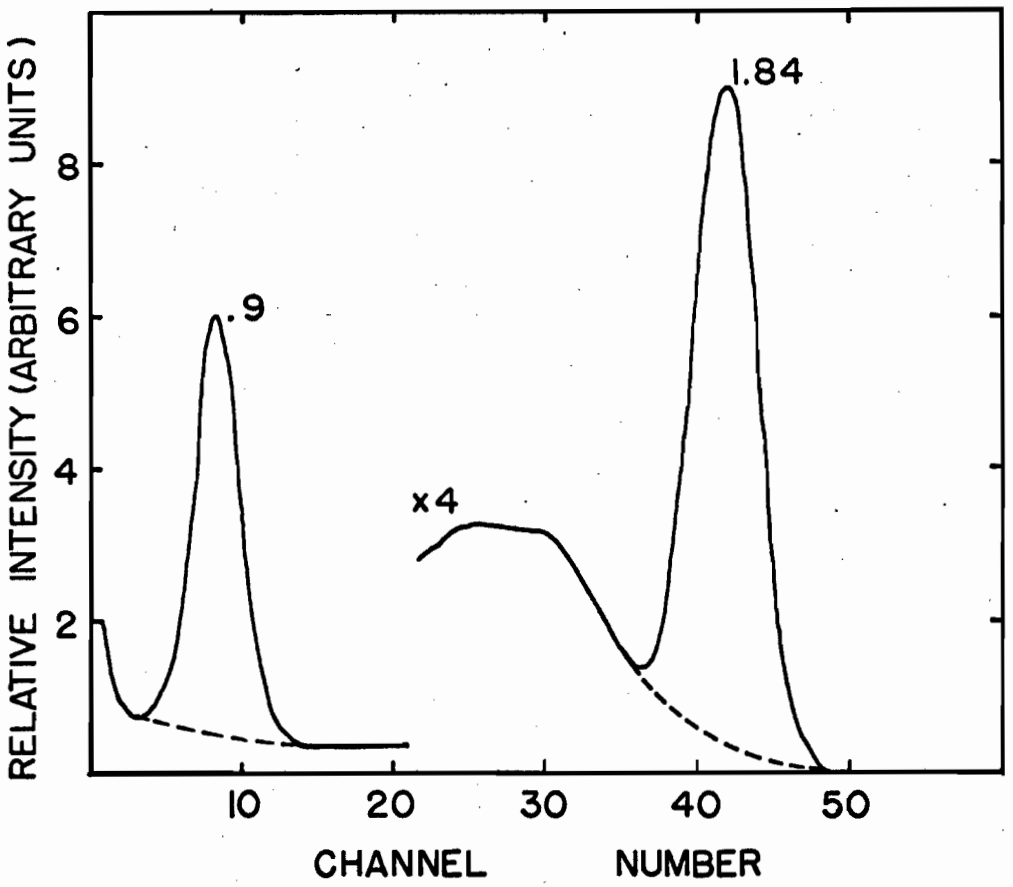

FIG. 5. Typical gamma-ray spectrum of yttrium sample, taken 74 days after bombardment at 30.5 Mev. Dotted lines indicate the estimated background. 0.9 Mev and 1.84 gamma rays are due to 105 day-Y^{88}.

FIG. 6. Typical gamma-ray spectra of yttrium samples, taken after milking experiments. Dotted lines indicate the estimated background.

(a) 37.25 hours after bombardment at 42 Mev. 0.381 Mev peak belongs to Y^{87m} and 0.48 Mev peak belongs to Y^{87g}.

(b) 2 hours after bombardment at 66 Mev. 0.208 Mev peak belongs to Y^{86m}.

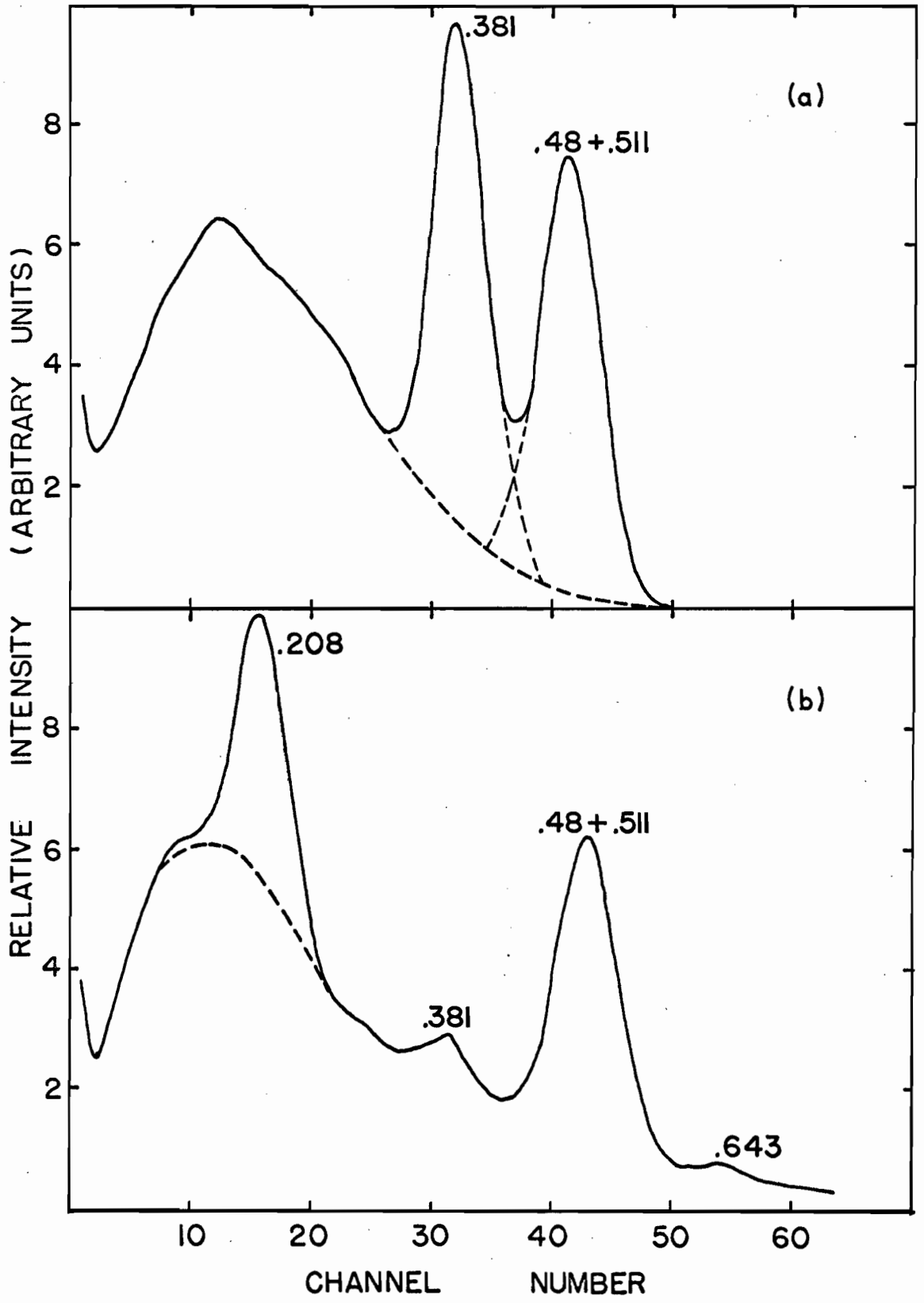
.381
(a)
.48+.511
8
6
4
2
(ARBITRARY UNITS)
.208
(b)
.48+.511
.381
.643
RELATIVE INTENSITY
10
20
30
40
50
60
CHANNEL NUMBER

D_o, making use of the following relation

$$D_o = N_o \times \frac{1 + \alpha_T}{B.R.} \qquad \ldots\ldots (II\text{-}2)$$

where α_T = internal conversion coefficient,

B.R. = branching ratio.

The internal conversion coefficients and branching ratios were taken from Nuclear Data Sheets (59) and more recent reports.

The integral counting rates of zirconium nuclides, as measured by the coincidence technique, were analysed by a graphical method. Yttrium data were resolved into components using the CLSQ Decay Curve Analysis Program* (60). Counting rates at the end of bombardment or separation, as given by the computer or graphical analyses, were converted to disintegration rates by applying the corrections for chemical yields, branching ratios, dilution factors and efficiency of the coincidence counter.

Corrections were applied, whenever needed, for the growth of a daughter from the parent during bombardment and separation time using the well known decay equations. In a case where the decay chain was of the type A ---> B ---> C, the complexity of the decay equations for the corrections of the disintegration rate of C led us to write and use a computer program (IBM-7040 at McGill Computing Centre). The equations are given in detail in the Appendix.

---

* I am indebted to Dr. N.T. Porile for kindly carrying out the computing with an IBM-7094 computer at Brookhaven National Laboratory.

II-7. Calculation of Cross-section

Once the disintegration rate of a particular nuclide at the end of bombardment was known, the formation cross-section of that nuclide could be calculated according to the following expression:

$$D_A^o = In_T \sigma_A (1 - e^{-\lambda_A t}) \qquad \ldots\ldots (II-3)$$

where D_A^o = disintegration rate of nuclide A at the end of bombardment,

σ_A = formation cross-section of the nuclide A,

I = proton intensity as the number of protons per second,

n_T = number of target nuclei per cm^2,

λ_A = decay constant of the nuclide A in sec^{-1},

t = period of bombardment in seconds.

As it was very difficult to determine the exact value of proton flux I, the proton beam was monitored by $Cu^{63}(p,n)Zn^{63}$ and $Cu^{65}(p,pn)Cu^{64}$ reactions whose formation cross-sections were well known. If the monitor is bombarded under similar conditions as the target itself, then the following relation holds good for the monitor too.

$$D_M^o = I\, n_M \sigma_M (1 - e^{-\lambda_M t}) \qquad \ldots\ldots (II-4)$$

where the subscript M refers to the monitor.

Now dividing Eqn. II-4 by Eqn. II-3 and rearranging, one gets

$$\sigma_A = \sigma_M \times \frac{n_M}{n_T} \times \frac{D_A^o}{D_M^o} \times \frac{(1 - e^{-\lambda_M t})}{(1 - e^{-\lambda_A t})} \qquad \ldots\ldots (II\text{-}5)$$

From a knowledge of the weight of the target or the monitor, the number of atoms can be calculated as

$$n = \frac{W}{A.W.} \times 6.02 \times 10^{23}$$

where W is the weight taken and A.W. the atomic weight of the target or the monitor.

Yttrium is monoisotopic, whereas copper has two stable isotopes, Cu^{63} (69.09%) and Cu^{65} (31.91%). Depending on the particular monitor reaction followed, this natural abundance enters into the above expression of 'n'. Taking all these considerations into account, the expression II-5 can finally be written as

$$\sigma_A = \sigma_M \times \frac{N.A_M}{N.A_T} \times \frac{A.W_T}{A.W_M} \times \frac{W_M}{W_T} \times \frac{D_A^o}{D_M^o} \times \frac{(1 - e^{-\lambda_M t})}{(1 - e^{-\lambda_A t})}$$

$\ldots\ldots (II\text{-}6)$

where N.A. represents the natural abundance, and T and M refer to the target and the monitor respectively. Eqn. II-6 was used to calculate the formation cross-section of a particular nuclide A.

II-8. Monitor Cross-sections

The $Cu^{63}(p,n)Zn^{63}$ reaction cross-sections were used for monitoring the proton beam at bombarding energies up to 15 Mev. The values of Ghoshal (3) were chosen and are given in Table I.

At bombarding energies from 18 Mev to 85 Mev the cross-sections

TABLE I

Monitor cross-sections from Mehgir (61) and Ghoshal (3) used in this calculation

Energy (Mev)	Zn^{63}-cross-section (3) (mb)	Cu^{64}-cross-section (61) (mb)
5	43	-
8.5	359	-
12	513	-
15	470	-
18.5		124
21.5		340
24.8		486
27		476
27.5		456
30.5		378
33.5		328
36.8		290
40		264
42		252
45		235
48		220
54		198
57		188
60		180
66		167
72		156
78		148
85		140

for the $Cu^{65}(p,pn)Cu^{64}$ reaction were used for monitoring. In the present calculation Mehgir's values (61) were used and are listed in Table I.

II-9. Errors

Errors involved in the determination of a reaction cross-section are of two kinds: systematic errors and random errors. Systematic errors are associated with branching ratios, internal conversion coefficients, half-lives reported in the literature and also the efficiencies of the counter. A large error due to uncertainty in the monitor cross-sections is reflected on our cross-section values. However, as the magnitudes of these errors except for that of the detection efficiencies are not definitely known, they are not quoted here. An error of $\pm$ 5% was quoted for the detection efficiencies (56).

Random errors include those associated with the determinations of disintegration rates, chemical yields, weights of the target and the monitor, and dilution factors. An estimation of each of these errors is given below.

The main source of error lies in the determination of the photopeak area. This error was estimated to be $\pm$ 6-18% depending on the complexity of the photopeaks.

An error of $\pm$ 5% was estimated for the decay curve analysis.

The chemical yields were determined in duplicate and sometimes in triplicate. They agreed within $\pm$ 3-5%.

The error associated with pipetting and diluting was assessed to be $\pm$ 1%.

The uncertainty in weighing the target materials on a micro-

balance did not exceed ± 1%.

In cases where the disintegration rates were determined by coincidence technique, the error was less. An error of ± 3-12% was assigned to the coincidence counting rates depending on whether they were determined by the graphical or computer analysis.

The total error was calculated by taking the square root of the sum of squares of individual errors cited above considering both the nuclide under study and the monitor. The value varied from ± 11% to ± 22% for various nuclides. The actual scatter of the experimental points is in most cases less than this estimate of error.

Since in a decay chain A ---> B ---> C ---> the disintegration rates of A and B affect that of C considerably, a large error of ± 25% was assumed for the formation cross-sections of B and C.

The spread in the bombarding energy was assumed to be ± 2 Mev, as reported by the Foster Radiation Laboratory Group of McGill University. This spread of energy would lead to an additional error at those energies where the excitation function for the monitor reaction has different slopes from that of the reaction under investigation. It is believed that this error overshadows any error due to the uncertainty in the beam energy.

An error of ± 9-28% was estimated for different isomer ratios.

The uncertainty in the bombarding energy is shown by the horizontal bar and that in the cross-section by the vertical bar at the points on the experimental excitation functions.

III. RESULTS

The counting procedures used for different nuclides of interest as well as the pertinent decay data are summarized in Table II. Described below are the details regarding the results of different reaction products.

III-1. (p,xn) Reactions

78.6 hr.-Zr^{89g}:- The formation cross-section of this product, formed by $Y^{89}(p,n)Zr^{89}$, was measured by detecting the 0.511 Mev annihilation radiation and the 0.908 Mev gamma ray. At energies higher than 12 Mev, the 0.908 Mev gamma ray could not be followed because Zr^{88} was formed and decayed to Y^{88} which contributed to the 0.908 Mev photo-peak. Therefore, at energies above this limit only the 0.511 Mev annihilation radiation was followed by the coincidence technique. A positron branching of 22% (62) (63) was used.

It should be mentioned that Zr^{89m}($t_{1/2}$ = 4.2 min.) could not be followed because of its very short half-life. Therefore, the total yields of the (p,n) reaction were obtained; these are tabulated in Table III. Also it is worth mentioning that about 7% of Zr^{89m} bypasses the isomeric transition and decays directly to the different levels of Y^{89}. Consequently our measured cross-sections are somewhat too low. The excitation function for the (p,n) reaction is shown in Fig. 9.

85 day-Zr^{88}:- The product of (p,2n) reaction, Zr^{88}, was measured by detecting the 0.39 Mev gamma ray with the pulse height analyser. Counting was started about 45 days after irradiation to avoid interference from shorter-lived activities.

TABLE II

Pertinent data and detection methods of the radioactive nuclides studied

Nuclide	Reaction	Half-life	Radiation followed	Branch Abundance	Detection Technique
Zr^{89}	(p,n)	78.6 h	β^+ .908 Mev	22% 100%	CC* PHA*
Zr^{88}	(p,2n)	85 d	.39 Mev	100%	PHA
Zr^{87}	(p,3n)	100 m	β^+	83%	CC
Zr^{86}	(p,4n)	17 h	.241 Mev	100%	PHA
Y^{88}	(p,pn)	105 d	.90 Mev 1.84 Mev	94% 100%	PHA
Y^{87m}	(p,p2n)	13.2 h	.381 Mev	100%	PHA
Y^{87g}	(p,p2n)	80 h	.48 Mev	97.7%	PHA
Y^{86m}	(p,p3n)	48.5 m	.208 Mev	100%	PHA
Y^{86g}	(p,p3n)	14.7 h	β^+	30%	CC
Y^{85m}	(p,p4n)	2.68 h	β^+	55%	CC
Y^{85g}	(p,p4n)	5 h	β^+	70%	CC
Y^{84}	(p,p5n)	40 m	β^+	86.5%	CC
Cu^{64}	(p,pn)	12.7 h	β^+	19%	CC PHA
Zn^{63}	(p,n)	38.3 m	β^+	93%	CC PHA

* PHA - 100 channel pulse height analyser

CC - 0.511 Mev gamma-0.511 Mev gamma coincidence counter.

A branching ratio of 100% and a value of 0.024 (64) for the total internal conversion coefficient of the 0.39 Mev gamma ray were used in the calculation. The results are tabulated in Table III and the excitation function is shown in Fig. 10.

100 min.-Zr^{87}:- Zr^{87}, produced by the (p,3n) reaction, was detected by 0.511 Mev gamma-0.511 Mev gamma coincidence measurements at all bombarding energies. At energies above 45 Mev, Zr^{86} which decayed to the 14.7 hr.-Y^{86g} was formed. The latter had a β^+ branching of 30% and so might interfere with the determination of the counting rate of Zr^{87}. It was, however, found from a simple theoretical calculation considering the worst possible factors that the contribution from the Y^{86g} positrons was negligible even after 4 hours. Under these circumstances, Zr^{87} was counted for an initial period of 2 hours and the decay curve was drawn through the initial points to give the activity at the end of bombardment.

A new gamma ray of energy 1.23 Mev decaying with a half-life of 100 minutes was observed. This is in agreement with a report in reference (65). The ratio of counting rates of positrons and the 1.23 Mev gamma ray was found to be about 20. So it could be assumed that 4-5% of Zr^{87} fed a level at 1.23 Mev above either Y^{87g} ground state or Y^{87m} metastable state. Nevertheless, in the absence of detailed knowledge of this decay behaviour a positron branch of 83%(59) was used in the calculation. The cross-sections are tabulated in Table III and also shown in Fig. 11.

17 hr.-Zr^{86}:- Zr^{86} resulting from the (p,4n) reaction decays by 100% electron capture, feeding a level of 0.241 Mev above the Y^{86g} ground state (66). This nuclide was measured by following the 0.241 Mev

gamma ray. The 0.241 Mev photopeak appeared on top of the back-scattered peak of all high energy gamma rays, especially the prominent 0.511 Mev annihilation photopeak of Zr^{87}. This gamma ray was, therefore, followed after the complete decay of Zr^{87}($t_{1/2}$ = 100 min.). As the remaining high energy gamma rays had comparable or longer half-lives, the back-scattered peak did not fluctuate too much throughout the period of measurement and a consistent background subtraction could be made.

Lacking knowledge of the conversion coefficient*, we assumed the photon abundance to be 100 per cent. The cross-sections are listed in Table III and the excitation function is presented in Fig. 12.

---

* A recent paper on the decay of Zr^{86} reported by Y. Awaya and Y. Tendow (J. Phys. Soc. (Japan) 19, 606 (1964)) came to our attention almost towards the end of this work. They reported a gamma ray of 0.247 Mev, among others, with a relative intensity of 100 and a conversion coefficient of 0.014 ± 0.015. This level was assigned a spin and parity of (1+). This gamma ray corresponds to the 0.241 Mev gamma ray that we followed. Though there will be a difference of 1 or 2% between the detection efficiencies of the 0.247 Mev and 0.241 gamma rays, we did not change our calculation.

III-2. (p,pxn) Reactions

105 day-Y^{88}:- This nuclide, formed by the (p,pn) reaction, was measured by following two characteristic gamma rays of 0.90 Mev and 1.84 Mev. Coincidence losses that might result from the summation of these gamma rays in cascade were reduced by counting the sources at low geometry. Branching ratios of 94% for the 0.90 Mev gamma ray and 100% for the 1.84 Mev gamma ray (67) were used for the calculation. Cross-sections were calculated using a mean value of these two disintegration rates which did not differ from each other by more than 3-5%. The cross-sections are presented in Table IV and the excitation function is shown in Fig. 14.

13.2 hr.-Y^{87m} + 80 hr.-Y^{87g}:- Both these isomers were formed through the (p,p2n) reaction and by the decay of their precursor, Zr^{87}, as well.

Y^{87m} decays by an isomeric transition of 0.381 Mev to the ground state. Yamazaki et al (68) suggested a positron branching of 5% going to the level of Sr^{87m}. But it was a mere suggestion rather than confirmed evidence, and hence a 100% isomeric transition was assumed. Since the 0.381 Mev gamma photopeak was obscured by the 0.388 Mev gamma ray of Sr^{87m} ($t_{1/2}$ = 2.8 hr.), grown through the chain Y^{87m} ---> Y^{87g} ---> Sr^{87m} ---> , yttrium was quickly separated from strontium by a milking experiment and Y^{87m} was counted immediately. About 10 mg of Sr carrier was added to the main yttrium solution. $Y(OH)_3$ was precipitated with conc. NH_4OH. The precipitate was centrifuged and decanted. Yttrium hydroxide was washed once with distilled water and dissolved in a few drops of conc. HCl and finally diluted to about 15-20 ml. An appropriate aliquot was taken and the

TABLE III

Experimental cross-sections for (p,xn) reactions

Bombarding Energy (Mev)	σ(p,n) (mb) ± 11% error	σ(p,2n) (mb) ± 13% error	σ(p,3n) (mb) ± 12% error	σ(p,4n) (mb) ± 16% error
5	50 ± 5.5			
8.5	352 ± 39			
12	720 ± 79			
15	712 ± 78	68 ± 8.8		
18.5	552 ± 61	352 ± 46		
21.5	395 ± 43	495 ± 64		
24.8	194 ± 21	1252 ± 163		
27	-	1248 ± 162		
27.5	103 ± 11	1318 ± 171		
30.5	61.4 ± 6.8	828 ± 108 896 ± 116	55 ± 6.6	
33.5	43 ± 4.7	506 ± 66	118 ± 14	
36.8	45 ± 5	329 ± 43	313 ± 38	
40	-	-	385 ± 46	
42	37 ± 4.1	172 ± 22	333 ± 40 349 ± 42	
45	-	-	299 ± 36	26.6 ± 4.3
48	29.4 ± 3.2	112 ± 15	168 ± 20	57 ± 9.1
54	29.7 ± 3.3	82.5 ± 11	91 ± 11	78 ± 12.5
57	-	-	-	81.5 ± 13
60	23.3 ± 2.6	73.4 ± 9.5	55.4 ± 6.6	63 ± 10
66	19.7 ± 2.2	60 ± 7.8	54 ± 6.5	42 ± 6.7
72	17 ± 1.9	54 ± 7	47.5 ± 5.7	32 ± 5.1
78	14.4 ± 1.6	46 ± 6	36.5 ± 4.4	27.7 ± 4.4
85	12 ± 1.3	41 ± 5.3	31.5 ± 3.8	22 ± 3.5

TABLE IV. Experimental cross-sections for (p,pxn) reactions

Bombarding energy (Mev)	σ(p,pn) (mb) ± 13%	σ(p,p2n)* (mb)	σ(p,p3n)* (mb)	σ(p,p4n)* (mb)	σ(p,p5n) (mb) ± 20%
15	3.6 ± .5				
18.5	38 ± 5				
21.5	141 ± 18				
24.8	257 ± 33	1.4			
27	-	3.5			
27.5	304 ± 40	-			
30.5	365 ± 47	95.7			
33.5	310 ± 40	229			
36.8	283 ± 37	284	10.7		
40	-	320	-		
42	231 ± 30	370 352	19.5		
45	-	395	61.5		
48	228 ± 30	340	126.5		
54	186 ± 24	263	208		
57	-	-	209		
60	199 ± 26	218	237	57.6	
66	177 ± 23	164	161	134.5 155	.37 ± .074
72	175 ± 23	158.6	121	163 141.4	-
78	162 ± 21	155.6	117.5	136.5 133	11 ± 2.2
85	144 ± 19	128.5	105.6	109 127	24 ± 4.8

* Errors have not been quoted for the total cross-sections given here for these reactions. Errors for the cross-sections of individual isomers are given in Tables V, VI, VII.

TABLE V

Experimental cross-sections and isomeric ratios of Y^{87m} and Y^{87g}

Bombarding energy (Mev)	σ_H(mb) ± 20% error	σ_L(mb) ± 20% error	σ_H/σ_L ± 21% error
24.8	.40 ± .08	1.0 ± .2	0.4 ± .08
27	1.8 ± .36	1.7 ± .34	1.06 ± .22
30.5	64 ± 13	31.7 ± 6.3	2.02 ± .42
33.5	159 ± 32	70 ± 14	2.27 ± .48
36.8	201 ± 40	83 ± 17	2.42 ± .51
40	230 ± 46	90 ± 18	2.56 ± .54
42	281 ± 56 251 ± 50	89.2 ± 18 101 ± 20	3.15 ± .66 2.5 ± .53
45	282 ± 56	113 ± 23	2.5 ± .53
48	245 ± 49	95 ± 19	2.6 ± .55
54	180 ± 36	83 ± 17	2.17 ± .46
60	146 ± 29	72 ± 14	2.03 ± .43
66	111 ± 22	53 ± 11	2.09 ± .44
72	111 ± 22	47.6 ± 9.5	2.33 ± .49
78	107 ± 21	48.6 ± 9.7	2.20 ± .46
85	88 ± 18	40.5 ± 8.1	2.17 ± .46

TABLE VI

Experimental cross-sections and isomeric ratios of Y^{86m} and Y^{86g}

Bombarding energy (Mev)	σ_H (mb) ± 25%	σ_L (mb) ± 25%	σ_H/σ_L ± 28%
45	17.5 ± 4.4	44 ± 11	.40 ± .11
48	56.5 ± 14	70 ± 18	.81 ± .23
54	115 ± 29	93 ± 23	1.24 ± .35
57	106 ± 27	103 ± 26	1.03 ± .29
60	135 ± 34	102 ± 26	1.32 ± .37
66	87 ± 22	74 ± 19	1.18 ± .33
72	64 ± 16	57.5 ± 14	1.11 ± .31
78	64.5 ± 16	53 ± 13	1.22 ± .34
85	55.2 ± 14	50.4 ± 13	1.10 ± .31

TABLE VII

Experimental cross-sections and isomeric ratios of $Y^{85m}(1/2-)$ and $Y^{85g}(9/2+)$

Bombarding energy (Mev)	σ_L(mb) ± 12%	σ_H(mb) ± 12%	σ_H/σ_L ± 9%
60	4.6 ± .55	53 ± 6.4	11.50 ± 1.03
66	32.5 ± 3.9 57 ± 6.8	102 ± 12 98 ± 12	3.14 ± .28 1.72 ± .15
72	58 ± 7 52.4 ± 6.3	105 ± 12 89 ± 11	1.81 ± .16 1.70 ± .15
78	46.5 ± 5.6 44 ± 5.3	90 ± 11 89 ± 11	1.94 ± .17 2.02 ± .18
85	43 ± 5.2 40 ± 4.8	66 ± 8 87 ± 11	1.53 ± .14 2.18 ± .20

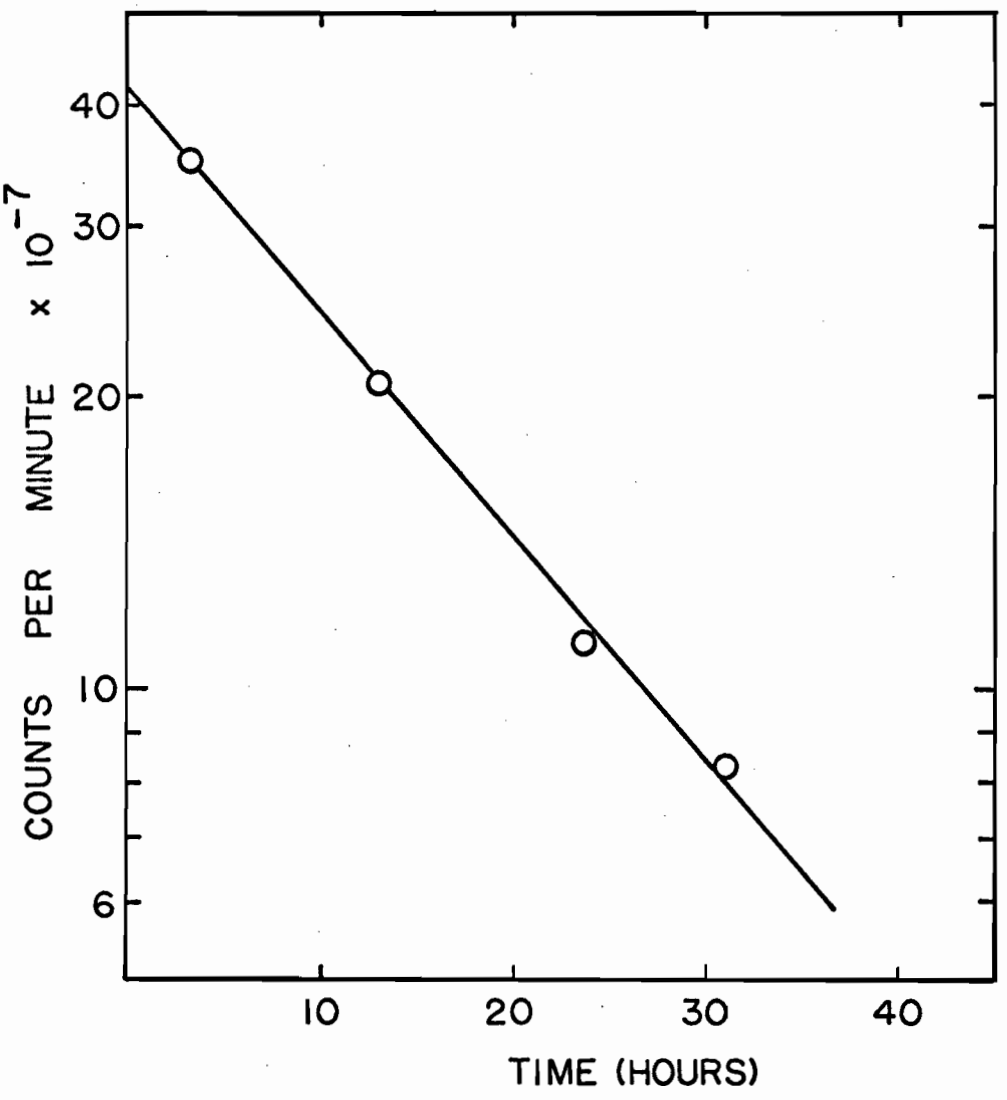

FIG. 7. Decay curve of 0.381 Mev photopeak due to 13.2 hr-Y^{87m}. Zero time is the separation time.

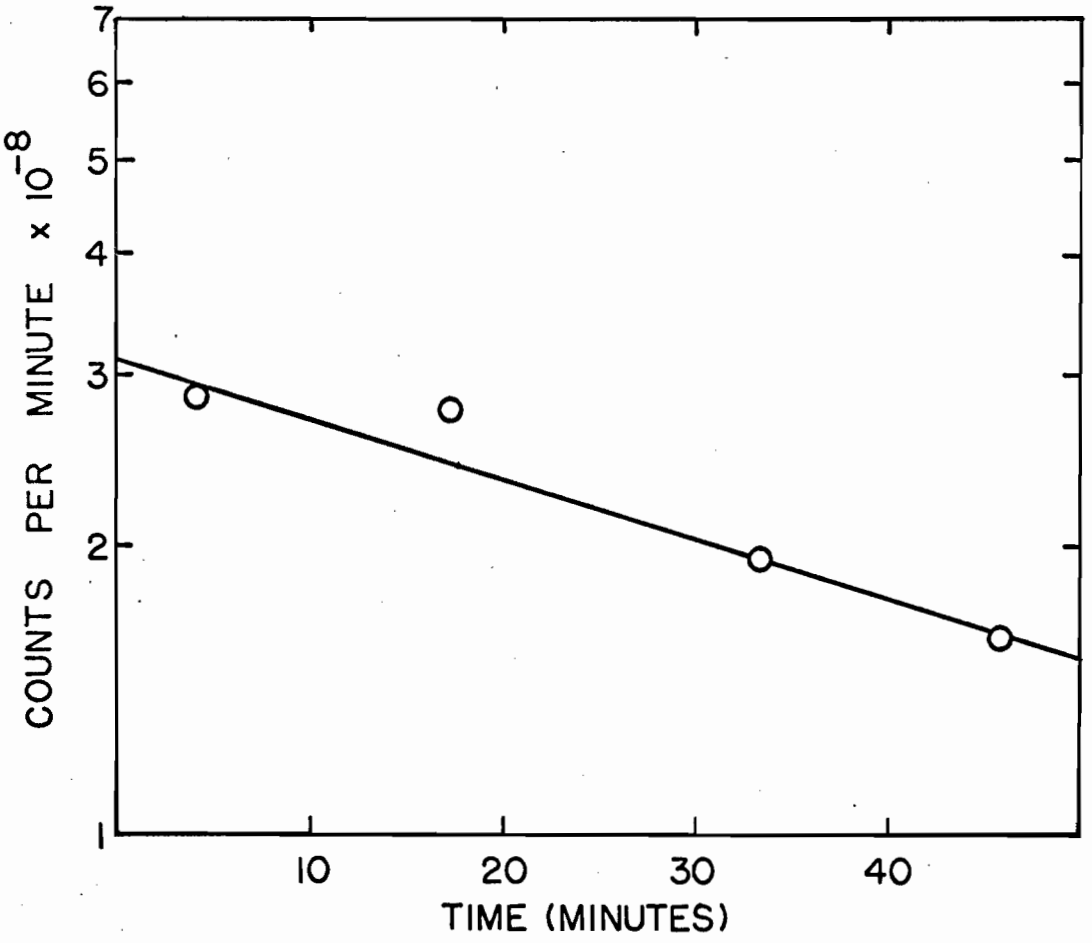

FIG. 8. Decay curve of 0.208 Mev photopeak due to 48.5 min-Y^{86m}. Zero time is the end of separation time.

0.381 Mev gamma ray of Y^{87m} was counted immediately. Four such separations were made for each sample. A typical decay curve is shown in Fig. 7.

Using a value of 0.28 for the internal conversion coefficient (59) of the 0.381 Mev gamma ray, the cross-sections were calculated and are presented in Table V. The excitation function is shown in Fig. 15.

Y^{87g} was measured by following the 0.48 Mev gamma ray after all the interfering nuclides decayed. At higher energies Y^{85m}($t_{1/2}$ = 2.68 hr.) and Y^{85g}($t_{1/2}$ = 5 hr.) were formed and decayed to Sr^{85m}($t_{1/2}$ = 70 min.) and Sr^{85g}($t_{1/2}$ = 65 days). Sr^{85g} decayed by 0.51 Mev gamma transition, which interfered with the 0.48 Mev photopeak of Y^{87g}. For this reason, the purified yttrium solution was set aside for about 10 days to let Y^{85m}, Y^{85g} as well as Y^{86g} decay completely. Yttrium was then removed from strontium by the precipitation of yttrium hydroxide and used for counting. An internal conversion coefficient of 0.0035 and a photon abundance of 98% were used (59). Both Y^{87m} and Y^{87g} disintegration rates were corrected for the growth of Y^{87m} from Zr^{87} and of Y^{87g} from Zr^{87} through Y^{87m} with a computer program.

Table V lists the cross-sections of both isomers and their ratios. Total cross-sections are tabulated in Table IV. The excitation function is presented in Fig. 15. A plot of isomer ratios against bombarding energy is given in Fig. 19.

48.5 min.-Y^{86m} + 14.7 hr.-Y^{86g}:- These two nuclides, formed by the (p,p3n) reaction as well as through the decay of Zr^{86}, presented the most difficult situation in the present study. This was due to the incomplete knowledge of the decay schemes of these nuclides.

Hyde et al (66) reported that Zr^{86} decayed by electron capture to an excited level 0.241 Mev above the Y^{86} ground state. The Y^{86m} isomer

remained undiscovered until 1961 when Haskin and Vandenbosch (69) reported its existence. Kim et al (70) studied this nuclide in more detail and stated that Y^{86m} decayed by a 10.15 Kev transition followed by a 0.208 Mev transition with a half-life of 48 ± 1 min. The 10.15 Kev transition was almost completely converted and the conversion coefficient of the 0.208 Mev gamma ray had a value of 0.04 ± 0.01. In agreement with the report of Kim et al (70) it was found by milking the yttrium daughter from zirconium samples that the isomeric level of Y^{86m} is not populated by the decay of Zr^{86}. With this information, the decay scheme shown in Fig. 13 was assumed for the decays of Zr^{86}, Y^{86m} and Y^{86g}.

$Y^{85m}(t_{1/2}$ = 2.68 hr.) and $Y^{85g}(t_{1/2}$ = 5 hr.), formed at higher energies, decayed to the 0.23 Mev isomeric level of $Sr^{85m}(t_{1/2}$ = 70 min.). The growth of this 0.23 Mev gamma photopeak interfered with the 0.208 Mev photopeak of Y^{86m}. Therefore, a fast separation of yttrium from strontium (milking) was made and Y^{86m} was counted as quickly as possible.

The 0.208 Mev photopeak of Y^{86m} appeared on top of the back-scattered peak arising from all the high energy gamma rays, especially the annihilation radiations due to $Y^{84}(t_{1/2}$ = 40 min.), $Y^{85m}(t_{1/2}$ = 2.68 hr.) and $Y^{85g}(t_{1/2}$ = 5 hr.). Due to short half-lives of these nuclides the back-scattered peak varied from count to count and as a result, consistent background subtraction could be achieved with only limited success. A typical decay curve is shown in Fig. 8.

A value of 0.05 was used for the internal conversion coefficient of the 0.208 Mev transition. The measured cross-sections are tabulated in Table VI, and shown in Fig. 16.

Y^{86g} was measured by detecting the annihilation radiations by coincidence technique. Confusion still exists about the positron branching

of this nuclide. Yamazaki et al (59) reported a positron branching ratio of 33.8%. The same authors (68) suggested later a branching of 28.1% whereas the sum of electron capture and positron branches from the decay scheme given adds to more than 100%. Under these circumstances a positron branching of 30% was arbitrarily assumed. The 1.08 Mev gamma transition could not be followed since within the resolution of the scintillation detector many other photons of similar energies appeared under this photopeak. The coincidence counting data were analysed by CLSQ Decay Curve Analysis Program (60). The corrections for the growth of Y^{86g} from Zr^{86} and Y^{86m} during the bombardment and separation time were applied. The results are shown in Table VI and Fig. 16.

Table IV shows the total cross-sections of Y^{86m} and Y^{86g}. Table VI shows the isomer ratios. Total cross-sections are plotted against the proton energy in Fig. 16. Fig. 20 shows the plot of the isomer ratio versus proton bombarding energy.

2.68 hr.-Y^{85m} + 5 hr.-Y^{85g}:- These nuclides are formed through the (p,p4n) reaction and the decay of Zr^{85}. They were measured by detecting the positron annihilation radiation by the coincidence technique.

The anomalous decay behaviour of Y^{85} was clarified by Horen and Kelley (71) who reported that it has two isomeric states. A thorough study of the decay scheme of Y^{85m} and Y^{85g}, accomplished by Dostrovsky et al (72), indicated that Y^{85m} had a positron branching of 55% with a half-life of 2.68 hr. and that Y^{85g} had a positron branching of 70% following a half-life of 5 hr. No isomeric transition was observed in their study.

The analysis of the result of coincidence measurements by CLSQ Decay Curve Analysis Program (60) gave the desired counting rates of these nuclides at the end of bombardment. Due to the unknown short half-life

of Zr^{85}, the correction for the growth of Y^{85m} and Y^{85g} from the decay of Zr^{85} could not be made. Therefore, the cumulative cross-sections were calculated on the basis of the positron branching ratios given by Dostrovsky et al (72). The results for Y^{85m} and Y^{85g} are listed in Table VII and shown in Fig. 17. The total cross-sections are given in Table IV. The isomer ratios are plotted against the bombarding energy in Fig. 21.

40 min.-Y^{84}:- This nuclide, formed by the (p,p5n) reaction, was measured by coincidence measurements of the positron annihilation radiations. The data were analysed by CLSQ Decay Curve Analysis Program (60). The half-life reported by Maxia et al (73) was 39 $\pm$ 1 min. and that in reference (59) was 43 min. A compromise value of 40 min. was decided on. A positron branching of 86.5% (59) was adopted in the calculation. Because of the short half-life of unknown Zr^{84} nuclide, the correction for the growth of Y^{84} through the decay of Zr^{84} could not be made. Hence the cumulative cross-sections are given in Table IV and the excitation function in Fig. 18.

12.7 hr.-Cu^{64} + 38.3 min.-Zn^{63}:- The annihilation radiations of Cu^{64} and Zn^{63} were measured by both the pulse height analyser as well as the coincidence counter. These two measurements did not differ from each other by more than 6%. An average value of two measurements was used to give the disintegration rates. Branching ratios of 19% (59) for copper and of 93% (74) for Zn^{63} were used.

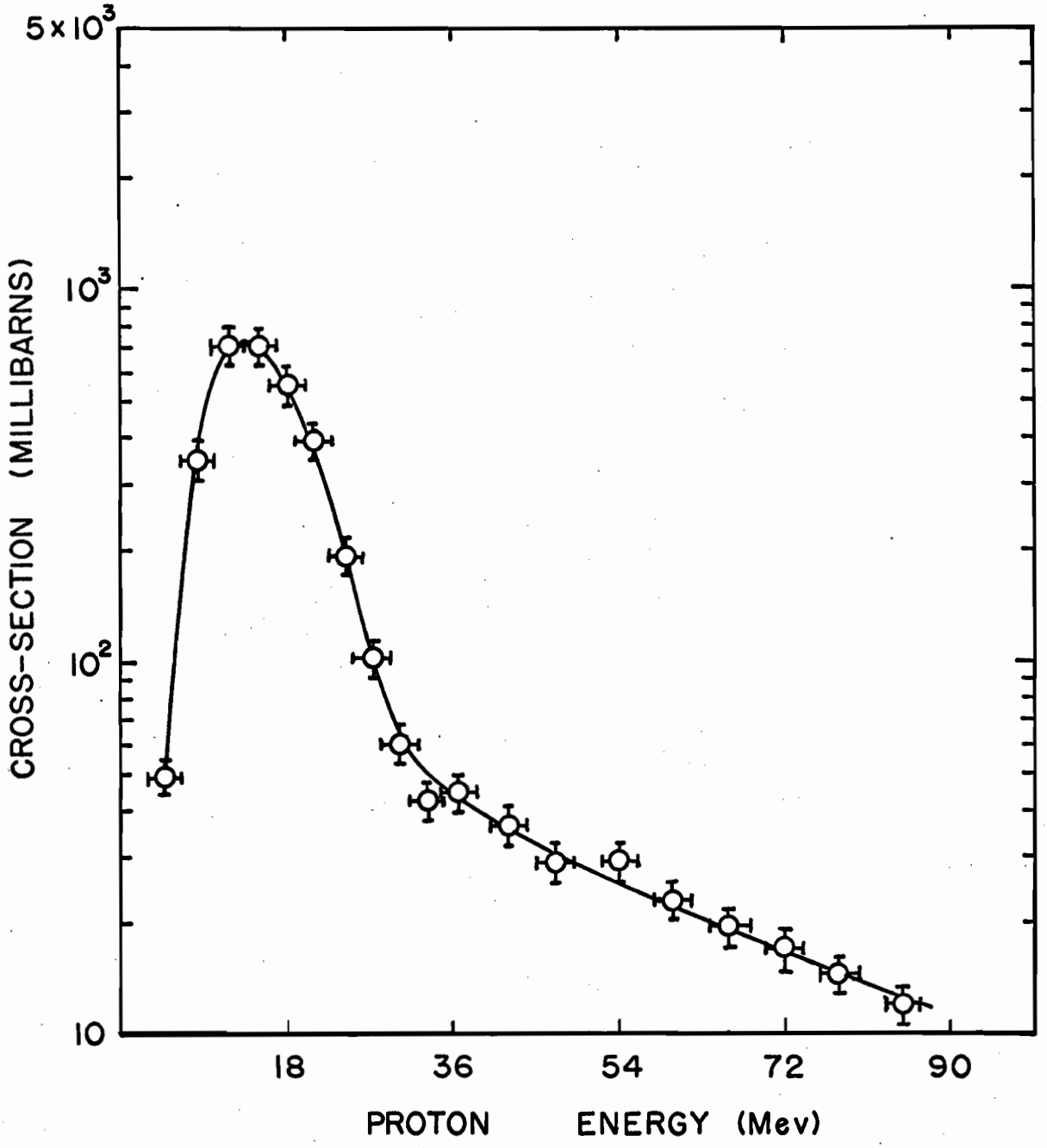

FIG. 9. Experimental Excitation Function of the (p,n) Reaction

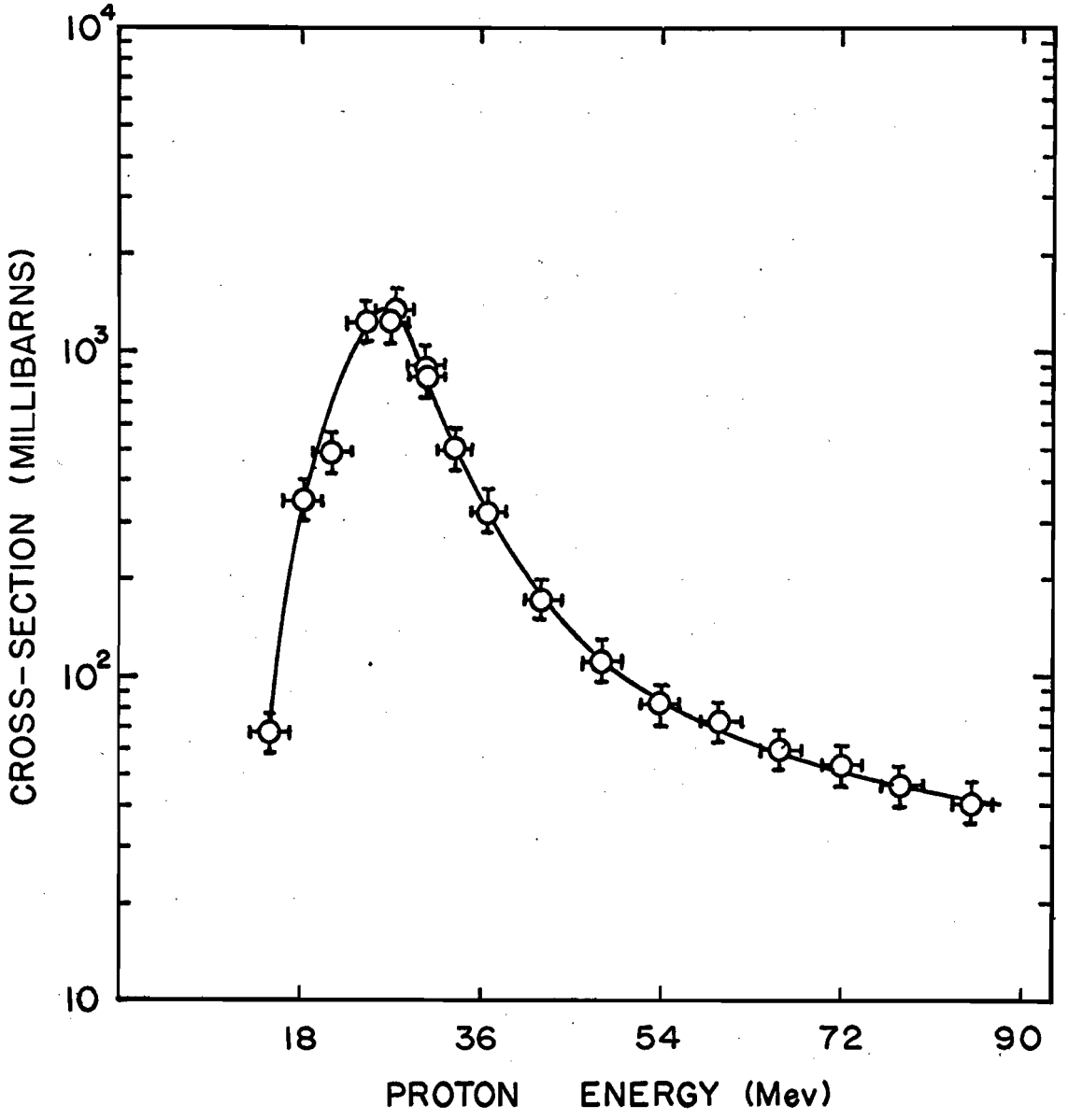

FIG. 10. Experimental Excitation Function of the (p,2n) Reaction.

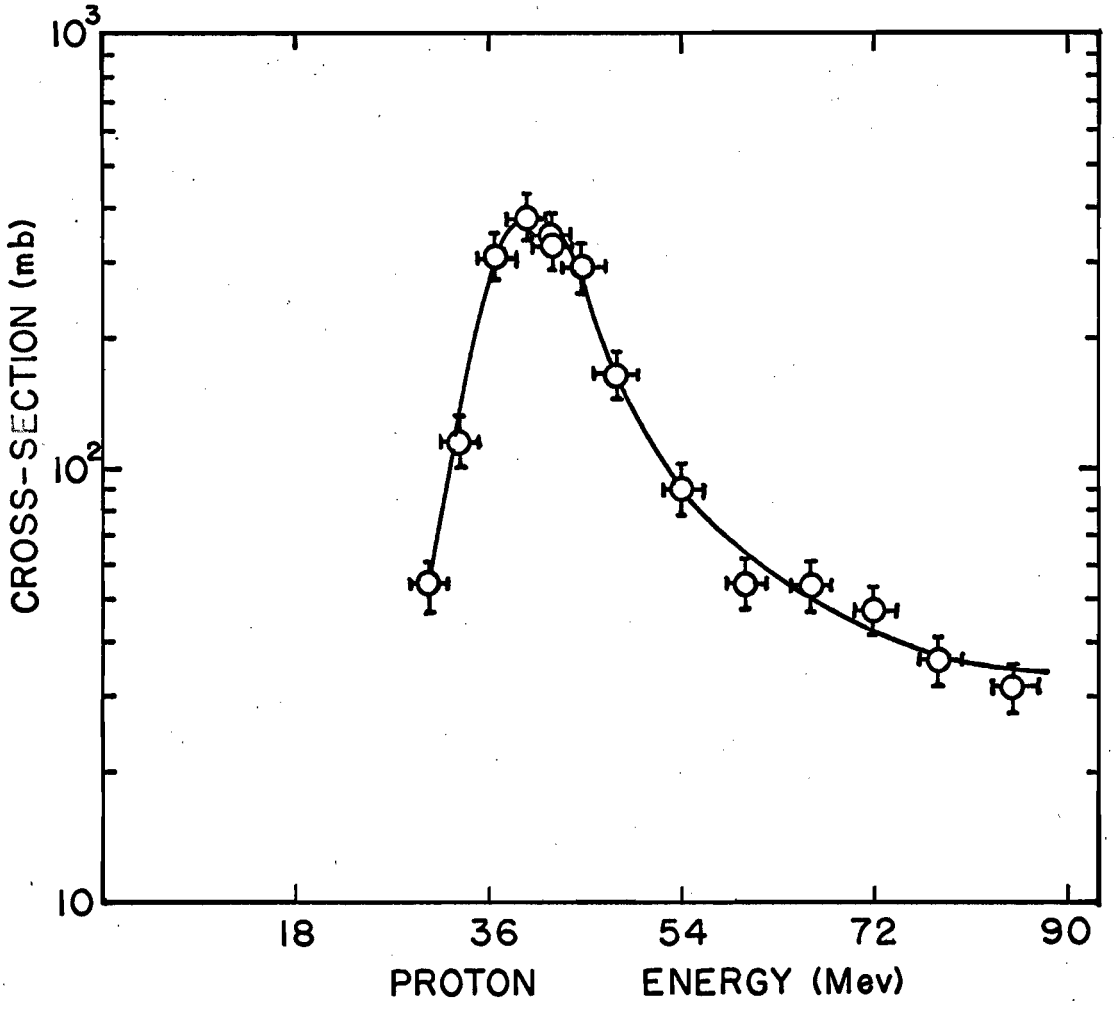

FIG. 11. Experimental Excitation Function of the (p,3n) Reaction.

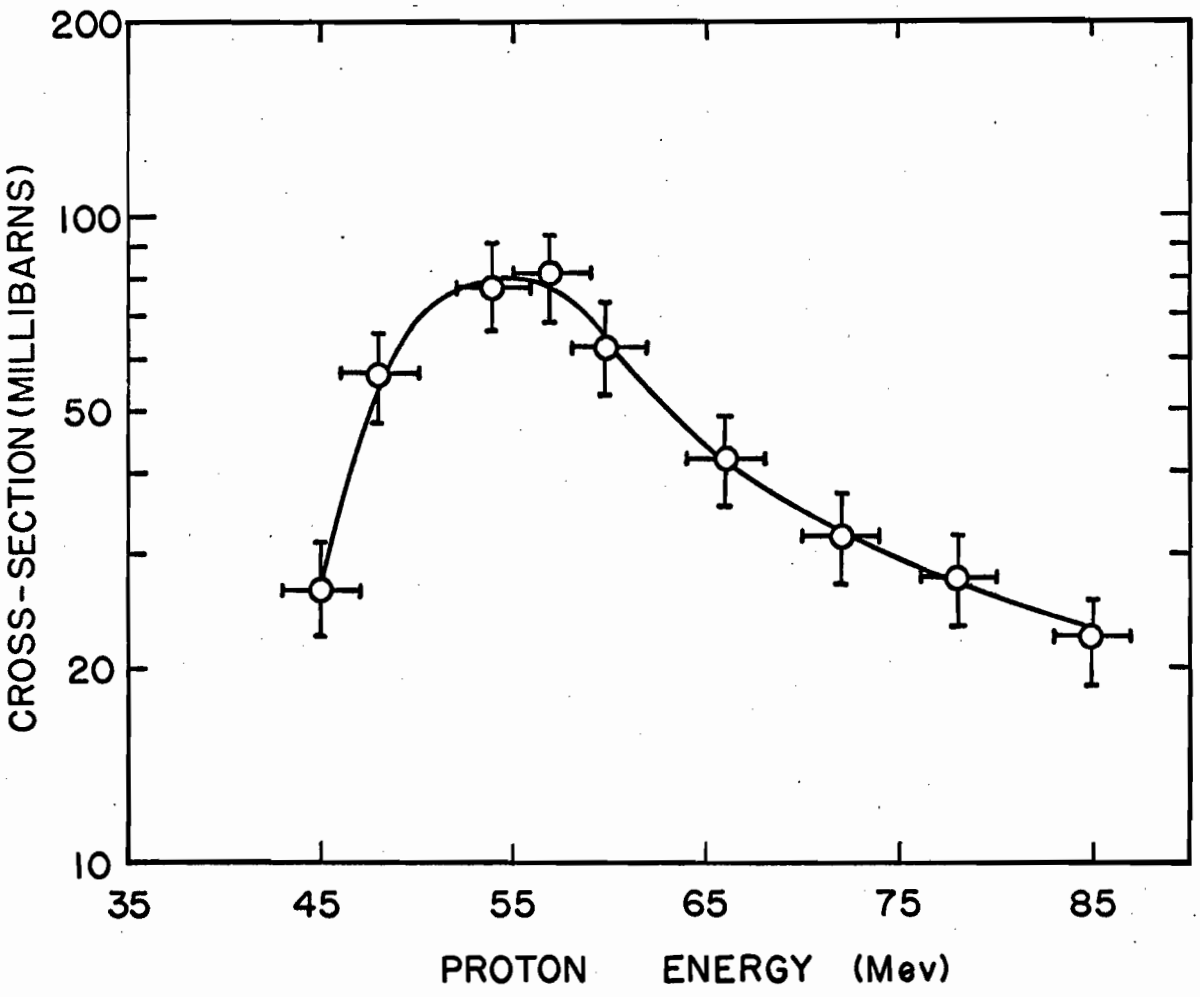

FIG. 12. Experimental Excitation Function of the (p,4n) Reaction.

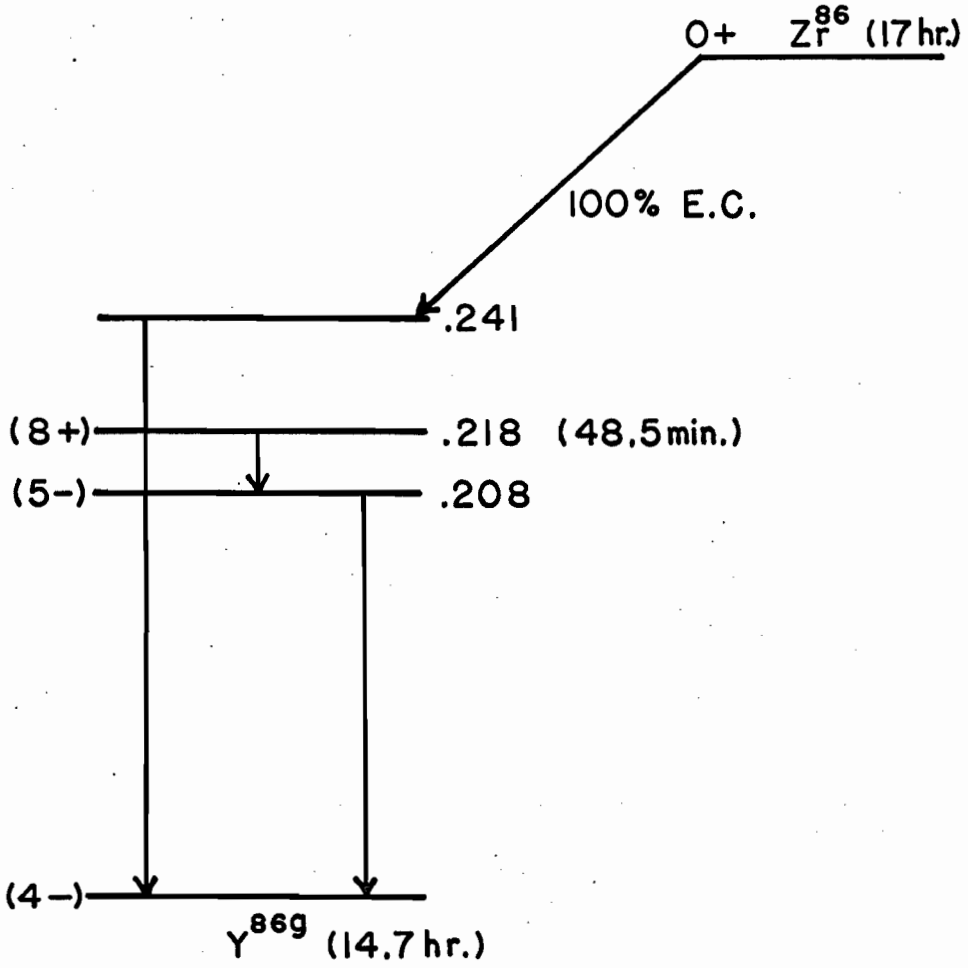

FIG. 13. Assumed Decay Scheme Pertaining to the Decay of Zr^{86}, Y^{86m} and Y^{86g}.

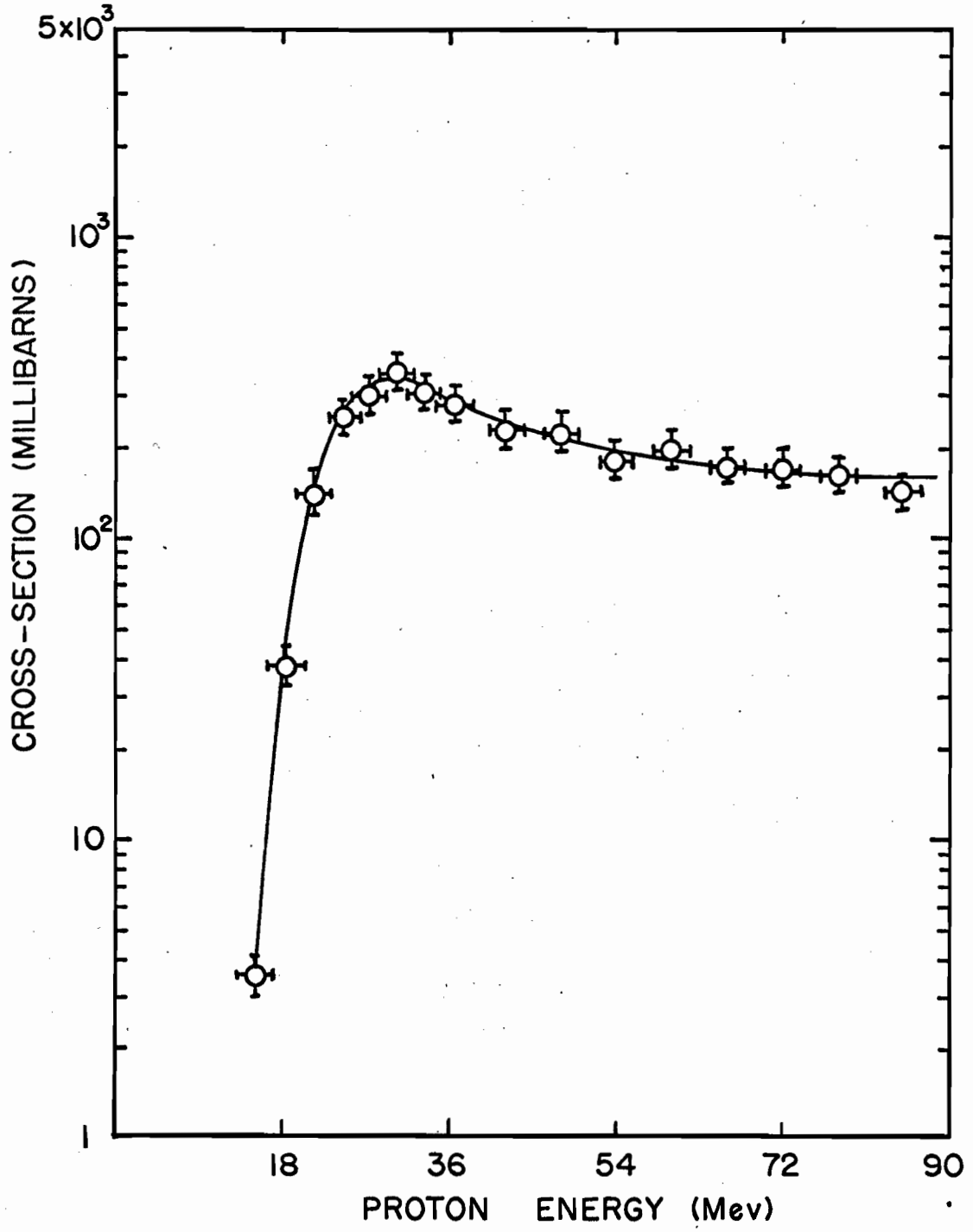

FIG. 14. Experimental Excitation Function of the (p, pn) Reaction.

FIG. 15. Experimental excitation functions of the (p,p2n) reaction.

□ Y^{87g} - cross-section

○ Y^{87m} - cross-section

◒ Total - cross-section

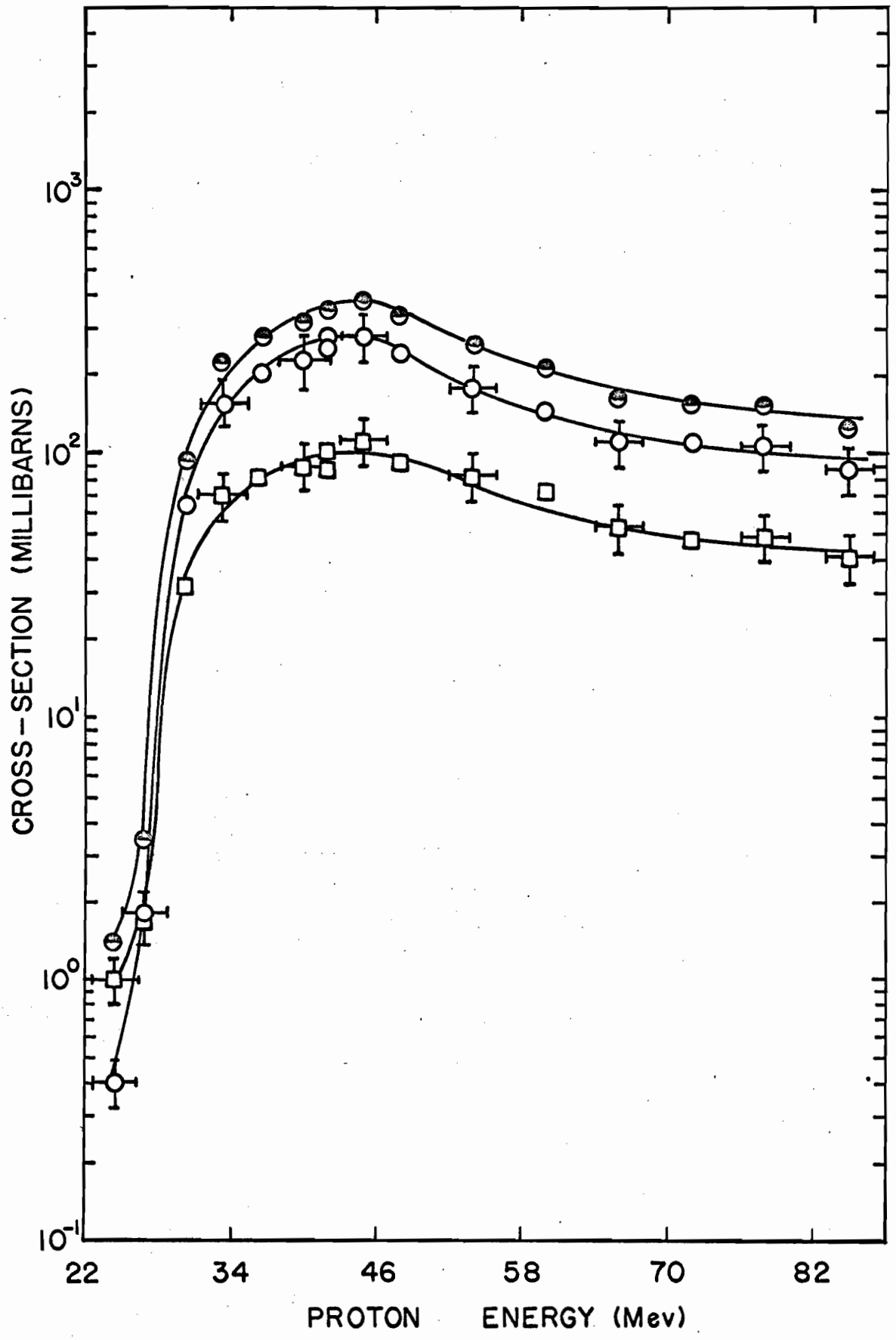
CROSS-SECTION (MILLIBARNS)
10^3
10^2
10^1
10^0
10^{-1}
22
34
46
58
70
82
PROTON ENERGY (Mev)

FIG. 16. Experimental excitation functions of the (p,p3n) reaction.

○ Y^{86g} - cross-section

□ Y^{86m} - cross-section

◒ Total - cross-section

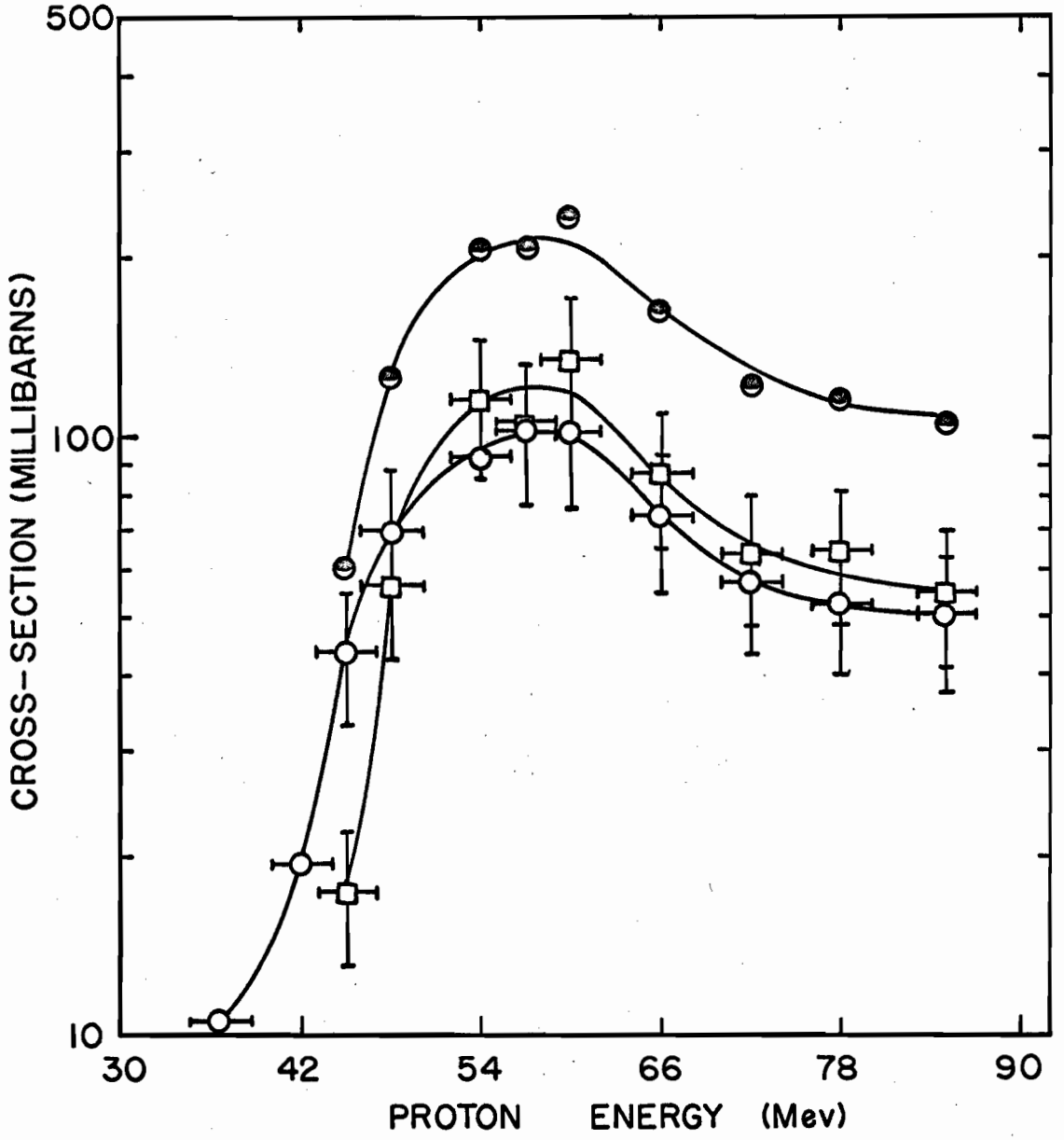
500
100
10
CROSS-SECTION (MILLIBARNS)
30
42
54
66
78
90
PROTON ENERGY (Mev)

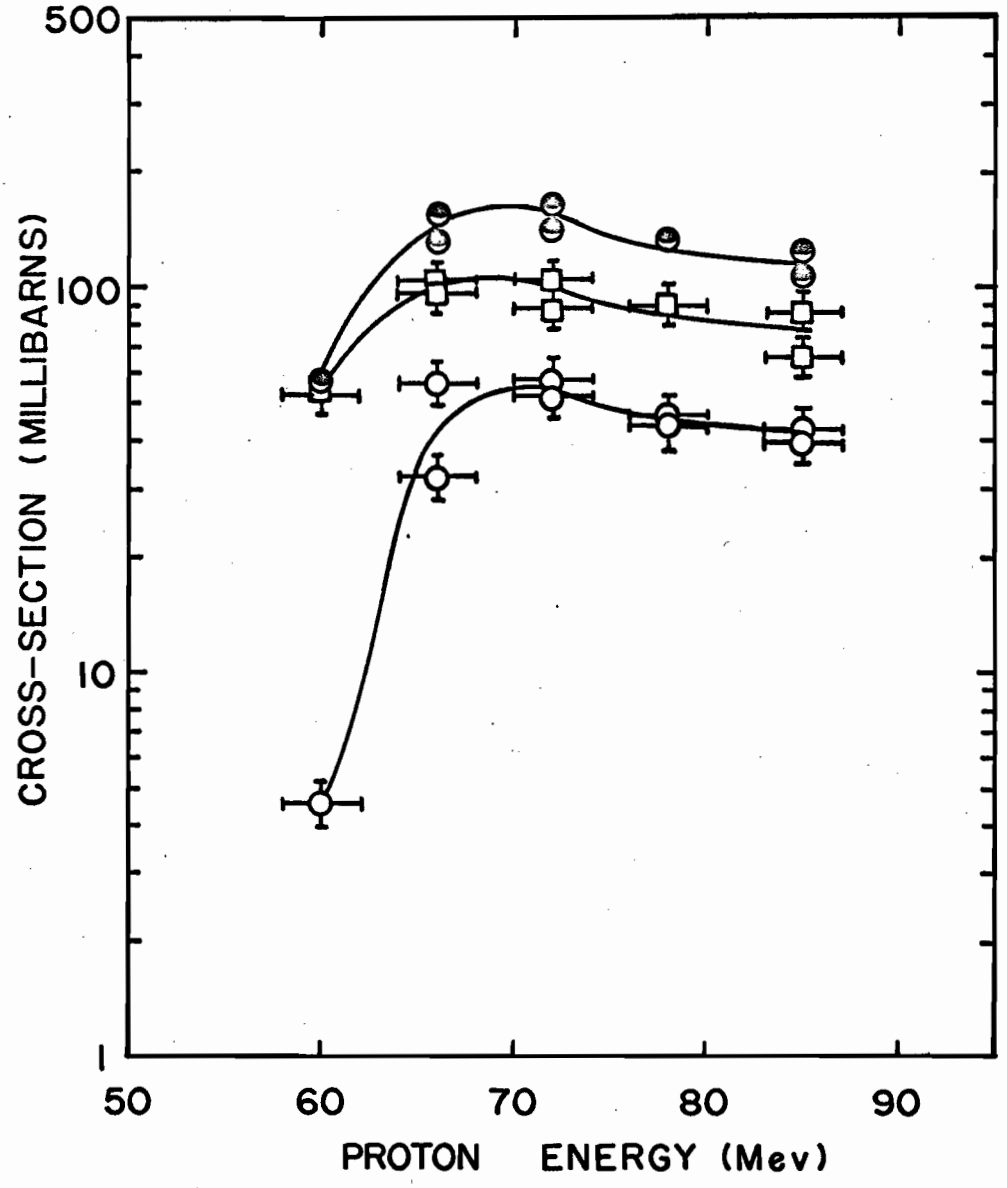

FIG. 17. Experimental Excitation Functions of the (p, p4n) Reaction.

□ Y^{85g} - cross-section

○ Y^{85m} - cross-section

● Total - cross-section

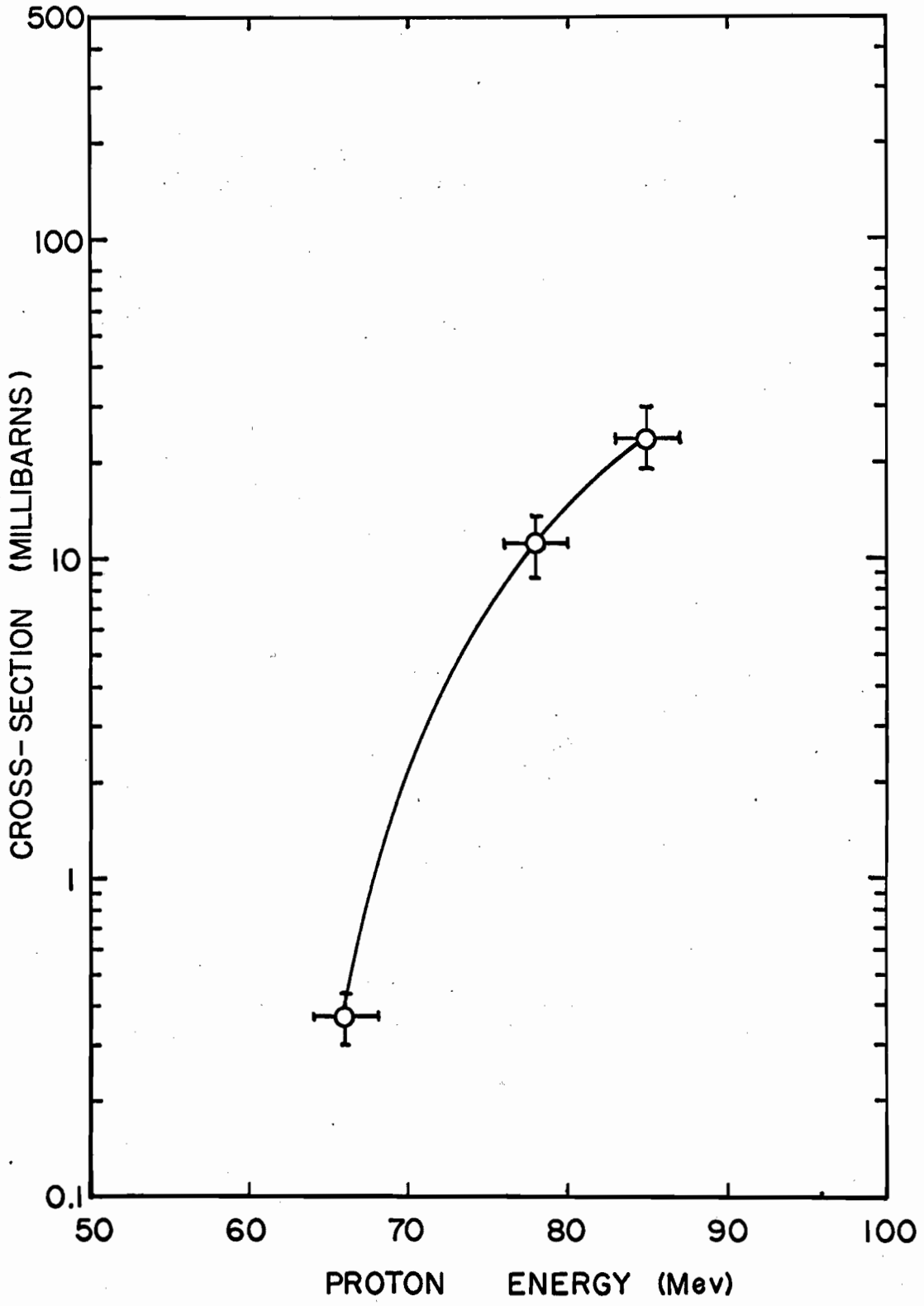

FIG. 18. Experimental Excitation Function of the (p,p5n) Reaction.

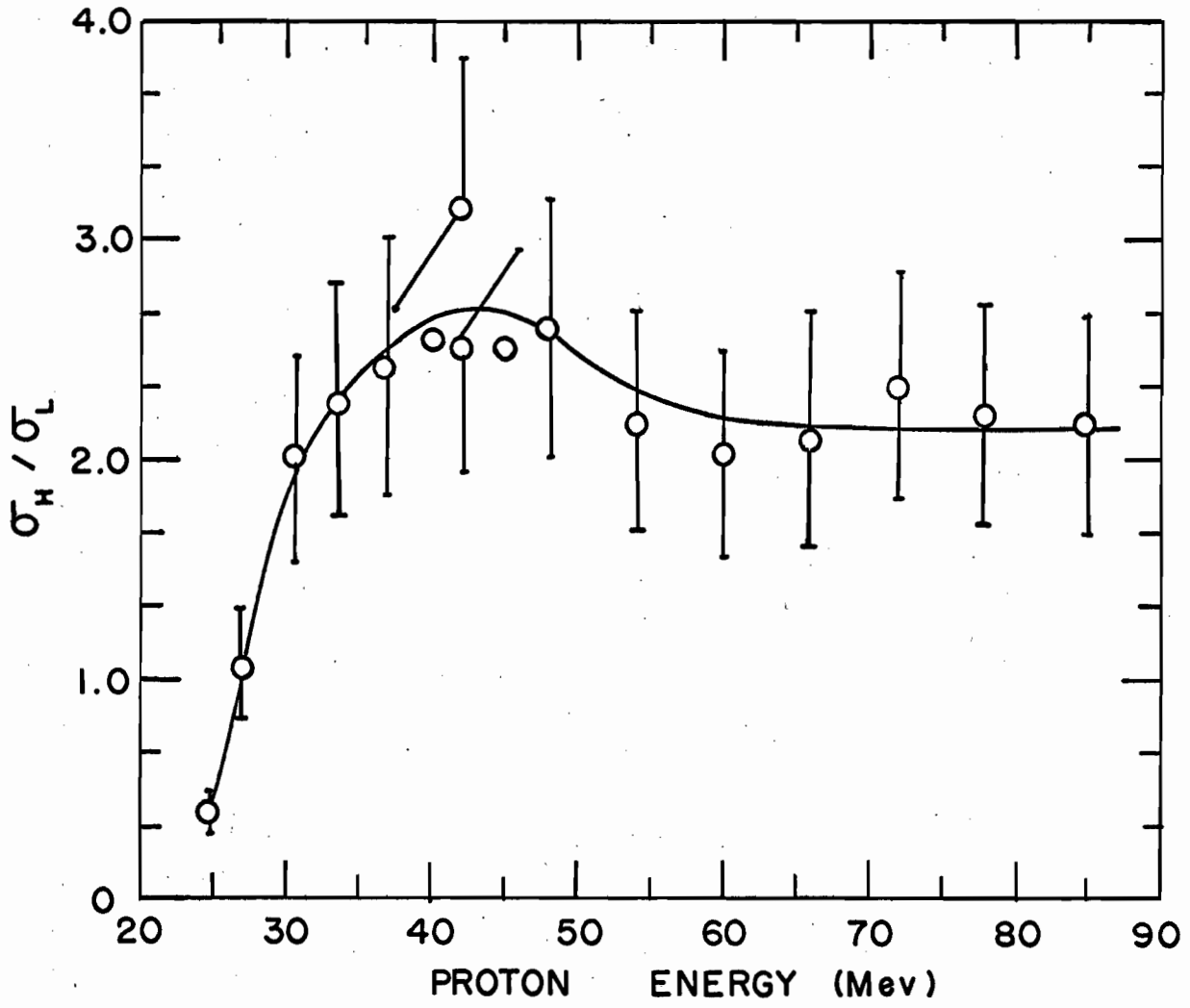

FIG. 19. Plot of Experimental Isomer Ratios versus Proton Energy for $Y^{89}(p,p2n)Y^{87m,g}$ Reactions.

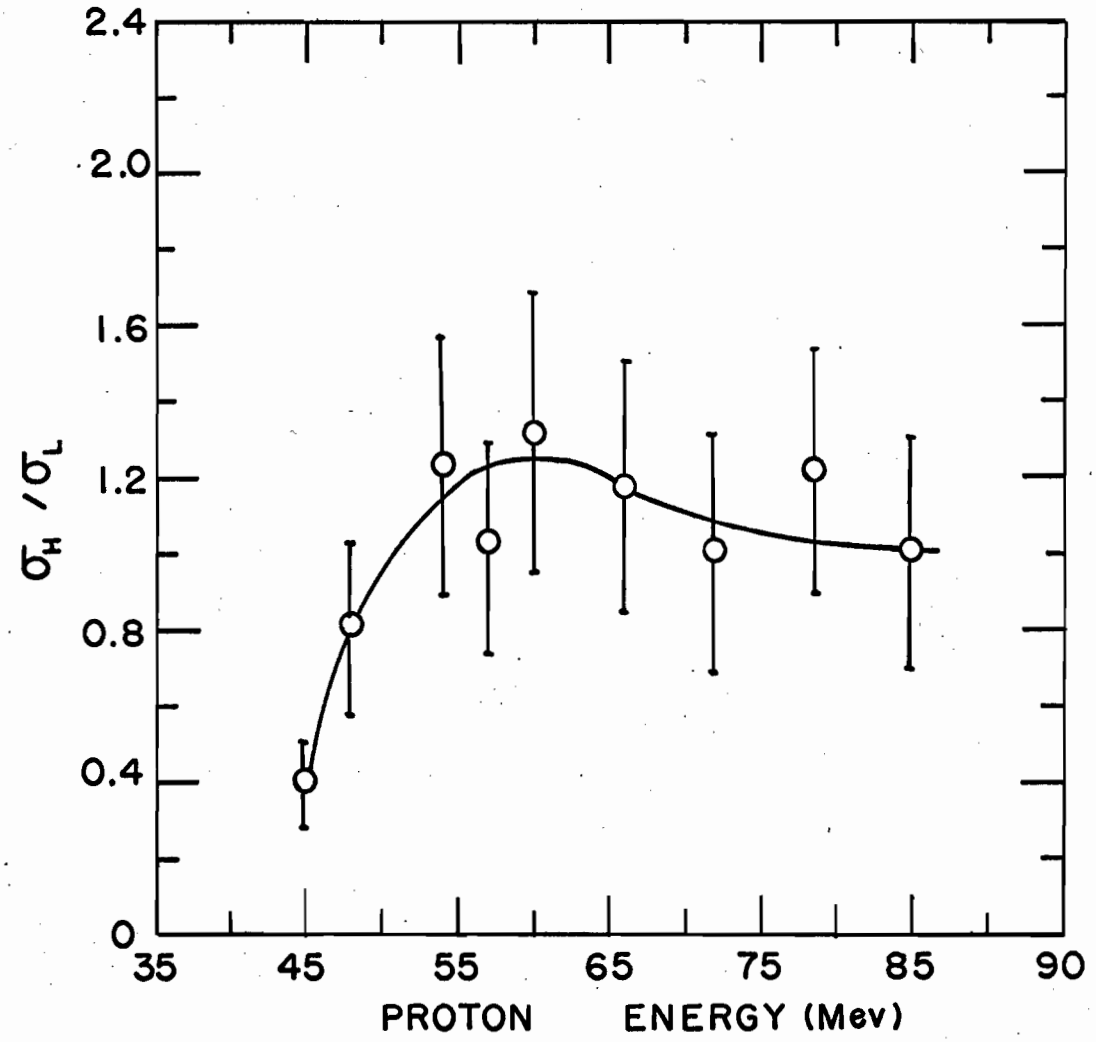

FIG. 20. Plot of Experimental Isomer Ratios versus Proton Energy for $Y^{89}(p, p3n)Y^{86m,g}$ Reactions.

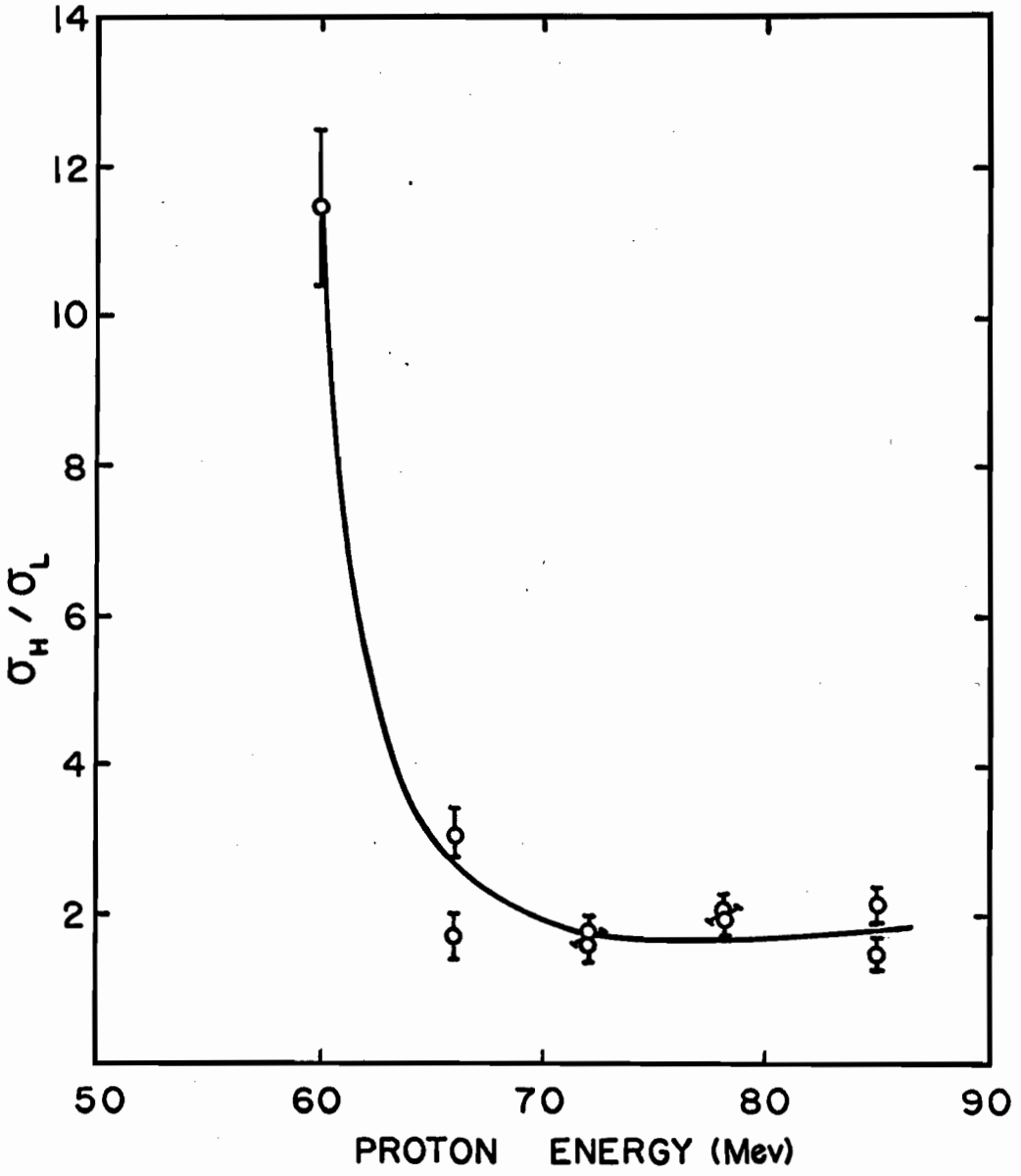

FIG. 21. Plot of Experimental Isomer Ratios versus Proton Energy for $Y^{89}(p, p4n)Y^{85m,g}$ Reactions.

IV. DISCUSSION

IV-1. Comparison with Previous Work

Our experimental results may be compared with the previous measurements of proton-induced nuclear reactions in Y^{89}. Caretto and Wiig (48) measured the cross-sections of different spallation products obtained by proton bombardment of Y^{89} at 60 Mev, 100 Mev, 150 Mev, 180 Mev and 240 Mev. Results of the 60 Mev bombardment, which can be compared with the present data, are shown in Table VIII.

TABLE VIII

Comparison of 60 Mev data

Reaction	Cross-section (mb) from Ref. (48)	Cross-section (mb) from present work
$(p,n)Zr^{89}$	44 ± 4	23.3 ± 2.6
$(p,2n)Zr^{88}$	140 ± 20	73.4 ± 9.5
$(p,4n)Zr^{86}$	72 ± 20	63 ± 10
$(p,pn)Y^{88}$	420 ± 50	199 ± 26
$(p,p2n)Y^{87g}$	82 ± 15	72 ± 14

In Table VIII, cumulative yields for $Y^{87m} + Y^{86}$, as reported by Caretto and Wiig, have not been included. They could not separate these two species because of their similar half-lives. Moreover, due to the recent report of the 48.5 min. Y^{86m} isomer, these values are incorrect.

The cross-section for Y^{85} has not been included because of the incorrect half-life assigned to this nuclide in the previous study. The cross-section for Zr^{87} has not been reported by these authors.

It is seen from the table that our experimental values are always smaller than those of Caretto and Wiig (48). Their cross-sections for the (p,n), (p,2n) and (p,pn) reactions are larger than the present values by a factor of about 2. The cross-sections of the (p,4n) and (p,p2n) reactions, on the other hand, agree within the experimental uncertainties. These authors reported an energy uncertainty of 20% at 60 Mev, which might affect their results considerably. However, as there is agreement in some cases and disagreement in others, no definite reasons for this discrepancy can be determined.

A value of 514 mb at 11.2 Mev for the Y^{89}(p,n) reaction measured by Delaunay-Olkowsky et al (75) is comparable to our 720 mb at 12 Mev. Gusakow (76) measured the cross-sections of the (p,pn) reaction induced in Y^{89} at medium energies. His results agree very well with our measured values at energies between 48.5 Mev to 87 Mev, but are lower by a factor of 1-2 in the low energy range. This low energy discrepancy may result from the use of different monitor reactions at energies where their excitation functions have a strong energy dependence. Gusakow (76) used the $C^{12}(p,pn)C^{11}$ reaction, whereas we used the $Cu^{65}(p,pn)Cu^{64}$ reaction for monitoring purposes.

Excitation functions of proton-induced reactions have been measured for copper (35), cobalt (36) and gallium (6) in the mass and energy range of present interest. The general features of these studies are similar to those of the present one, although minor differences may be noted. The shapes of the excitation functions for Co^{59} (36), Ga^{69} and

Ga^{71} (6), and Cu^{63} and Cu^{65} (35) are similar to those noted for Y^{89}. The peak cross-sections show the expected decrease with increasing number of emitted neutrons. The peak cross-sections of the (p,pn) reactions appear to decrease with increasing mass number. As evidence of this trend we cite values of about 700 mb for Co^{59}, 500 mb for Cu^{65}, 420 mb for Ga^{69}, 350 mb for Y^{89} and 185 mb for Au^{197} (49). Moreover, in all cases, this excitation function has a substantial tail at higher energies. For example, the cross-section of this reaction for Y^{89} at 85 Mev is only a factor of 2.5 lower than the peak value.

IV-2. Phenomenological Aspects of the Results

The experimental excitation functions for the (p,xn) reactions shown in Figs. 9-12 and those for the (p,pxn) reactions shown in Figs. 14-18 generally exhibit the expected shapes and magnitudes. Several qualitative remarks will be made about these excitation functions in the following paragraphs.

The general trend of the (p,xn) reactions indicates several characteristics that may be interpreted in terms of an evaporation mechanism at low energies and a cascade-evaporation mechanism at higher energies. On the other hand, the (p,pxn) excitation functions show several features which can mainly be related to a cascade-evaporation mechanism. All these excitation functions pass through maxima and then decrease with increasing proton energy. However, the decrease of the (p,pxn) excitation functions above the peak energies is not as prominent as that of the (p,xn) excitation functions. The high energy tails of the excitation functions are indicative of a direct process, as one cannot

expect them from the evaporation mechanism. The peak cross-sections and energies of the reactions whose excitation functions pass through maxima in the present energy range are summarised in Table IX.

TABLE IX

Peak cross-sections and peak energies for different reactions studied

Reaction	Peak energy (Mev)	Peak cross-section (mb)
(p,n)	13	720
(p,2n)	26	1380
(p,3n)	40	380
(p,4n)	55	80
(p,pn)	30	350
(p,p2n)	44	370
(p,p3n)	59	218
(p,p4n)	70	165

It is seen from this table that for reactions involving the emission of more than two neutrons, the peak cross-sections decrease with increasing number of emitted neutrons. This decrease results from the competition of other energetically possible reactions. Since the total reaction cross-section tends towards a constant value at higher energies, an increase in the number of possible reactions will lead to a decrease in the individual reaction cross-sections.

Here we define two quantities, f_n and f_p, which may be of some

use in understanding the general trend of the results. f_n is defined as the fraction of the calculated total reaction cross-section in which no charged particle is emitted and f_p is defined as the fraction of the calculated total reaction cross-section in which one singly charged particle (one proton or one deuteron) and a number of neutrons are emitted. The quantity, f_n, is obtained by dividing the sum of all experimental (p,xn) reaction cross-sections at a particular energy by the total reaction cross-sections calculated according to Eqn. IV-20 in Section IV-3B. Similarly f_p is obtained by dividing the sum of all experimental (p,pxn) reaction cross-sections at a particular energy by the calculated total reaction cross-section. The values of f_n and f_p have been plotted versus the proton bombarding energy in Fig. 22. The upward arrows on the points of the f_n curve represent the contribution from the unmeasured cross-sections of the (p,5n) and (p,6n) reactions. The upward arrows on the points of the f_p curve below 50 Mev indicate the unmeasured contribution from the (p,p') reaction. The upward or downward arrows on the points of the f_p curve above 55 Mev represent the net contribution from the (p,p') reaction and the (p,5n) and (p,6n) reactions. The cross-sections of the latter have been included in the (p,p4n) and (p,p5n) reactions respectively. All these unmeasured contributions have been estimated from the cascade-evaporation calculation discussed in Section IV-3.

It is seen from Fig. 22 that at low energies, reactions involving only neutron emission are predominant. These reactions decrease with increasing bombarding energy. This is due to the effect of the Coulomb barrier in inhibiting proton emission at low energies and to the onset of many additional reactions at higher energies. On the other

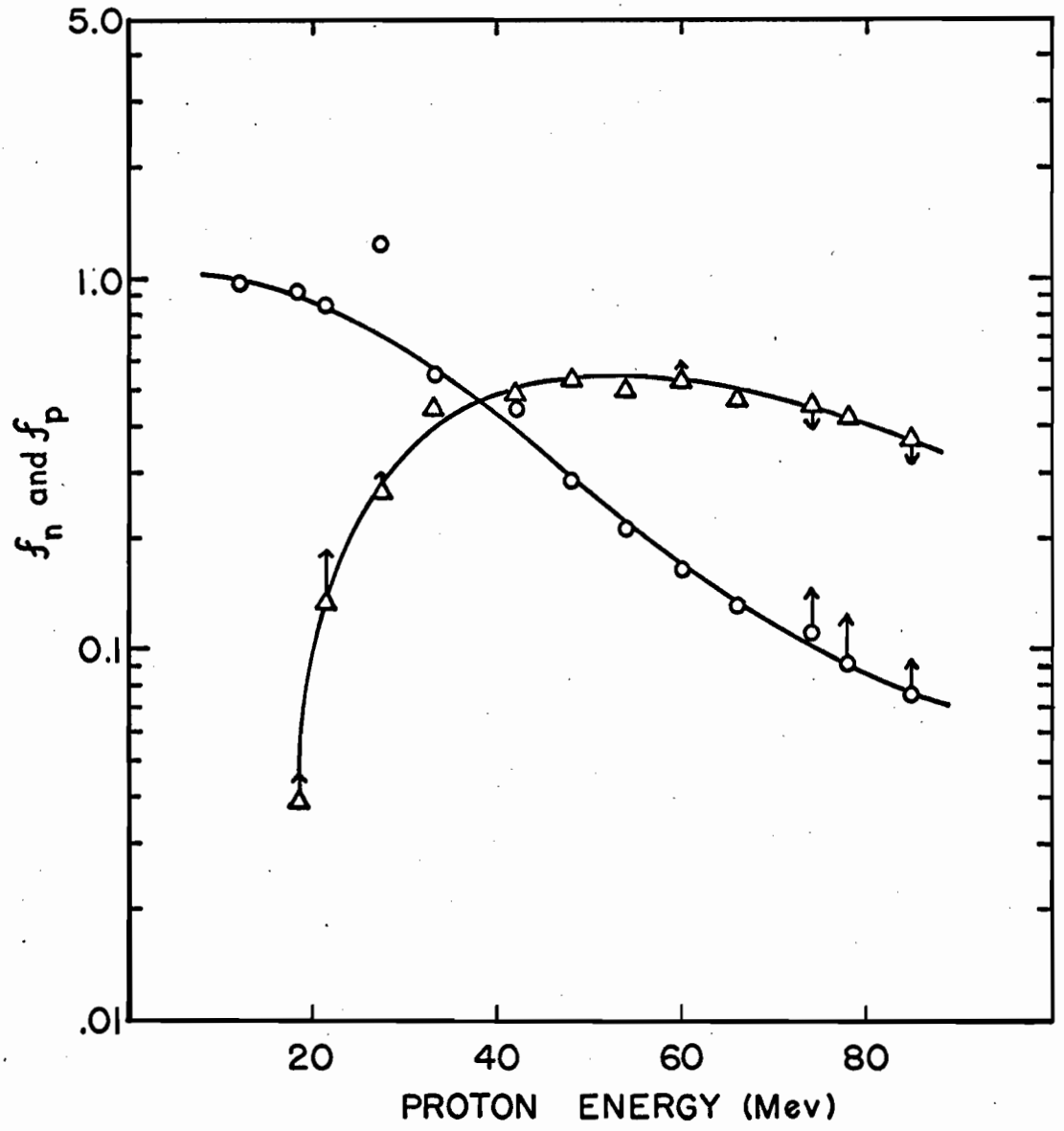

FIG. 22. Plots of f_n and f_p versus proton bombarding energy.

o - f_n (fraction of total reaction involving only neutron emission)

Δ - f_p (fraction of total reaction involving one proton and a few neutrons emission).

hand, reactions involving the emission of one singly charged particle and several neutrons increase sharply as the effect of the Coulomb barrier decreases. At higher energies f_p decreases only slowly indicating the importance of proton re-emission. At bombarding energies up to about 30 Mev f_n and f_p add to about unity indicating that at these energies the (p,xn) and (p,pxn) reactions are the only important de-excitation paths. At energies of 40 Mev - 70 Mev, approximately half of the reaction cross-section involves the emission of a single proton and a few neutrons. At high energies other competing processes are energetically possible and hence the sum of the two fractions decreases.

It is instructive in connection with the above discussion to examine the relative yields of the isobaric products. The ratios of cross-sections for the (p,2n) and (p,pn) reactions, the (p,3n) and (p,p2n) reactions, and the (p,4n) and (p,p3n) reactions are plotted as a function of proton energy in Fig. 23. The most striking features of these ratio curves are the preponderance of proton emission over neutron emission and the decrease of all the ratios at higher energies towards a constant value of 0.2-0.3. The thresholds of the (p,2n), (p,3n) and (p,4n) reactions are higher than those of the (p,pn), (p,p2n) and (p,p3n) reactions respectively. Thus all the ratio curves should start from an initial zero value. While this is evident in the $\sigma(p,3n)/\sigma(p,p2n)$ and $\sigma(p,4n)/\sigma(p,p3n)$ ratio curves, the $\sigma(p,2n)/\sigma(p,pn)$ ratio curve does not show such an initial increase. The difference of thresholds of these reactions is about 1 Mev. Therefore, the large spread of the proton beam energy ($\sim$2 Mev) and the rapid decrease of the reaction cross-section at low energies make it impossible to observe this effect.

It is found that beyond about 50-55 Mev the ratios for these

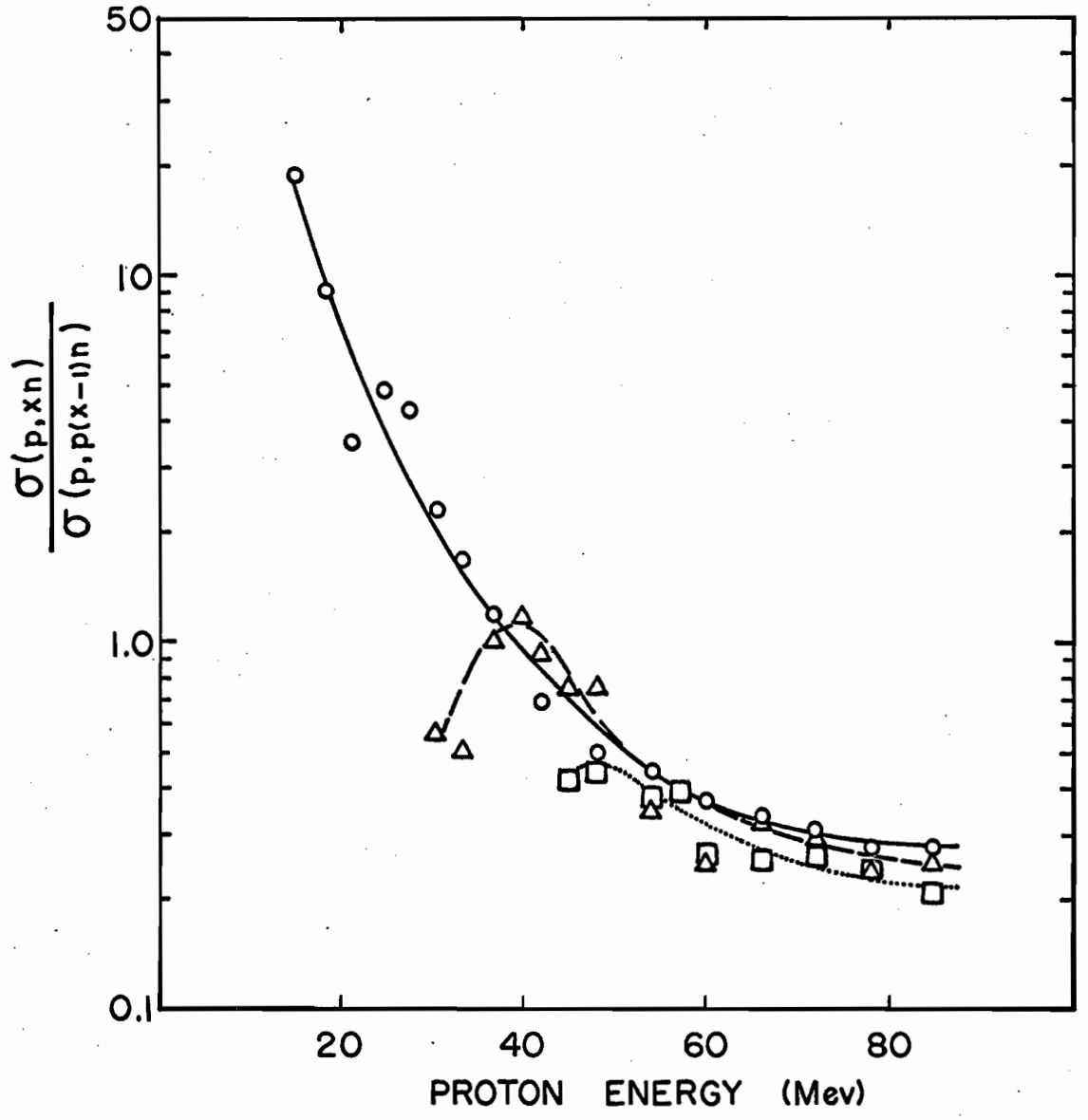

Fig. 23. Plots of the ratios of cross-sections of the isobaric nuclides versus proton bombarding energy.

o - $\sigma(p,2n)/\sigma(p,pn)$ - (solid line)

Δ - $\sigma(p,3n)/\sigma(p,p2n)$ - (dashed line)

□ - $\sigma(p,4n)/\sigma(p,p3n)$ - (dotted line)

three sets of reactions decrease almost at the same rate with energy tending towards a constant value of 0.2-0.3. The constant value of a particular isobaric ratio is explained by Miller and Hudis (77) as due to the evaporation process. The insensitivity of the isobaric ratio to the bombarding energy implies that the energy distribution of the excited progenitors of a given set of isobaric products is nearly independent of the bombarding energy. The isobaric yield ratio is then primarily determined by the branching ratios for neutron and proton emission in the final evaporation step. In turn these branching ratios depend on the binding energies, odd-even effect, etc., of the residual nucleus.

Although evaporation effects can account for the constancy of a given isobaric ratio at higher energies, it is curious that all the isobaric ratios have nearly the same value at 70-85 Mev. We believe that this reflects the effect of the cascade process. A reasonable mechanism for all these reactions at 70-85 Mev is a (P,P') or a (P,N) cascade followed by the evaporation of (x-1) neutrons. The cascade calculation discussed in Section IV-3 confirms this assumption. Under this condition the isobaric ratio will be primarily governed by the relative probability of (P,N) and (P,P') cascades leading to residual nuclei with sufficient excitation energy to evaporate (x-1) neutrons. As a first approximation the branching ratios for the evaporation of (x-1) neutrons from $(Zr^{89})^*$ or $(Y^{89})^*$ will cancel. The following simple calculation can then be performed to estimate the isobaric yield ratios.

We assume that, as already mentioned, only one nucleon is emitted in the cascade, followed by the evaporation of (x-1) neutrons. The incident proton is assumed to collide with a stationary nucleon at a large impact parameter. Trajectories involving small impact parameter can be

expected to lead to compound nucleus formation in this energy range and, therefore, need not be considered. This localisation of the reaction site enables us to neglect the important effect of the absorption of the incident and emitted particles. This follows from the small traversal distance inside the nucleus required for a peripheral interaction as well as from the reduced nuclear density in the surface region. Furthermore, it is reasonable to assume that the effects of reflection, refraction as well as absorption are approximately the same for both (P,P') and (P,N) cascades. Hence these effects need not be considered in our approximate treatment. It is assumed that after collision one of the collision partners is directly emitted and the other is captured giving rise to an excited residual nucleus. The energy transfer in the collision is such that the residual nucleus can just evaporate the required number of neutrons to give the desired reaction. It is clear that for an incident proton, emission of a proton in the cascade process can arise from either a proton-proton or a proton-neutron collision, whereas neutron emission arises only from a proton-neutron collision. It is further assumed that the probability for collision with a neutron or a proton at the nuclear surface is proportional to the number of neutrons or protons in the nucleus. With these points in mind, we can write to a first approximation,

$$\frac{\sigma(p,xn)}{\sigma(p,p(x-1)n)} = \frac{\sigma(P,N)}{\sigma(P,P')} = \frac{\sigma_{p-n} \cdot a_{p-n} \cdot N_n}{\sigma_{p-n} \cdot a_{p-n} \cdot N_n + \sigma_{p-p} \cdot a_{p-p} \cdot N_p} \quad \ldots\ldots \text{(IV-1)}$$

where σ_{p-n} and σ_{p-p} = total proton-neutron and proton-proton elastic cross-sections,

N_n and N_p = number of neutrons and protons in the nucleus,

a_{p-n} and a_{p-p} = fractions of σ_{p-n} and σ_{p-p} leading to the desired excitation energy needed to evaporate the required number of neutrons.

The quantities 'a' are defined as

$$a = \frac{\int_0^{2\pi} \int_{\theta_{min}}^{\theta_{max}} \frac{d\sigma}{d\Omega} \, d\Omega}{\int_0^{2\pi} \int_0^{\pi} \frac{d\sigma}{d\Omega} \, d\Omega}$$

$$= \frac{2\pi \int_{\theta_{min}}^{\theta_{max}} \frac{d\sigma}{d\theta} \sin\theta \, d\theta}{\sigma_{p-p} \text{ (or } \sigma_{p-n})} \qquad \ldots\ldots \text{(IV-2)}$$

Here the limits θ_{min} and θ_{max} are the centre of mass scattering angles. They are determined by the range of energy transfer which is required to evaporate the desired number of neutrons. We have chosen the following energy intervals for different reactions:

10-20 Mev - 1 neutron is evaporated to give (p,2n) or (p,pn) reactions.

20-30 Mev - 2 neutrons are evaporated to give (p,3n) or (p,p2n) reactions.

35-45 Mev - 3 neutrons are evaporated to give (p,4n) or (p,p3n) reactions.

These intervals were chosen from a knowledge of the peak energies of the (p,xn) reactions. The lower limits of these energy intervals give θ_{min} and the upper limits give θ_{max}. As the centre of mass scattering angle is the same for both incident and struck nucleons, it can be calculated from a knowledge of the initial velocity and the velocity of either

particle after collision. It has been calculated from a formula given by Evans (78), which in the case of equal mass particles reduces to

$$V^2_{cap.} = \frac{1}{2} V^2_{inc.} (1 - \cos\theta_{c.m.}) \quad \ldots\ldots (IV\text{-}3).$$

Here $V_{inc.}$ is the velocity of the incident proton and $V_{cap.}$ is that of the captured nucleon. The latter is determined by the above-mentioned energy intervals. The calculation has been performed for 85 Mev incident protons. Since the target nucleons have been assumed to be stationary, it is consistent to neglect the effect of the nuclear potential on the energy of the incident proton.

The values of σ_{p-p} and σ_{p-n} have been calculated by the empirical formula given by Metropolis et al (31) and are 31.23 mb and 77.2 mb respectively. The angular distribution of p-p scattering is isotropic and that of p-n scattering is anisotropic. Empirical formulae for $d\sigma/d\Omega$ have been given by Bertini (39) in the following forms.

$$\left.\begin{aligned} \frac{d\sigma}{d\Omega}(p\text{-}p) &= A_p \\ \frac{d\sigma}{d\Omega}(p\text{-}n) &= A_n + B_n \cos^3\theta \end{aligned}\right\} \quad \ldots\ldots (IV\text{-}4)$$

Putting Eqns. IV-4 in Eqn. IV-2 and integrating we have

$$\left.\begin{aligned} a_{p-p} &= \frac{2\pi \left[-A_p \cos\theta\right]_{\theta_{min}}^{\theta_{max}}}{\sigma_{p-p}} \\ a_{p-n} &= \frac{2\pi \left[-A_n \cos\theta - B_n \frac{\cos^4\theta}{4}\right]_{\theta_{min}}^{\theta_{max}}}{\sigma_{p-n}} \end{aligned}\right\} \quad \ldots\ldots (IV\text{-}5)$$

The value of A_p was taken as 5.5 mb/str. by an interpolation between the 70 Mev and 90 Mev results given by Hess (79). The values of A_n and B_n have been given by Bertini (39). A_n and B_n were taken as 4.8 mb/str. and 8.2 mb/str. respectively at 85 Mev. Thus a_{p-p} and a_{p-n} were determined from Eqn. IV-5. Once the values of σ_{p-p}, σ_{p-n}, a_{p-p} and a_{p-n} are known, $\sigma(P,N)/\sigma(P,P')$ can be calculated according to Eqn. IV-1.

The calculated ratios corresponding to $\sigma(p,2n)/\sigma(p,pn)$, $\sigma(p,3n)/\sigma(p,p2n)$ and $\sigma(p,4n)/\sigma(p,p3n)$ are 0.62, 0.56 and 0.53 respectively. In view of the many approximations that have been made, the factor of 2 difference from the experimental values is probably not significant. It thus appears that the cascade process may be the decisive factor in giving the same value of all the isobaric ratios at 70-85 Mev. It is amusing to note that the far more realistic cascade-evaporation calculation, described in the subsequent section, predicts isobaric ratios that are in poorer agreement with experiment than those given by the present calculation.

Another possible way of analysing our results is to plot the cross-sections versus the total kinetic energy (K.E.) associated with emitted nucleons and photons. These plots are presented in Fig. 24 for the (p,xn) reactions and in Fig. 25 for the (p,pxn) reactions. In either case the total K.E. associated with emitted nucleons and photons has been obtained by subtracting the reaction Q-value from the centre of mass K.E. of the incident proton. The reaction Q-values have been obtained by using Wapstra's (80) mass excess values.

It is obvious that the K.E. spectra can range from zero up to the kinematically determined maximum energy. Each curve passes through a maximum which characterises the most probable total K.E. of the particular

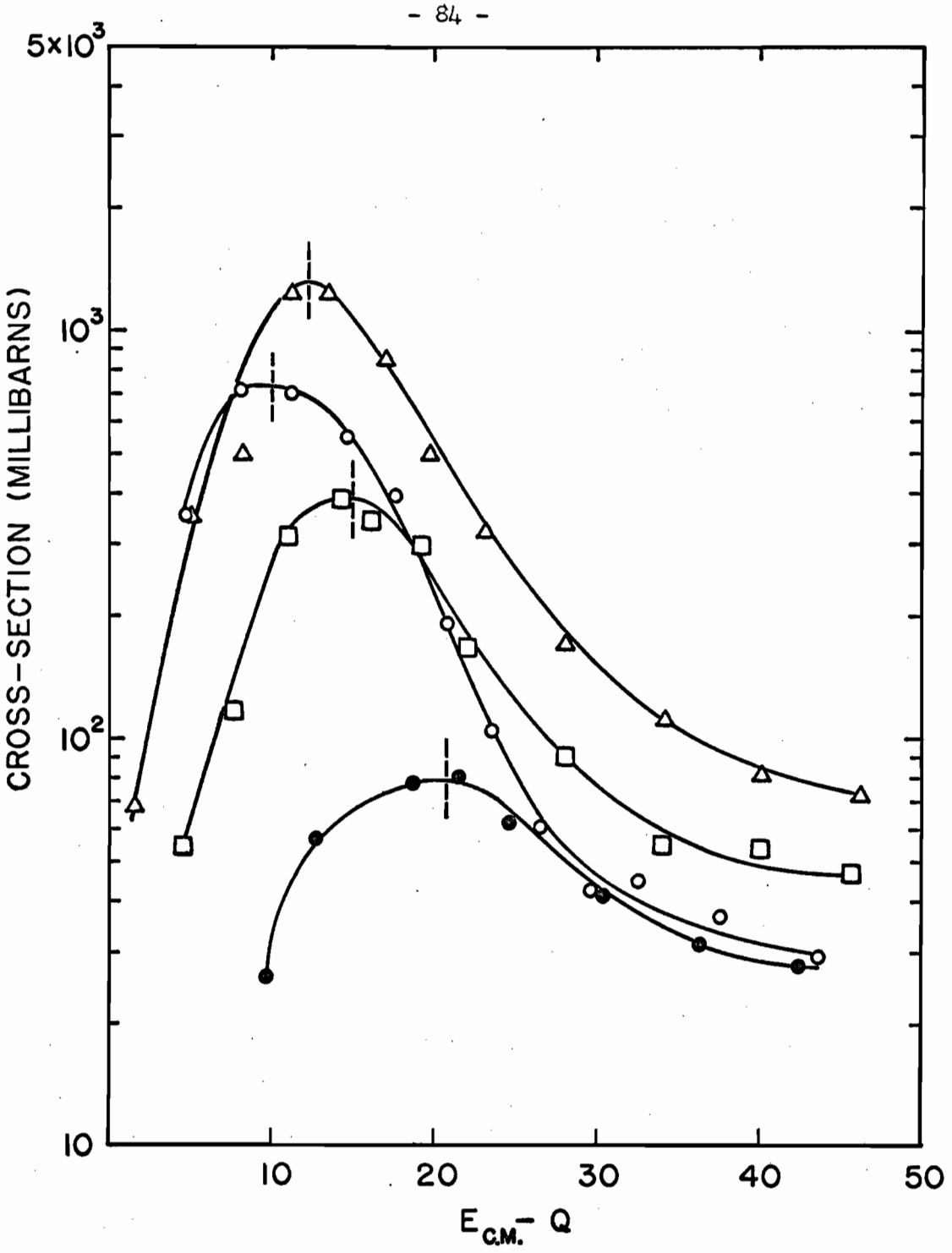

FIG. 24. Plots of cross-sections versus total K.E. ($E_{c.m.}$ – Q) of emitted neutrons and photons, for the (p,xn) reactions.

o - (p,n)

□ - (p,3n)

Δ - (p,2n)

● - (p,4n)

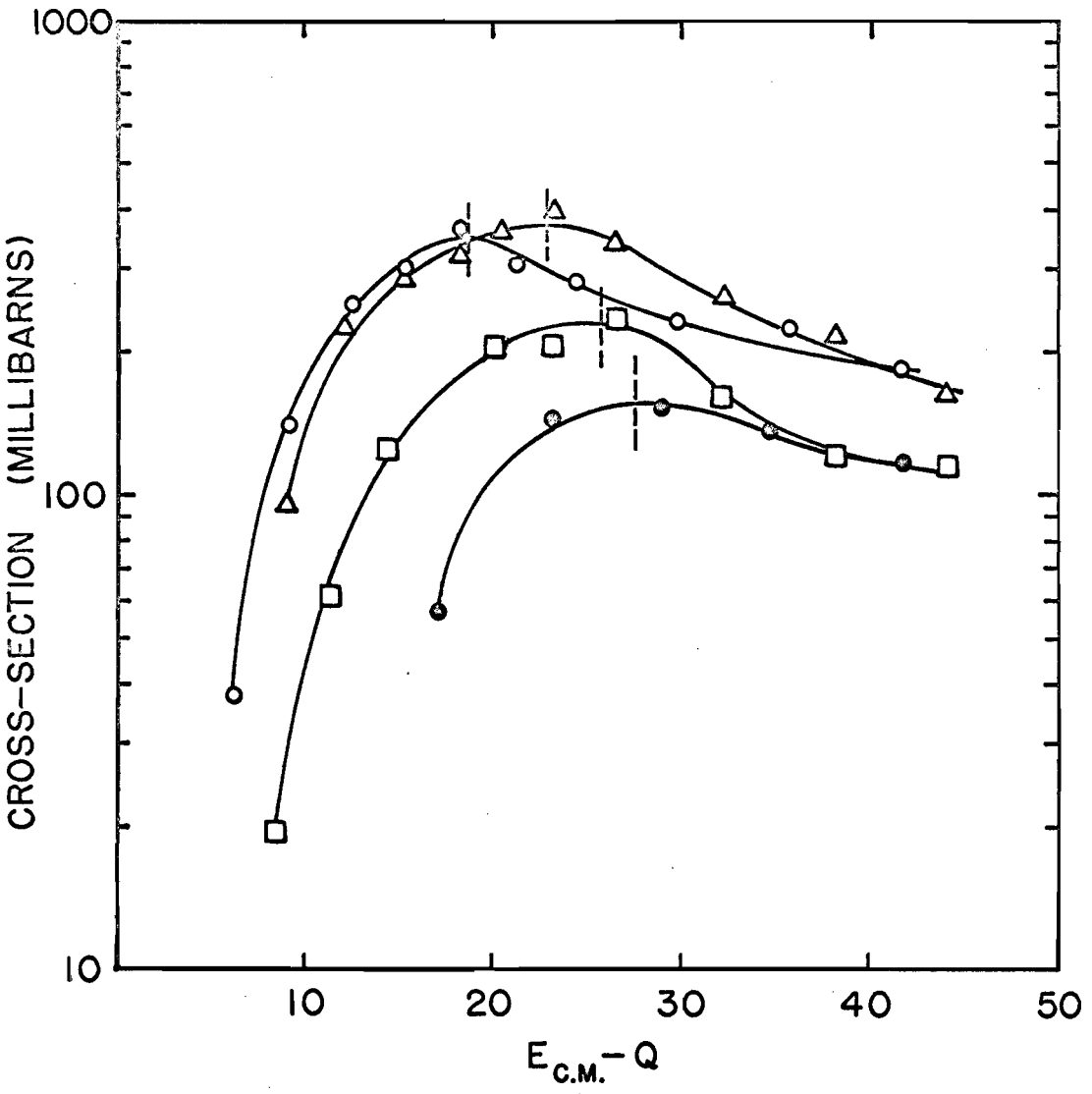

FIG. 25. Plots of cross-sections versus total K.E. ($E_{c.m.}-Q$) of emitted nucleons and photons, for the (p,pxn) reactions.

o - (p,pn)
Δ - (p,p2n)
□ - (p,p3n)
◉ - (p,p4n)

group of nucleons and photons in question. In order to avoid confusion in the terminology of the discussion that follows, we shall instead refer to this quantity as the average total K.E. The difference between the most probable and the average energy is, in fact, rather small in the case of the (p,xn) reactions in view of the approximate symmetry of the curves. On the other hand, the curves for the (p,pxn) reactions exhibit a pronounced asymmetry. It is thus seen that the probability for the emission of nucleons with large kinetic energy is substantial, reflecting the large probability of (P,P') cascades in which an energetic proton is emitted. It is also apparent that the probability of occurrence of these reactions for kinetic energies below 10 Mev is negligibly small. This is certainly due to the suppressive effect of the Coulomb barrier which is 8.4 Mev for the Y^{89} + p system.

It can be seen from Figs. 24 and 25 that there is an increase in the average total K.E. with increasing number of emitted neutrons. In order to understand this behaviour more explicitly, we have made the following analysis. The probability of the evaporation of a neutron with kinetic energy ε is approximately given by the Maxwellian equation

$$P(\varepsilon) \propto \varepsilon e^{-\varepsilon/T} \qquad \ldots\ldots \text{(IV-6)}$$

where T is the temperature of the residual nucleus evaluated at its maximum excitation energy. The above relation implies that the average K.E. carried away by each emitted neutron is equal to 2T. The nuclear temperature T is given by the simple expression

$$T = \sqrt{\frac{E^*_{max}}{a}} \qquad \ldots\ldots \text{(IV-7)}$$

where 'a' is chosen as A/10 in this analysis and E^*_{max} is the maximum excit-

ation energy of the residual nucleus. Eqn. IV-7 is the equation of state for a Fermi gas at moderately high excitation energy. When a neutron is emitted from a nucleus with excitation energy E, the maximum excitation energy E^*_{max} of the residual nucleus is

$$E^*_{max} = E - B \qquad \ldots\ldots \text{(IV-8)}$$

where B is the binding energy of the emitted neutron. Therefore,

$$T = \sqrt{\frac{E - B}{a}} \qquad \ldots\ldots \text{(IV-9)}.$$

Consequently, the average excitation energy of the residual nucleus after neutron emission is

$$\bar{E}_r = E - B - 2\sqrt{\frac{E - B}{a}} \qquad \ldots\ldots \text{(IV-10)}.$$

The maximum excitation energy of the next residual nucleus is obtained by subtracting the binding energy of the next neutron to be emitted, from $\bar{E}_r$. Then T is calculated according to Eqn. IV-9 and $\bar{E}_r$ of the next residual nucleus is obtained by Eqn. IV-10. This is repeated as long as sufficient energy is available for neutron emission.

The above analysis has been carried out for the (p,xn) reactions. The average excitation energy of the initial nucleus has been obtained by converting the peak energy of each reaction to excitation energy according to $E_{c.m.} + Q$. Here Q is the Q-value for compound nucleus formation, and it has been obtained by using Wapstra's (80) mass excess values. The neutron binding energies have also been obtained from Wapstra's (80) mass excess values. The results of the analysis are shown in Table X.

It can be seen that the average total K.E. of the emitted neutrons increases with increasing number of emitted neutrons. The average K.E.

TABLE X

Results of analysis for the average total K.E. carried by neutrons and photons in the (p,xn) reactions

Reaction	Peak energy (lab.) (Mev)	E* (Mev)	Number of neutrons	$E_n = 2T$ (Mev)	Average residual energy (Mev)	Average total K.E. of emitted neutrons and photons
(p,n)	13	21.18	1	2.03	---> 7.20	----> 9.23
(p,2n)	26	34.03	1	3.14	18.94	
			2	2.05	---> 7.28	----> 12.47
				5.19		
(p,3n)	40	47.88	1	4.00	31.93	
			2	3.17	19.15	
			3	1.78	---> 5.80	----> 14.75
				8.95		
(p,4n)	55	62.71	1	4.75	46.01	
			2	4.04	32.36	
			3	3.03	17.14	
			4	1.88	---> 5.84	---> 19.54
				13.70		

per emitted neutron displays a similar, although less marked, trend. The average residual energy, dissipated in photon emission, displays a less consistent trend with the number of emitted neutrons. The total K.E., given in column 7 of Table X, does however increase with the number of emitted neutrons, and thus explains the trend noted in Figs. 24 and 25.

IV-3. Calculations of Cascade-evaporation and Statistical Theories and Their Comparison with Experimental Results

In order to make a quantitative comparison of our experimental results with the predictions of the statistical and cascade-evaporation theories, Monte Carlo calculations have been performed. The general scheme of each of these calculations is outlined below.

IV-3A. Calculation of Cascade Process

The recent Monte Carlo calculation of Chen et al (40) which is the most sophisticated to date has been adopted for the present purpose. In this calculation the nuclear density distribution is represented by 7 concentric step-function regions of constant density. Proper choice of radius and density of each region is made so that the whole distribution approximates the Fermi distribution,

$$\rho(r) = \frac{\rho_0}{1 + \exp\left[\frac{(r-c)}{a}\right]} \qquad \ldots\ldots \text{(IV-11)}.$$

Here ρ_0 is the maximum density at the centre of the nucleus, $c = 1.07\ A^{1/3}$ fermi and

$$a = \frac{r(10\%) - r(90\%)}{4.4} \qquad \ldots\ldots \text{(IV-12)}$$

with r(10%) and r(90%) equal to the radii at which density has dropped to $0.1\rho_o$ and $0.9\rho_o$ respectively.

The momentum distribution of the protons and the neutrons in each region is assumed to be that of a degenerate Fermi gas with Fermi energy,

$$E_{F_i} = \frac{\hbar^2}{2m_i} (3\pi^2\rho_i)^{2/3} \qquad \ldots\ldots \text{(IV-13)}$$

where m_i is the mass of proton or neutron. ρ_i is the density of protons or neutrons in the region of interest.

A purely central potential is used for each region. The radial component of the particle momentum is changed as the particle enters a different density region and reflection and refraction of the particles at the boundary between different zones are taken into account. The angle of refraction is given by an equation which is the inverse of Snell's law of optical refraction (at non-relativistic energies)

$$\frac{\sin\theta}{\sin\theta'} = \frac{p'}{p} \qquad \ldots\ldots \text{(IV-14)}$$

where p' and p are the momenta of the particle in the regions in question. The critical angle for total reflection is

$$\cos\theta_{cr.} = \frac{\sqrt{E^2 - E'^2}}{p} \qquad \ldots\ldots \text{(IV-15)}$$

where E and E' are the total energies of the particle in these regions.

In contrast to the previous calculations in which one particle at a time from among the collision partners was followed sequentially, the present calculation proceeds on a time-like basis. The Fermi sphere of momentum is divided into 'n' portions of equal volume. The mean free path of the incoming particle is calculated by

$$\Lambda = \frac{A}{\rho_{max}} \left[Z\sigma_p + (A - Z)\sigma_n \right]^{-1} \quad \ldots\ldots \text{(IV-16)}$$

where ρ_{max} is the <u>total</u> nucleon density at the centre of the nucleus. σ_n and σ_p are the cross-sections for collision of the incident particle with a neutron or a proton respectively. Λ will be underestimated if the particle is at the diffuse edge of the nucleus where the density is considerably smaller than ρ_{max}.

The time interval is then calculated by

$$t = \frac{\Lambda}{n\beta} \quad \ldots\ldots \text{(IV-17)}$$

where β is the velocity of the incoming particle in units of the velocity of light. A collision partner is chosen at random out of the momentum distribution. It is then checked whether an interaction has taken place in the path length βt and, if not, the particle is advanced by the path length βt. A new t is calculated and the process is repeated until the particle makes an interaction or escapes from the nucleus. Reflection and refraction of the cascade particles at the surfaces of different density regions are considered. An interaction is checked to see whether it is allowed or forbidden by the exclusion principle. In an allowed collision both collision partners are followed. The calculation proceeds until the struck particles either escape from the nucleus or are captured. The latter eventuality is assumed to occur when their total energy drops below an arbitrary cut-off energy.

The cascade calculation gives the type, number and energy of the emitted particles and also the excitation energy of the residual nuclei. In order to complete the analysis the latter are then used as the starting nuclei in an evaporation calculation, described in the following subsection.

IV-3B. Calculation of Evaporation Process

The general basis for the evaporation calculation is the formalism of the statistical theory as derived by Weisskopf (2). According to Weisskopf's formalism the probability $P(E_j)dE_j$ that a nucleus excited to the energy E_i will emit a particle j with kinetic energy between E_j and $E_j + dE_j$ is

$$P(E_j)dE_j = \frac{g_j m_j}{\pi^2 \hbar^3} \cdot \sigma^*(E_j) \cdot \frac{w(E_f)}{w(E_i)} \cdot E_j \cdot dE_j \qquad \ldots\ldots \text{(IV-18)}.$$

Here $w(E_i)$ and $w(E_f)$ are the level densities of the initial and final nuclei at their respective energies E_i and E_f. The emitted particle of mass m_j has the statistical weight factor $g_j = 2s_j + 1$ due to its spin. $\sigma^*(E_j)$, the so-called inverse cross-section, is the cross-section for the formation of the initial compound nucleus when the particle j with kinetic energy E_j is incident upon the excited residual nucleus.

For the present purpose a Monte Carlo calculation has been performed according to the program written by Dostrovsky et al (34). The integration of Eqn. IV-18 to give the total emission width of the particle j requires explicit expressions for the inverse cross-sections $\sigma^*(E_j)$ and the level density w(E). These are briefly outlined below.

The present understanding of the inverse cross-section is quite incomplete due to lack of knowledge about the properties of excited nuclei. Under these circumstances the inverse cross-section is evaluated by assuming that it equals the total reaction cross-section for particles incident upon a nucleus in its ground state. The inverse cross-section is given by

the empirical formula

$$\sigma_c = \sigma_g.\alpha.(1 + \frac{\beta}{E_n}) \qquad \ldots\ldots \text{(IV-19)}$$

for a neutron with kinetic energy E_n in the centre of mass system. α and β are two parameters chosen as $\alpha = 0.76 + 2.2A^{-1/3}$ and $\beta = (2.12A^{-2/3} - 0.05)/(0.76 + 2.2A^{-1/3})$ to give the best fit to the continuum theory cross-sections given by Blatt and Weisskopf (81). σ_g, the geometric cross-section, is equal to πR^2 with radius $R = r_o \times A^{1/3}$ cm.

The inverse cross-section for charged particle emission is given by the empirical formula

$$\sigma_c = \sigma_g(1+c_j)\ (1 - \frac{k_j V_j}{E_j}) \qquad \ldots\ldots \text{(IV-20)}$$

where c_j and k_j are two adjustable parameters to give the best fit to the continuum theory cross-sections given by Shapiro (82) and Blatt and Weisskopf (81). $k_j V_j$ is the effective Coulomb barrier and the constant k_j approximates the effect of potential tunnelling. V_j is calculated as

$$V_j = \frac{Z_1 Z_2 e^2}{R} \qquad \ldots\ldots \text{(IV-21)}$$

with $R = r_o \times A^{1/3} + \rho_j$ as the interaction radius between the charged particle and the residual nucleus of atomic numbers Z_1 and Z_2 respectively. ρ_j is taken as 1.2 fermi for deuterons and alpha particles and zero for protons. E_j is the kinetic energy of the incident particle in the centre of mass system. The values of c_j and k_j have been given by Dostrovsky et al (34) for several values of Z and any intermediate value can be obtained by interpolation.

The simplest and most widely used level density formula is given as

$$w(E) = C.\exp\left[2(aE)^{1/2}\right] \quad \ldots\ldots (IV\text{-}22).$$

Here E is the excitation energy and 'a' is the level density parameter given as a function of mass number A. C is assumed to be constant, although the most correct formulation indicates that it is energy dependent. The level densities depend on whether the neutron or proton numbers of the residual nucleus are odd or even. Hurwitz and Bethe (83) pointed out that odd-even effects on nuclear level densities could be considered as arising from the displacement of the ground state energy due to nucleon pairing. A fraction of the total excitation energy, equal to the pairing energy 'δ', is utilised to break a pair of nucleons without giving rise to any level within this energy interval. Therefore, the excitation energy in the level density formula is measured from a characteristic state displaced upward from the true ground state by the pairing energy. With these considerations the level density formula becomes

$$w(E) = C.\exp\left\{2\left[a(E-\delta)\right]^{1/2}\right\} \quad \ldots\ldots (IV\text{-}23)$$

where $\delta = 0$ for odd-odd nuclei and $\delta > 0$ for all other types.

The nuclear level densities are also affected by the shell structure of the nucleus. The level density of a magic nuclide is much smaller than that of an intermediate nuclide. Newton (84) and Cameron (85) have discussed these shell effects elaborately. However, the shell effect has not been taken into account in the level density formula in the present calculation.

The total emission width of a neutron j is obtained by the integration of Eqn. IV-18

$$\Gamma_j = \frac{g_j m_j}{\pi^2 \hbar^3} \int_0^{E_i - S_j} \sigma^*(E_j) \frac{w(E_f)}{w(E_i)} \cdot E_j . dE_j \quad \ldots\ldots (IV\text{-}24)$$

where S_j is the separation energy of the neutron. In the case of charged particle emission the lower limit of integration should be the effective Coulomb barrier $k_j V_j$. Moreover, if the residual nucleus is even-even or odd-A, a pairing energy 'δ' has to be subtracted from the upper limit. Using Eqns. IV-19 and IV-20 for the inverse cross-sections for neutrons and charged particles respectively and Eqn. IV-23 for the level density, Γ_j can be calculated from Eqn. IV-24. The integrated forms of Γ_j have been given by Dostrovsky et al (34). The probability of emission of a particle j is then obtained by

$$P_j = \frac{\Gamma_j}{\sum_j \Gamma_j} \qquad \ldots\ldots \text{(IV-25)}$$

where the summation runs over all the particles.

In an actual Monte Carlo calculation the relative emission widths of neutron, proton, deuteron, alpha particle, triton and He^3 are computed. The total emission width is then normalised to unity. A random number is chosen to select the type of the particle emitted. Whether the residual nucleus will emit any more particles or not is determined by the kinetic energy carried away by the first particle. This kinetic energy is selected by the choice of a random number weighted by the energy spectrum given by Eqn. IV-18. If the residual nucleus has enough energy to evaporate a particle, it is treated as a new starting nucleus and the calculation is performed in the same fashion as described above. The procedure is repeated until further particle emission is energetically impossible. The calculation gives the Z and A distribution of the reaction products.

IV-3C. Present Calculations

Two Monte Carlo calculations have been performed - one according to the statistical theory assuming compound nucleus formation throughout the energy range i.e. up to 85 Mev; the other according to the cascade-evaporation theory. Both calculations have been carried out according to the procedures outlined in Sections IV-3A and IV-3B, with an IBM-7094 computer at Brookhaven National Laboratory*.

In the statistical or evaporation theory calculation, the values of parameters c_j and k_j used for the inverse cross-sections for charged particle emission were taken from the interpolation of the values given by Dostrovsky et al (34). A value of A/20 for the level density parameter 'a' and Cameron's (85) pairing energy values 'δ' were used in the level density formula IV-23. A value of $r_o = 1.5 \times 10^{-13}$ cm was chosen for the radius parameter. Separation energies were taken from Wapstra's (80) table. One thousand evaporations were followed with the same initial set of parameters at each of several energies.

In the cascade calculation of the cascade-evaporation process the cut-off energy chosen was 16.4 Mev above the Fermi energy for neutrons. The corresponding value for protons was 15.9 Mev. An average binding energy of 8.2 Mev was used for both neutron and proton. The cut-off and binding energies were not changed throughout the calculation in spite of the change in mass number of the residual nuclei at different cascade steps. The cascade calculation gives a number of residual nuclei each of

---

* I am deeply indebted to Dr. N.T. Porile and Dr. G. Friedlander for kindly performing these calculations at Brookhaven National Laboratory.

which is characterised by its Z, A and excitation energy values. These were then taken as the starting nuclei for the evaporation calculation. The latter was carried out with the same set of parameters as used in the statistical theory calculation. Five hundred cascades were run at each of several energies and three evaporations for each residual nucleus were performed for better statistical accuracy.

The formation cross-sections of the product nuclides are obtained by multiplying their calculated formation probabilities by the total reaction cross-section. The latter was calculated from Eqn. IV-20 with $c_p = 0.06$, $k_p = 0.75$ and $r_o = 1.5 \times 10^{-13}$ cm. In the case of the cascade-evaporation calculation a correction for nuclear transparency was applied. This was given by the cascade calculation.

IV-3D. Comparison Between Calculations and Experimental Results

The calculated and experimental cross-sections for the (p,xn) and (p,pxn) reactions have been plotted as a function of proton bombarding energy in Figs. 26-34 inclusive.

It is seen that both statistical theory and cascade-evaporation calculations agree very well with the experimental results of the (p,n), (p,2n), (p,pn) and (p,p2n) reactions up to the peaks of the excitation functions. Agreement between the two types of calculations indicates, of course, that the cascade-evaporation calculation predicts compound nucleus formation at energies up to 30 Mev to 35 Mev. The calculated cross-sections according to the statistical theory decrease sharply as the bombarding energy increases beyond the peaks of these excitation functions. The experimental excitation functions for the (p,n), (p,2n)

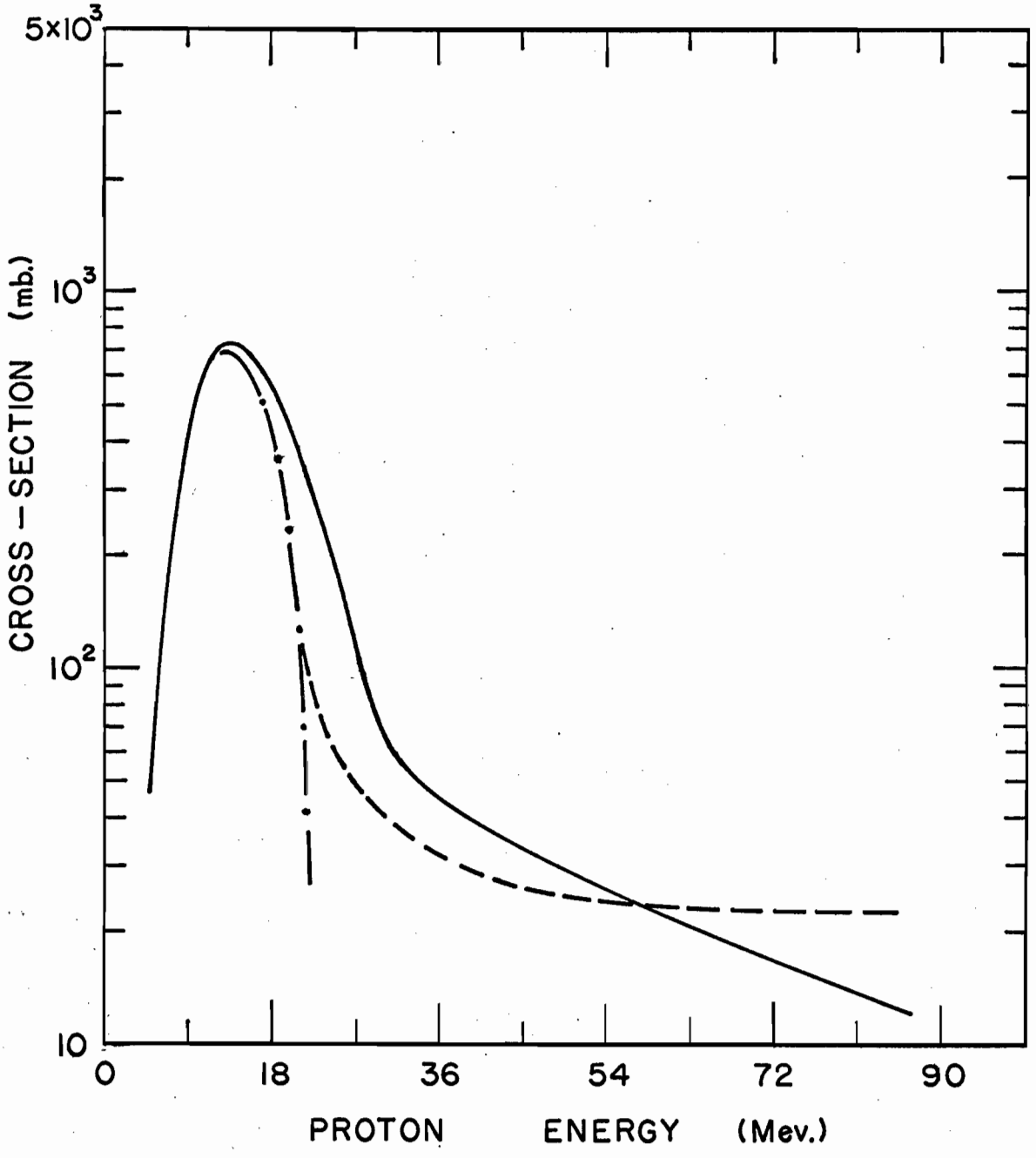

FIG. 26. A comparison of the experimental (p,n) excitation function with the statistical theory and cascade-evaporation calculations. ———— experimental. -·-·-·-·-·-·-·-·- statistical theory. - - - - - cascade-evaporation.

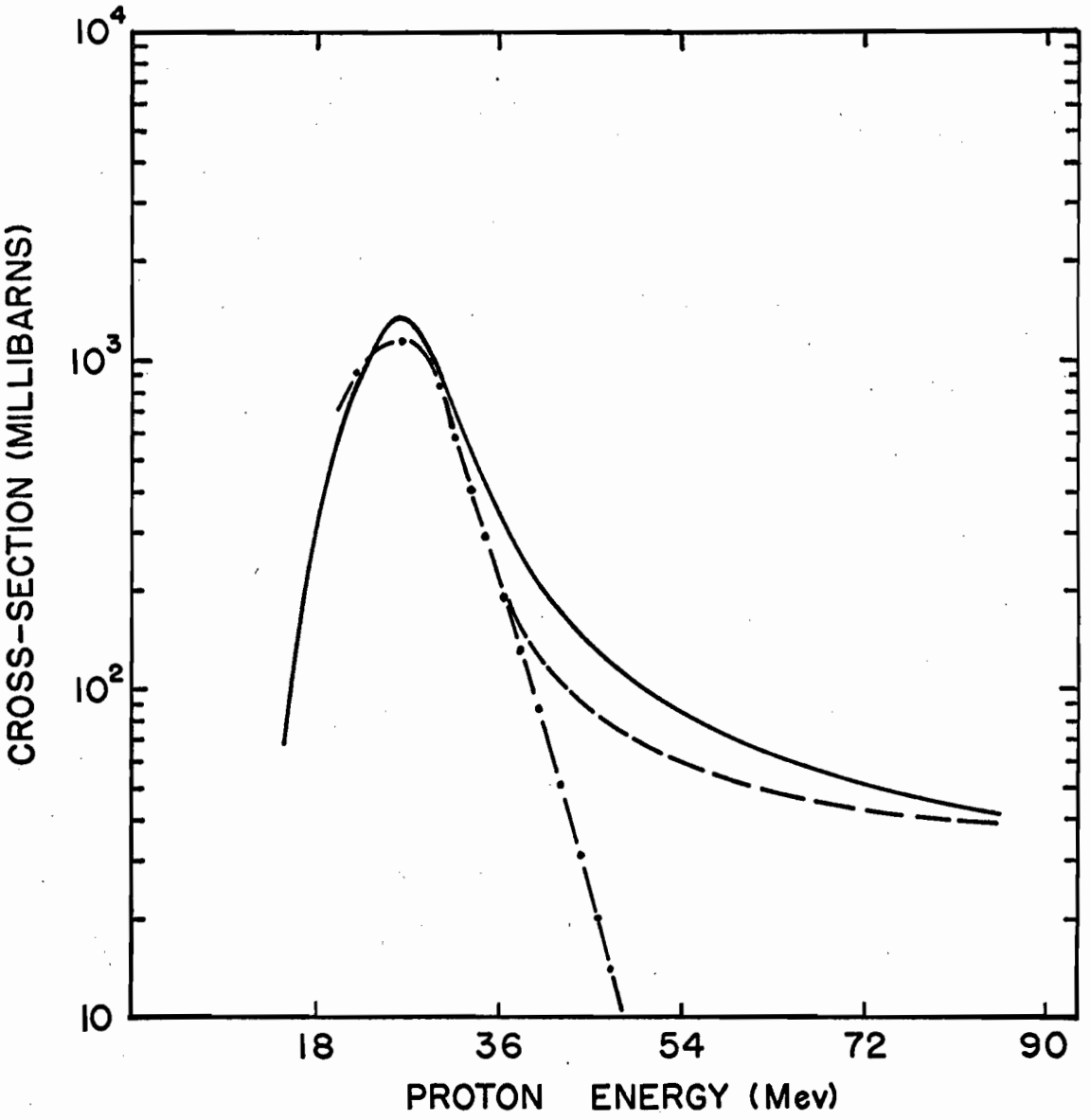

FIG. 27. A comparison of the experimental (p,2n) excitation function with the statistical theory and cascade-evaporation calculations. ———— experimental. -·-·-·-·- statistical theory. - - - - - cascade-evaporation.

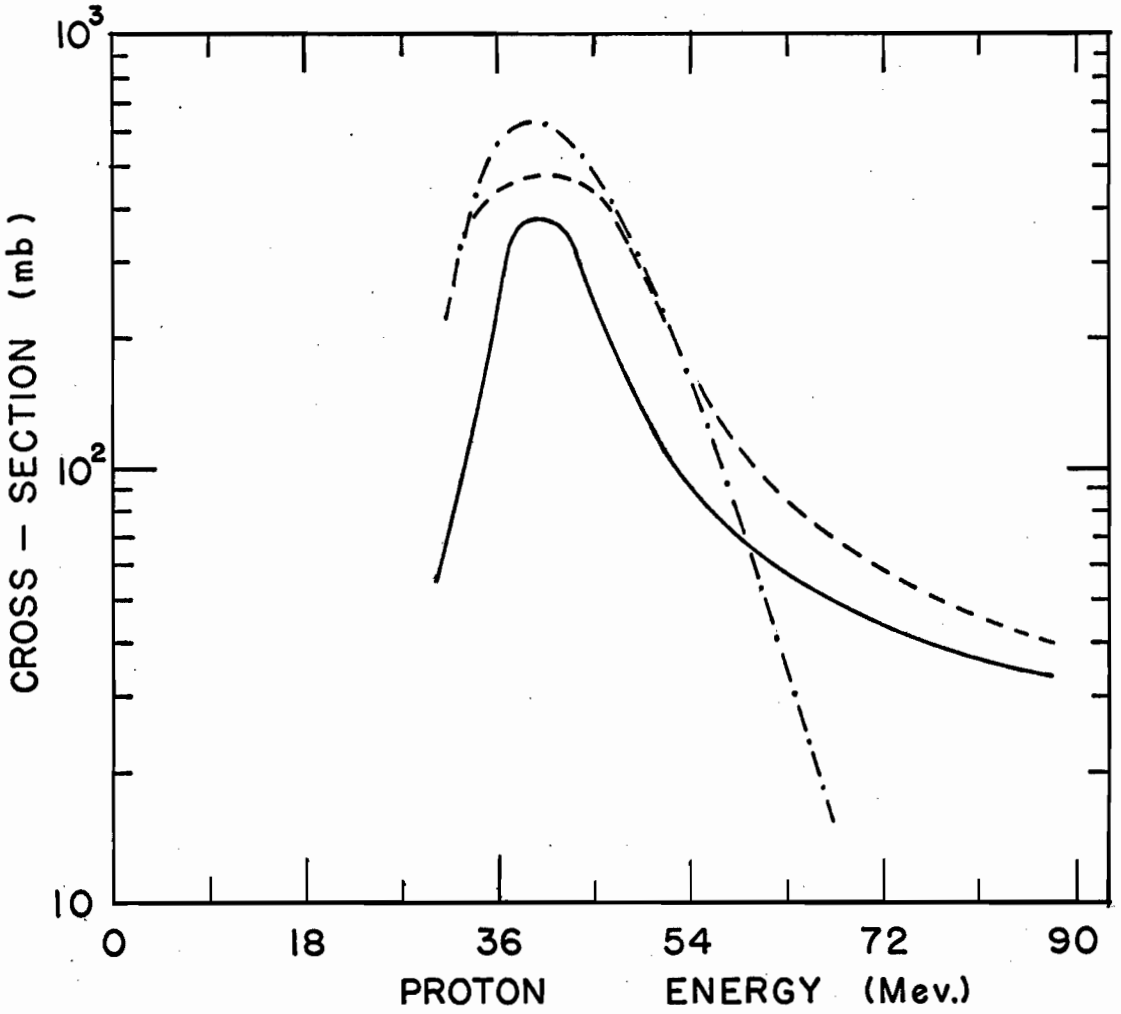

FIG. 28. A comparison of the experimental (p,3n) excitation function with the statistical theory and cascade-evaporation calculations. ———— experimental. -·-·-·-·- statistical theory. - - - - - cascade-evaporation.

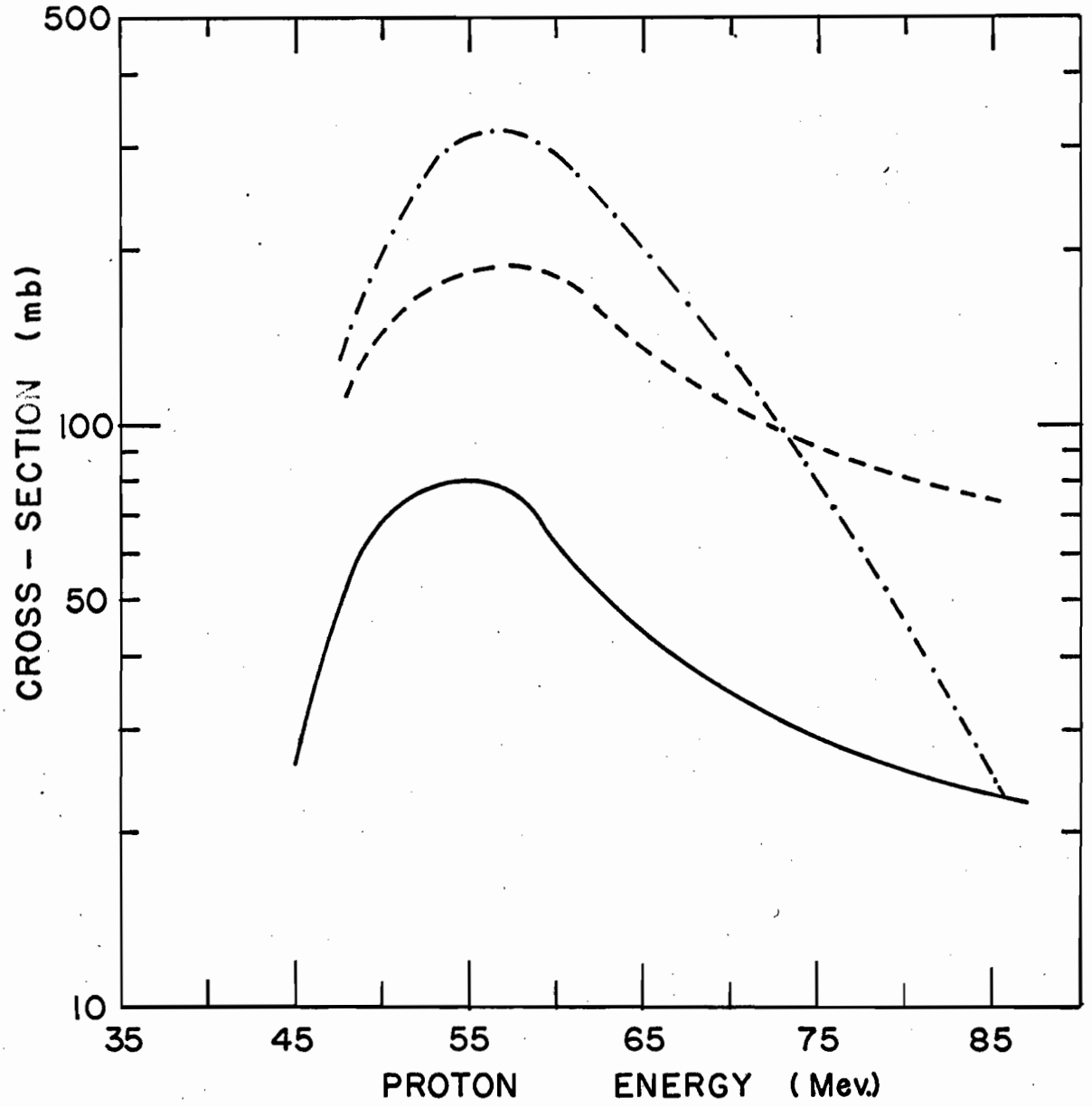

FIG. 29. A comparison of the experimental (p,4n) excitation function with the statistical theory and cascade-evaporation calculations.

——————— experimental.
—·—·—·— statistical theory.
– – – – – cascade-evaporation.

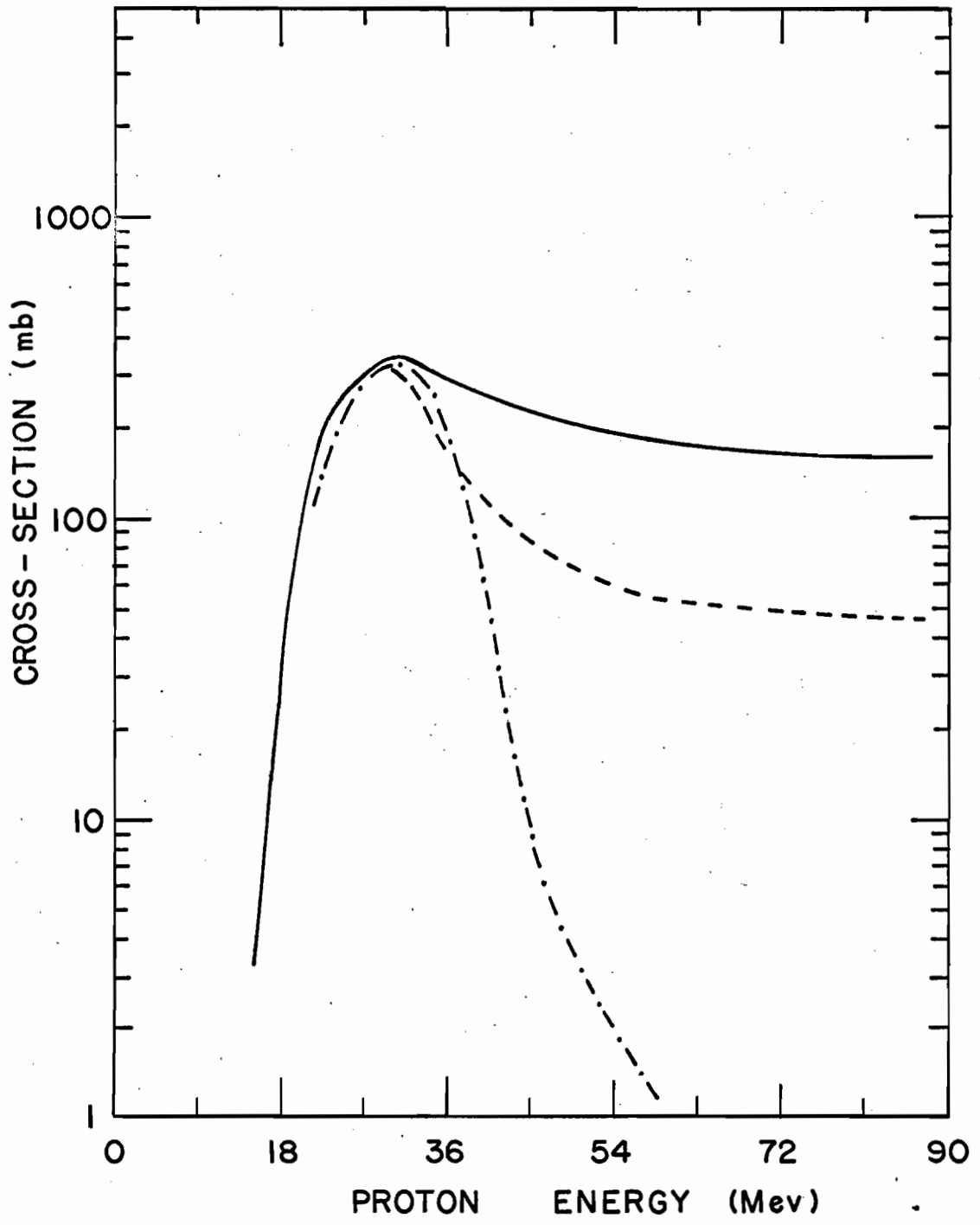

FIG. 30. A comparison of the experimental (p,pn) excitation function with the statistical theory and cascade-evaporation calculations.

———— experimental.
-·-·-·-·- statistical theory.
- - - - - cascade-evaporation.

FIG. 31. A comparison of the experimental (p,p2n) excitation function with the statistical theory and cascade-evaporation calculations.

———— experimental.

·–·–·–·–·–·–· statistical theory.

– – – – – – cascade-evaporation.

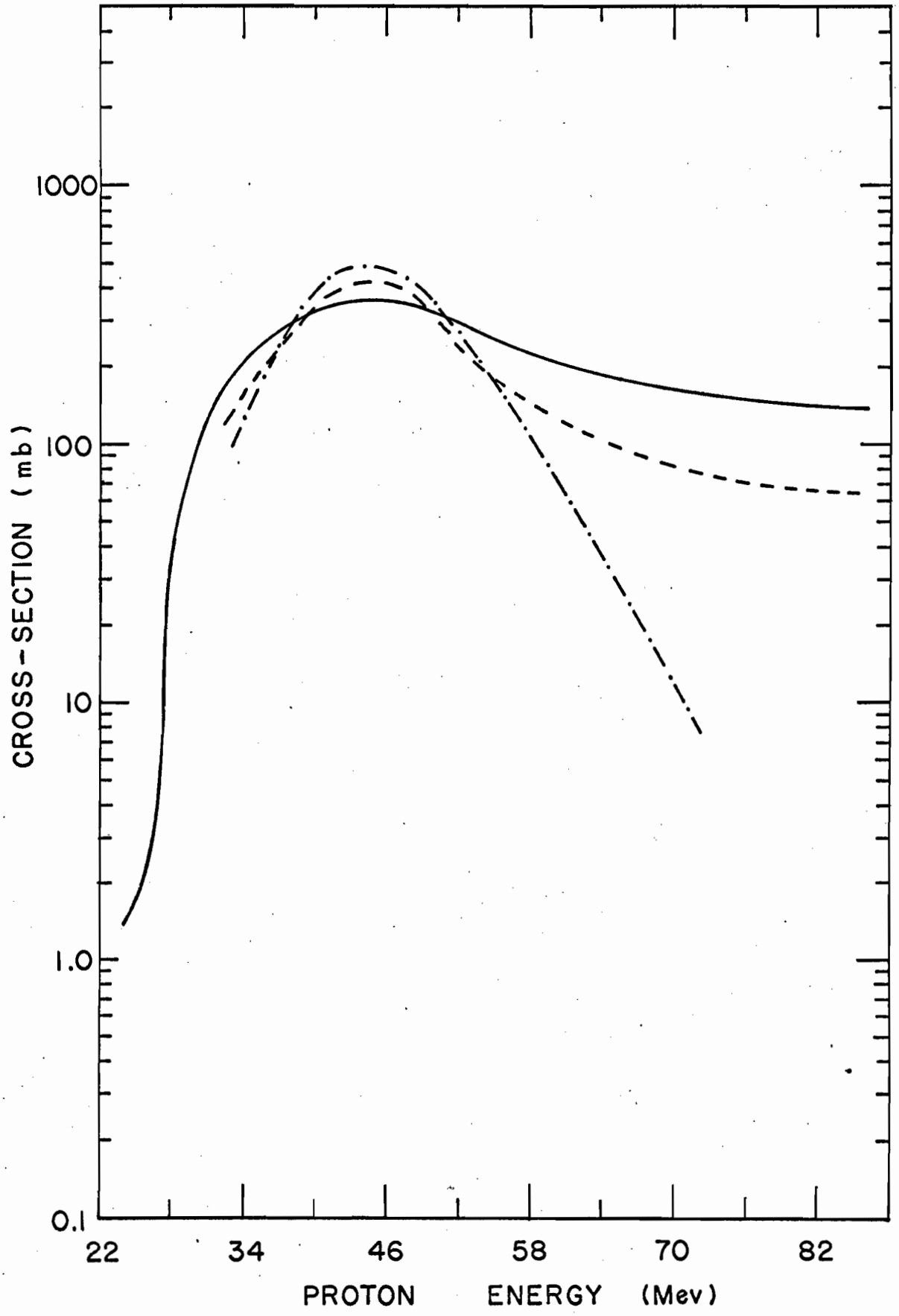
1000
100
10
1.0
0.1
CROSS-SECTION (mb)
22
34
46
58
70
82
PROTON ENERGY (Mev)

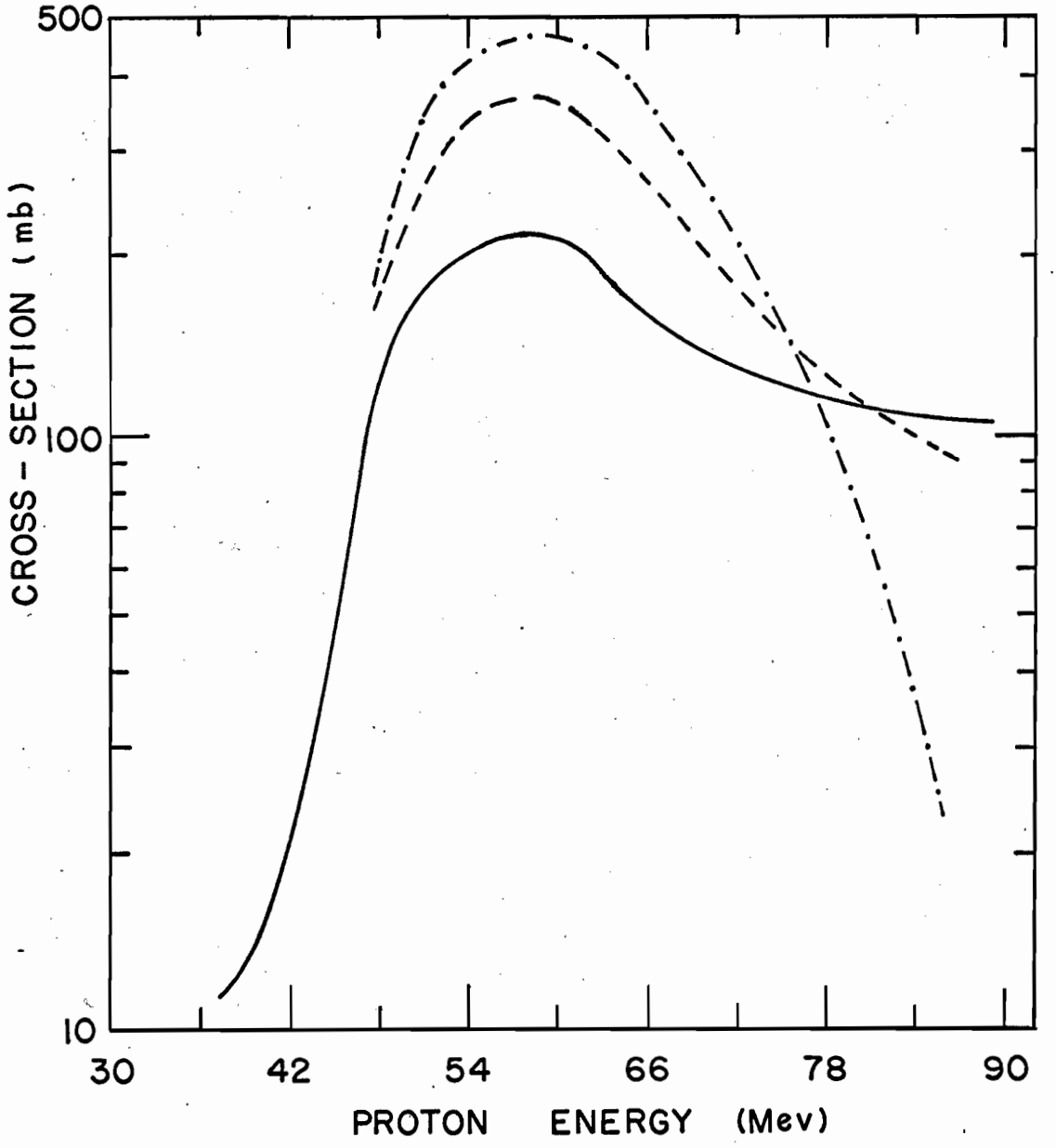

FIG. 32. A comparison of the experimental (p,p3n) excitation function with the statistical theory and cascade-evaporation calculations.

——————— experimental.
—·—·—·— statistical theory.
– – – – – cascade-evaporation.

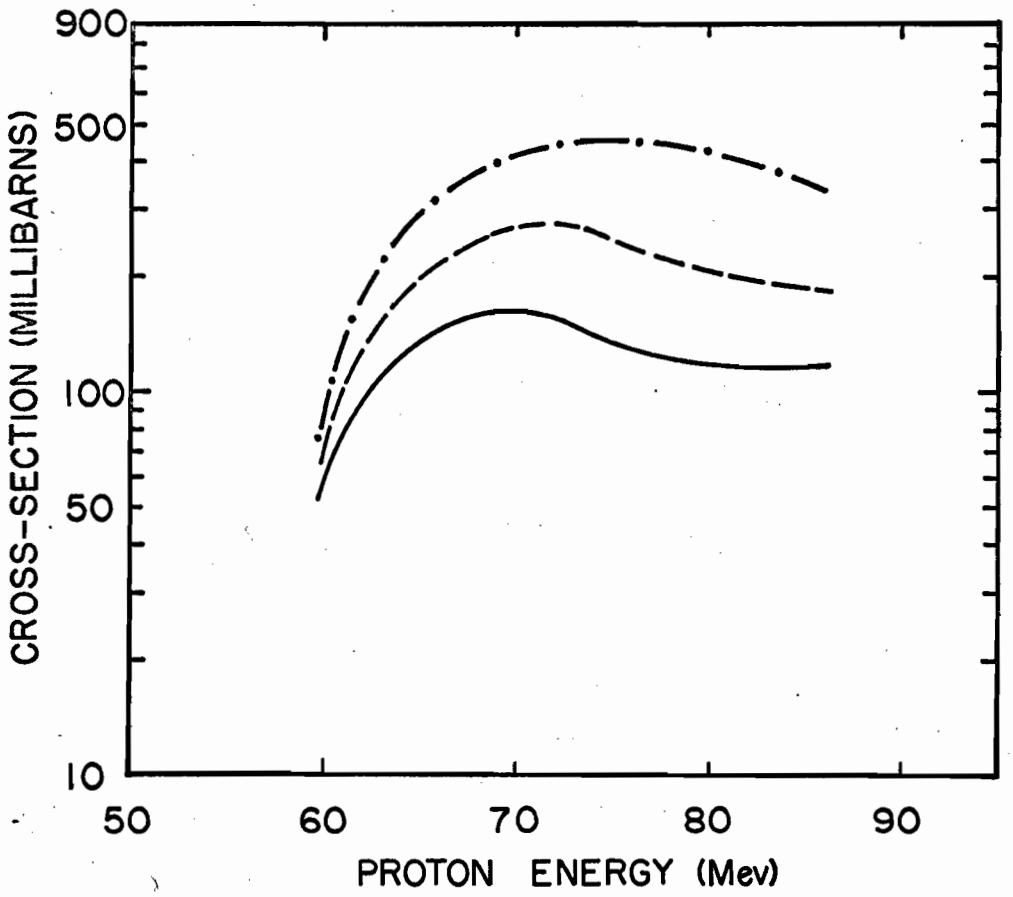

FIG. 33. A comparison of the experimental (p, p4n) excitation function with the statistical theory and cascade-evaporation calculations.

———— experimental.
—·—·—·— statistical theory.
– – – – – cascade-evaporation.

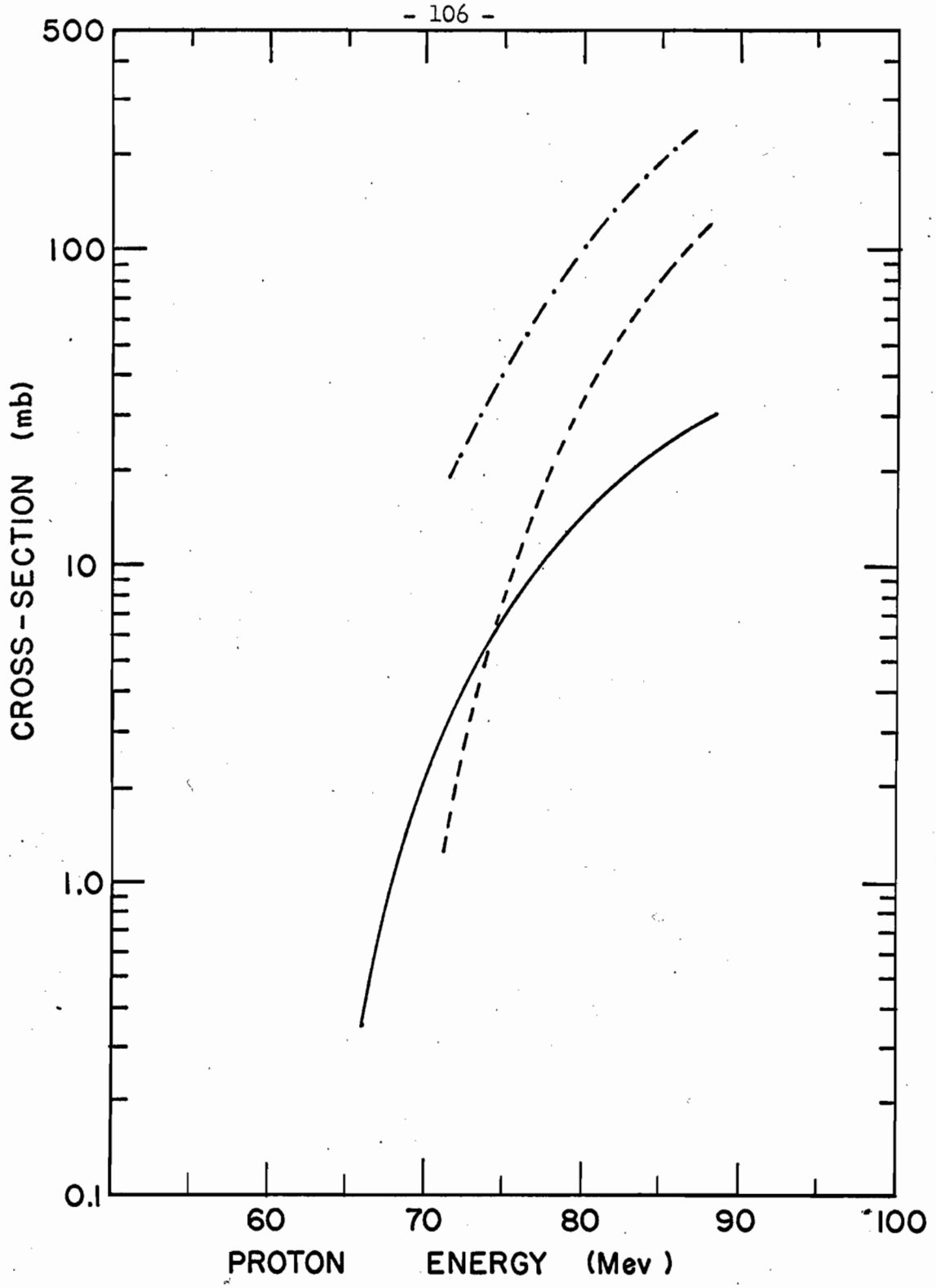

FIG. 34. A comparison of the experimental (p,p5n) excitation function with the statistical theory and cascade-evaporation calculations.

——— experimental.
-·-·-·-·- statistical theory.
– – – – – cascade-evaporation.

reactions match this decrease for some 8-15 Mev beyond the peak energy. At higher energies the experimental excitation functions are not reproduced by the statistical theory calculation. On the other hand, the cascade-evaporation calculation gives better predictions of the shapes of these excitation functions at higher energies, although the calculated values are lower than the experimental results.

The statistical theory calculation predicts large peak cross-sections for the complex reactions having higher thresholds, such as the (p,3n), (p,4n), (p,p3n), (p,p4n) reactions. The cascade-evaporation calculation is, on the other hand, somewhat more realistic. The shapes of these experimental excitation functions are well reproduced by the calculation, but the calculated values are still larger than the experimental results.

Comparisons of the experimental results with calculations show good agreement at energies up to 25-30 Mev and disagreement at higher energies. The observed discrepancy at higher energies cannot be attributed to a shortcoming of the evaporation calculation. The values of the inverse cross-sections, level density parameter 'a' and pairing energy 'δ' used in the present calculation have been shown to result in agreement with experiments in the mass region of interest. Moreover, the good agreement obtained at low energies in the present study lends support to this argument. This suggests that direct interaction processes are responsible for this discrepancy. The large cross-sections predicted by the evaporation calculation for the complex reactions are due to the fact that the inverse reaction cross-section for compound nucleus formation is taken as the total reaction cross-section. However, direct reactions reduce the total cross-section for compound nucleus formation. As a result, the experimental

values will be lower than the statistical theory predictions.

At this point we wish to comment on the validity of the statistical theory. This theory is based on the assumptions of the formation of a compound nucleus, the random phases of the levels of the compound nucleus and the independence of its decay from the mode of formation. Agreement between a statistical model calculation and an experiment provides only a ncesssary but not a sufficient condition for the proof that these assumptions are indeed correct. Any reaction, irrespective of mechanism, is governed by an apparent threshold and eventually its cross-section diminishes as other competing processes become energetically possible. We also note that the independence hypothesis is at present under question. Cohen and Rubin (86) observed from their 14.5 Mev (p,p') scattering studies that there was a preferential emission of a proton rather than a neutron when the former is the incident particle. As their observed spectra had an evaporation character and were taken at 90 degrees, one has no clear basis for ascribing the proton excess to an ordinary direct interaction. This phenomenon goes against the independence hypothesis. They gave the explanation that the incident proton may transfer most of its energy to a collective excitation of the target nucleus rather than to particle excitation and still be re-emitted. Bodansky (87) suggested that these effects could be attributed to processes for which emission does not occur in a time as short as nuclear transit time (as in conventional direct interaction processes), but still occurs so quickly that statistical equilibrium cannot be achieved. These effects are outside the predictions of the statistical theory.

As we have seen, the cascade-evaporation gives a more realistic prediction about the shapes and magnitudes of the excitation functions than

the statistical theory. In spite of the disagreement between the calculation and the experimental results, it is obvious that direct interaction plays an important role in the overall reaction mechanism. We shall, therefore, concentrate our attention on the cascade-evaporation theory.

The cascade-evaporation calculation underestimates the formation cross-sections of the simple reactions at higher energies, whereas it overestimates those of the complex reactions having higher thresholds. This may arise from the fact that the cascade calculation probably overestimates compound nucleus formation. Also it may be due to the fact that the relative number of cascades involving high energy transfer after the emission of one or two cascade particles is large. In either case the compound or residual nuclei with high excitation energy will evaporate a number of nucleons and thus result in large cross-sections for the complex reactions. Consequently, as a compensation, the simple reaction cross-sections will be underestimated.

It may be of interest at this point to scrutinise the output of the cascade calculation to see how the excitation energy is distributed in the residual nuclei. It is found from the output of the calculation that at the highest energy i.e. at 85 Mev, cascades involving the emission of 2 and 1 nucleons constitute 8 and 231 events respectively out of the initial 500 cascades. One hundred and seventy-eight events involve compound nucleus formation and 83 events lead to transparency. Thus only one nucleon-out cascades are important in the cascade process in the energy range of our interest. In order to examine the energy spectrum of the residual nuclei, the fraction of the total number of inelastic events per 10 Mev interval has been plotted versus residual excitation energy in Fig. 35. Figs. 35a, 35b, 35c correspond to bombarding energies of 33.5 Mev, 60

FIG. 35. Excitation energy spectra of residual nuclei obtained from cascade calculation at different energies. (a) 33.5 Mev (b) 60 Mev (c) 85 Mev (d) fraction of the cascades leading to compound nucleus formation at different energies.

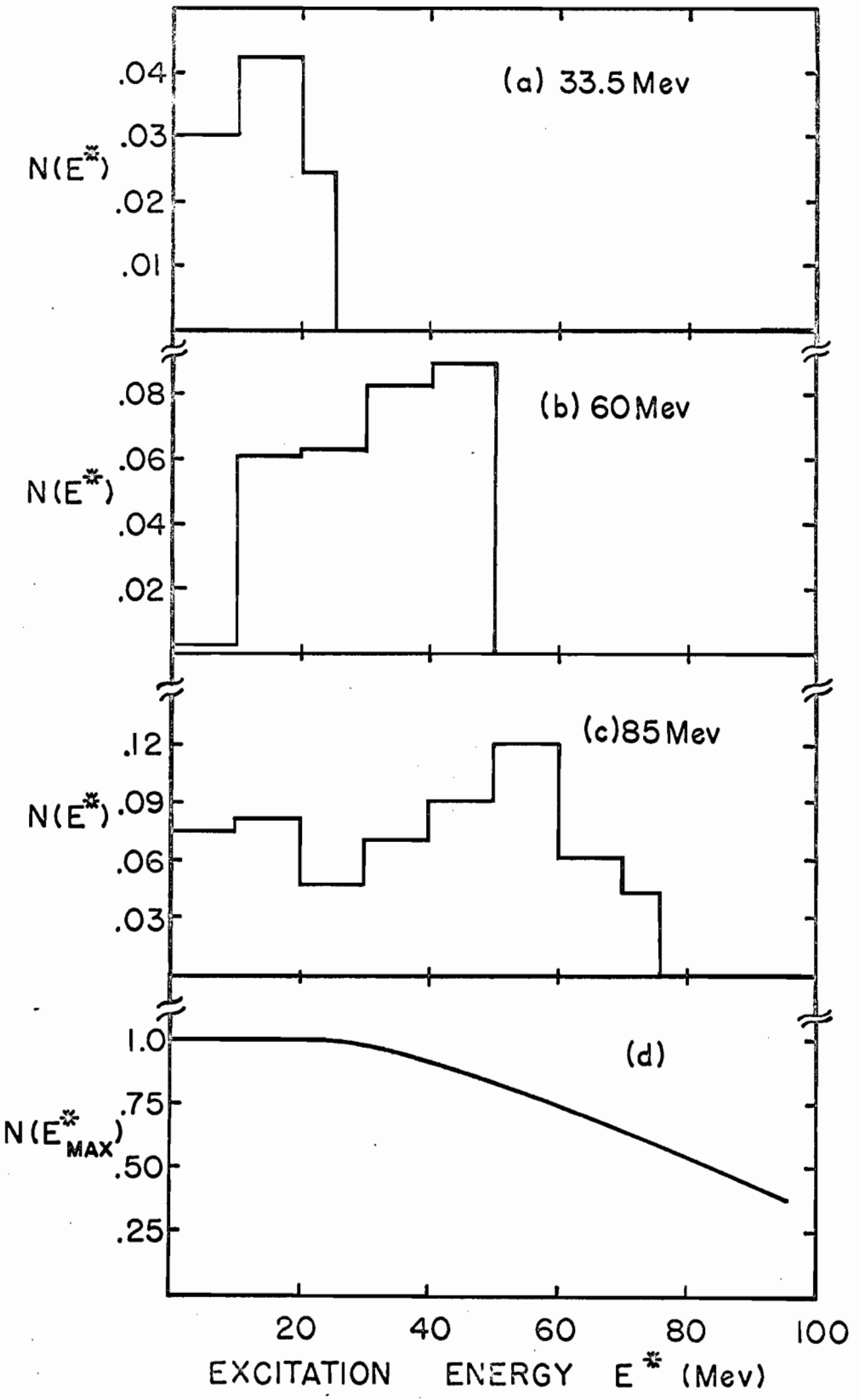
(a) 33.5 Mev
(b) 60 Mev
(c) 85 Mev
(d)
N(E*)
N(E*MAX)
.04
.03
.02
.01
.08
.06
.04
.02
.12
.09
.06
.03
1.0
.75
.50
.25
20
40
60
80
100
EXCITATION ENERGY E* (Mev)

Mev and 85 Mev respectively, and Fig. 35d shows the fraction of the total number of cascades that lead to the formation of compound nuclei. It is seen that the excitation energy E* is almost uniformly distributed between 0 and E^*_{max}. Such a flat excitation energy spectrum was also observed in the calculation of Metropolis et al (31). Furthermore, as was found there (31), the average deposition energy appears to be a slowly increasing function of the incident energy. From Fig. 35d it can be seen that even at the highest excitation energy of 92 Mev (corresponding to a bombarding energy of 85 Mev), compound nucleus formation is a surprisingly large 40 per cent. Therefore, the observed discrepancy between the calculation and the experiment may be attributed to the overestimation of compound nucleus formation at higher energies.

Now the question arises - what factors might be responsible for this possibility? The present calculation has considered the reflection and refraction of the collision partners as they enter into the new density regions of the nucleus. An unrealistic angle of refraction may overestimate the reflection of the particles at these surfaces. According to Peaslee (22), the reflection coefficient of a surface is known to be maximum when it is sharp and to decrease to zero for an infinitely diffuse surface. In view of this reasoning, the incident proton may be able to enter into the outer region of lower density, but the subsequent collision partners will be reflected more effectively from the inner surfaces of the denser regions. Consequently all or most of the collision partners will be absorbed inside the nucleus. This will lead to an overestimate of the number of compound nuclei or of residual nuclei with high excitation energy. This may give rise to the observed discrepancy between the calculation and the experiment.

A detailed analysis of the (p,pn) and (p,2n) reactions may throw some light on the actual mechanism of these simple reactions. The various reaction mechanisms mentioned below contribute to these reaction cross-sections. (a) Two nucleons are emitted in the knock-on process and the residual excitation energy is insufficient for further particle evaporation. (b) One of the collision partners is emitted in the cascade process leaving a residual excitation energy large enough to evaporate just one nucleon. (c) The (p,pn) reaction product can also be produced by the evaporation of one proton and one neutron or a deuteron from a compound nucleus. Similarly the (p,2n) reaction can also be formed by the evaporation of two neutrons. Contributions from these different mechanisms have been estimated from an approximate analysis of the calculation at 85 Mev. The analysis has been made from a knowledge of the numbers of events leading to $(Y^{88})^*$, $(Y^{89})^*$ and $(Zr^{89})^*$ in the proper energy interval and the branching ratios of proton and neutron emissions from $(Zr^{89})^*$ and $(Y^{89})^*$. The former are obtained from the output of the cascade calculation and the latter are calculated using the formulae of emission widths given by Dostrovsky et al (34). Evaporation of two nucleons at 85 Mev has a negligible contribution according to the statistical theory calculation. The results are summarised in Table XI.

The analysis shows that though there is a large difference between the calculated and the experimental values, the major portion of the cross-sections is due to the direct knock-out of one nucleon followed by the evaporation of another nucleon. The (p,pn) reaction arises mainly from the preferential proton emission in the cascade process followed by the evaporation of a neutron. A similar analysis has been made by Porile et al (6) for these same reactions of Ga^{69} at 46.5 Mev using the cascade

TABLE XI

Analysis of the (p,pn) and (p,2n) reactions of Y^{89} at 85 Mev

Reaction Mechanisms	σ(p,pn) (mb)	σ(p,2n) (mb)
Knock-out of two nucleons	5.5	-
Evaporation of one neutron	50.7	35.9
Evaporation of one proton	4.6	-
Evaporation of two nucleons (or a deuteron)	-	-
Total	60.8	35.9
Experimental	144	41

calculation of Metropolis et al (31). In contrast to the present results they found that the two nucleon knock-out process constituted about 20% of the (p,pn) reaction. This is consistent with the above finding that the calculation of Chen et al (40) underestimates the emission of energetic cascade nucleons.

An alternative way of presenting our results is to plot the mass-yield curves for different energies. The sums of cross-sections of the isobaric nuclides having mass number A have been plotted against A in Figs. 36 and 37. Since only the (p,xn) and (p,pxn) reaction cross-sections have been measured, the sums represent the partial yields of the isobaric chain. The shaded band represents the corresponding calculated values according to the cascade-evaporation theory. It is indicated by these plots

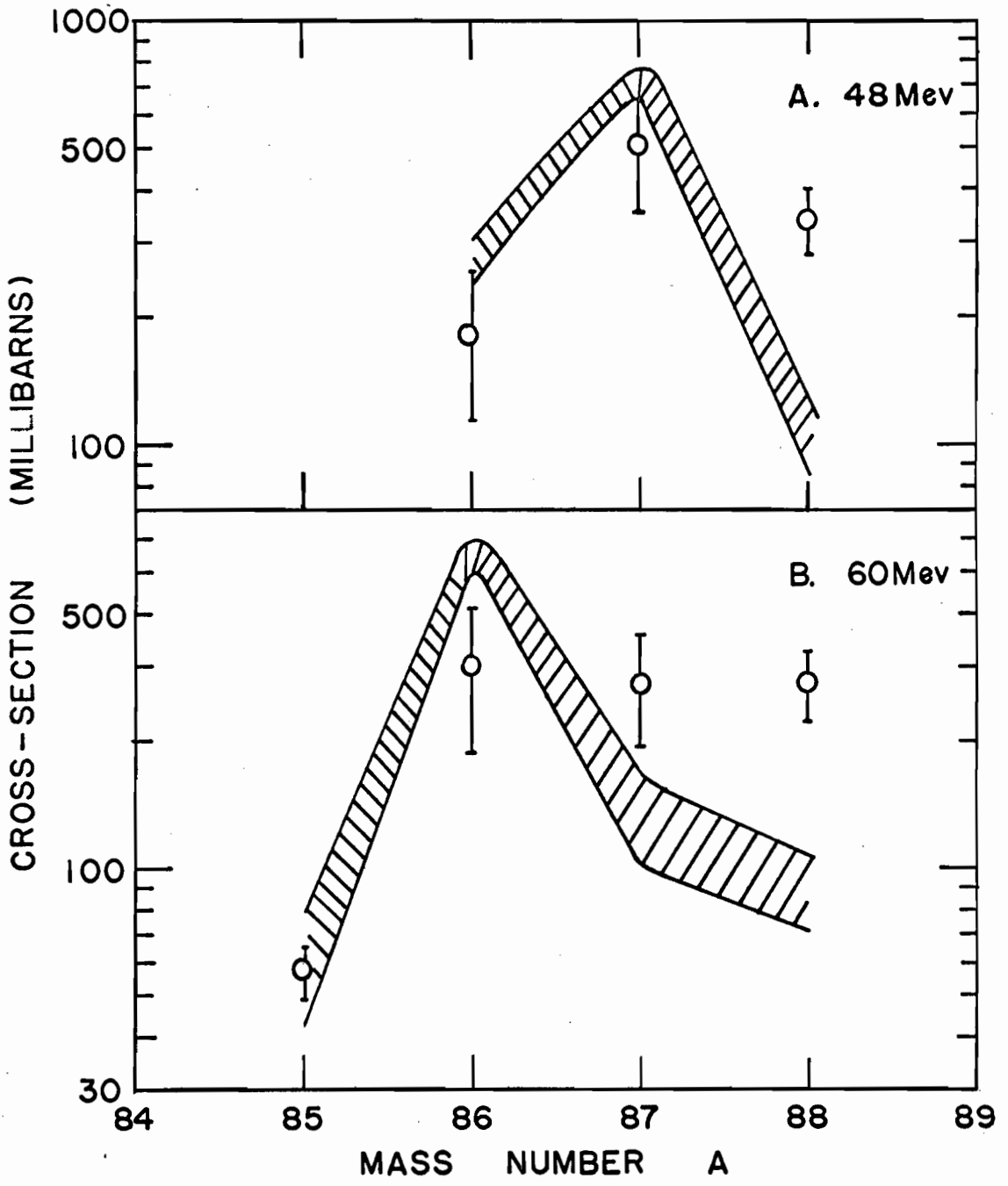

FIG. 36. A comparison of the experimental and calculated (cascade-evaporation) mass-yield curves at different energies. (A) at 48 Mev (B) at 60 Mev.

FIG. 37. A comparison of the experimental and calculated (cascade-evaporation) mass-yield curves at different energies (A) at 72 Mev (B) at 85 Mev.

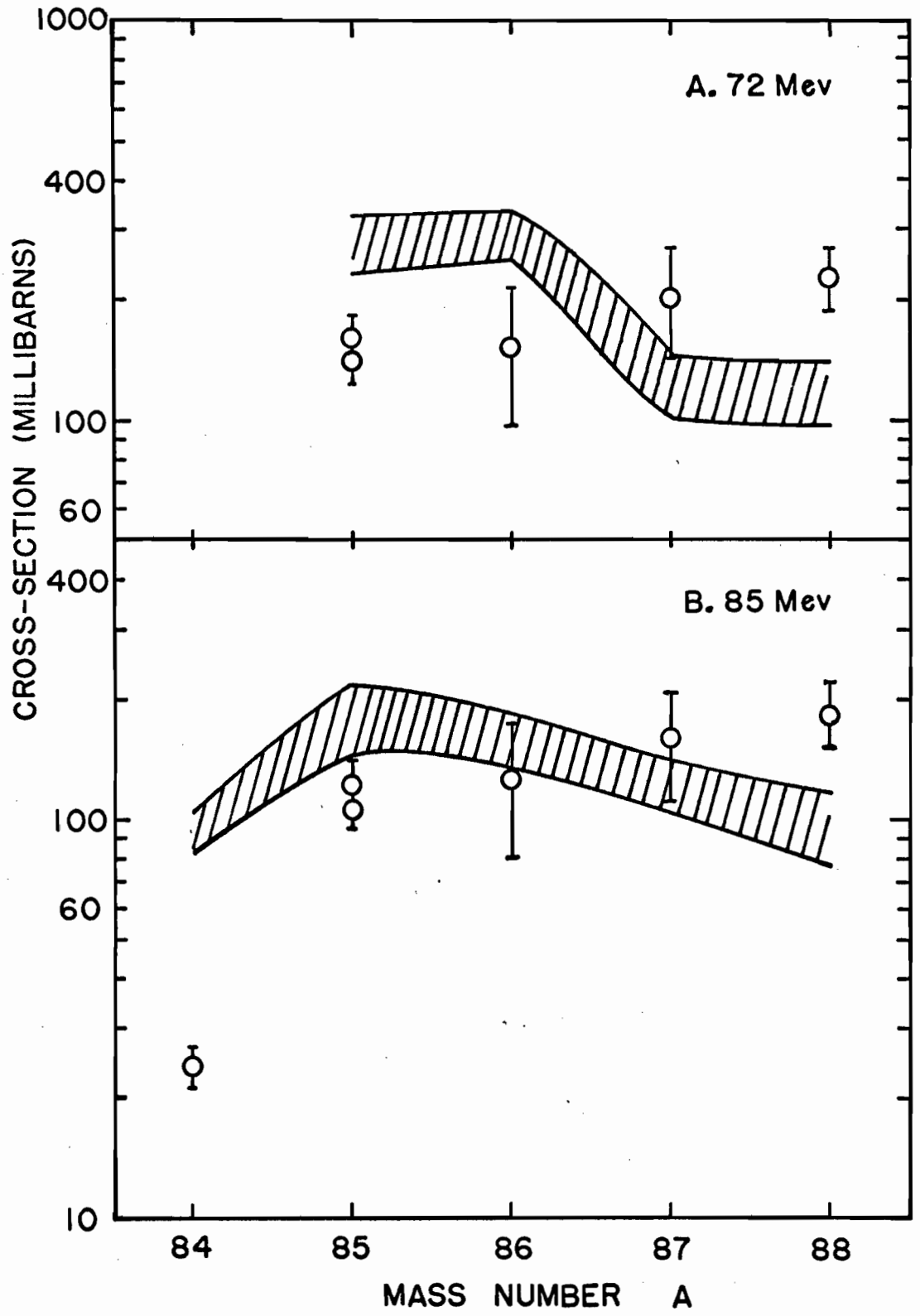
1000
400
100
60
A. 72 Mev
400
100
60
10
B. 85 Mev
CROSS-SECTION (MILLIBARNS)
84
85
86
87
88
MASS NUMBER A

that almost all the experimental points lie within 2σ (σ is the standard deviation) of the calculated values, showing a moderate agreement.

Finally, in Fig. 38 the calculated and experimental total reaction cross-sections have been plotted as a function of proton energy. The calculated values are those of the cascade-evaporation calculation. It is to be mentioned that the total reaction cross-sections presented are the sums of the (p,xn) and (p,pxn) reaction cross-sections only. When we remember the large discrepancy between the calculation and the experiment for individual excitation functions, it is amazing to find an excellent agreement in the case of the total reaction cross-sections. This is due to the fact that underestimation of the simple reaction cross-sections has been compensated by overestimation of the complex reactions. The statistical theory calculation also gives practically the same values for the total reaction cross-section as the cascade-evaporation calculation does. These facts indicate that Eqn. IV-20 in Section IV-3B is a good approximation to the total reaction cross-section.

Although we have a good deal of evidence for the importance of direct interactions, their detailed mechanism is still a conjecture. In interpreting the inelastic scattering results of 31 Mev protons on Pb, Au, Ta and Sn, Eisberg and Igo (18) proposed that the direct process occurs through free two-body collisions at the diffuse surface of the nucleus. Because of the extremely reduced nucleon density in the surface of the nucleus, either of the collision partners might escape from the nucleus without further collision. Alternatively, Hayakawa et al (88) considered inelastic scattering as due to the knock-on processes taking place throughout the nuclear volume. Butler et al (89) and Kikuchi (90) also made semi-classical calculations considering direct interactions taking place through-

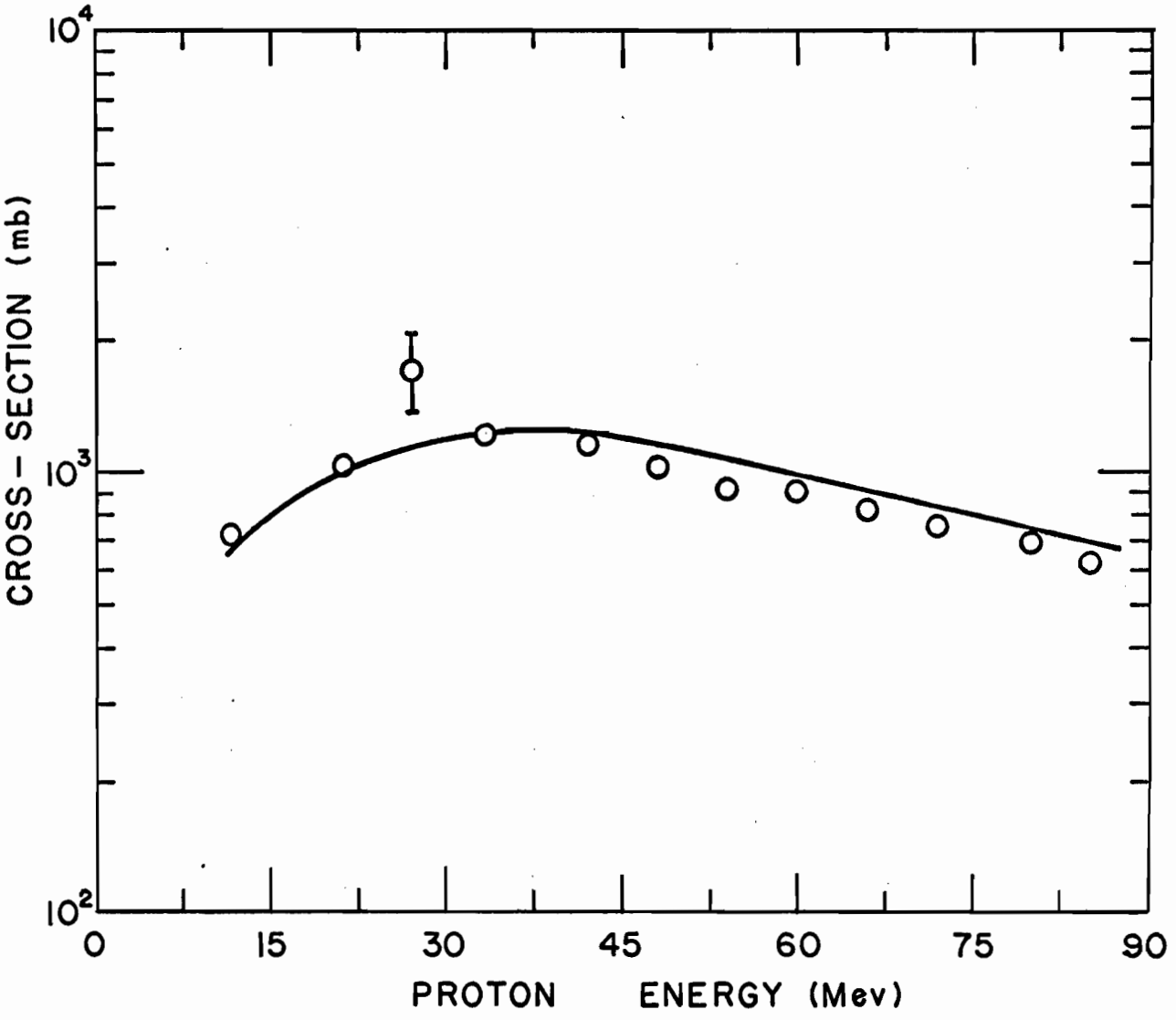

FIG. 38. A comparison of the experimental total reaction cross-section (sum of the (p,xn) and (p,pxn) reaction cross-sections) with the cascade-evaporation calculation.

out the nuclear volume. On the other hand, as already mentioned, Cohen and Rubin (86)(91) suggested a collective excitation of the nucleus due to the knock-on process occurring at the nuclear surface.

Elton and Gomes (92) calculated the angular distribution due to inelastic scattering of 31 Mev protons. They considered in one calculation the knock-on process occurring at the diffuse surface and in the other throughout the volume of the nucleus. They concluded that knock-on processes occurring at the nuclear surface make the main contribution to the inelastic scattering, while those involving the total nuclear volume contribute only a minor fraction.

It is apparent from the above discussion and also clear from physical reasons that at low energies the direct processes are likely to occur at the diffuse surface of the nucleus. However, as the bombarding energy is increased, the incident particle can lead to knock-on processes throughout the nuclear volume. These facts can also be envisaged in terms of the optical model. It is known that the imaginary part of the optical potential peaks at the nuclear surface, and broadens throughout the nuclear volume with increasing bombarding energy. Consequently, at low energies surface absorption takes place, whereas at higher energies volume absorption occurs. Thus the direct processes are likely to occur at the nuclear surface at low energies.

Though the calculation of Elton and Gomes (92) indicated a surface interaction for 31 Mev protons, this would also be the case to some extent throughout the energy range of our interest. If the collision occurs within the far interior of the nuclear volume, it is more likely for the proton to be absorbed than emitted as a cascade particle. The substantial tails of the simpler reactions indicate that the incident

proton undergoes a collision with other nucleons at the diffuse surface of the nucleus causing a small momentum transfer to the struck nucleon. The proton will then be emitted with large kinetic energy. Moreover, these high energy tails substantiate the fact that the main effect of increasing the bombarding energy is merely to increase the kinetic energy of the outgoing particles. These tails also indicate that competition as new channels open is not as strong an effect as in the low energy region.

The detailed discussion presented so far leads us to the conclusion that compound nucleus formation is the principal mechanism for proton energies up to 25-30 Mev. As the energy increases, compound nucleus formation decreases and the direct interaction process becomes predominant. High energy tails of the excitation functions arise from the direct interaction probably occurring at the nuclear surface.

Comparison between the statistical theory calculation and experimental excitation functions shows agreement at low energies and disagreement at high energies. The cascade-evaporation calculation, though far from expectation, gives somewhat more realistic predictions of both the shapes and magnitudes of the excitation functions.

NOTE: When the bulk of the thesis had been typed, Dr. G. Friedlander brought to our attention that a change in the cascade calculation was necessary in order to take into account the refraction of the incident protons at the Coulomb barrier. Dr. G. Friedlander kindly sent us the results of the modified cascade calculation at 85 Mev for the Y^{89} + p system. The modification does not significantly change the results of the cascade calculation. For example, for an initial 500 cascades, the modified calculation predicts 187 events for compound nucleus formation, 194 events for one nucleon-out cascades, 11 events for two nucleon-out cascades and 108 events for transparencies. The corresponding values given by the calculation presented here are 178, 231, 8 and 83 respectively, agreeing with the modified calculation within the statistical error. We conclude that this modification will have a negligible effect on the results of the cascade-evaporation calculations presented in this thesis.

IV-4 Isomer Ratios

IV-4A. Qualitative Aspects

The experimentally determined isomer ratios for the (p,p2n), (p,p3n) and (p,p4n) reactions have been shown in Figs. 19-21. The spins and parities of the metastable states Y^{87m}, Y^{86m} and Y^{85m} are (9/2+), (8+) and (1/2-) respectively and the corresponding values of the ground states are (1/2-), (4-) and (9/2+). In all the figures the ratios of the formation cross-section of the high spin state to that of the low spin state have been plotted against the proton bombarding energy.

It can be seen from Fig. 19 that the isomer ratios for Y^{87} increase from an initial value of less than 1 at 25 Mev to a maximum value of 2.7 at 42 Mev and then decrease to a constant value of about 2.2 at higher energies. Similarly in Fig. 20 one can see that the isomer ratios for Y^{86} increase from a value of 0.4 at 45 Mev to a maximum value of about 1.2 at 60 Mev and then decrease slowly at higher energies. The initial increase is due to the fact that as the bombarding energy is increased, the orbital angular momentum brought in by the proton becomes larger and, therefore, the total angular momentum of the compound nucleus increases. Consequently, the high spin state will be increasingly favoured. At higher energies direct interactions predominate leading to a lower energy and angular momentum transfer. As a result, the high spin isomeric state is less favoured. The initial increase and final decrease are also due to the fact that at low excitation energies the contribution of the intrinsic spins to the angular momentum of the compound nucleus will be most important. The effect of intrinsic spins is to favour the formation of the state with spin closer to that of the target nucleus

(spin of Y^{89} is 1/2-). Moreover, near the threshold, the ground state is always preferably produced, regardless of its spin. This effect is strictly due to the difference in Q-values for the formation of the two states.

It is to be noted that in the energy range of 45-60 Mev where the isomer ratios for the (p,p2n) reaction decrease due to direct interactions, the ratios for the (p,p3n) reaction increase due to the compound nucleus mechanism. This indicates that both compound nucleus formation and direct interaction contribute to the reaction mechanism in this energy range. This is consistent with the analysis in Section IV-3D where the same conclusion was drawn. The constancy of the isomer ratios at higher energies may result from the fact that the knock-on mechanism produces a spin distribution of the residual nuclei, which is approximately independent of the bombarding energy.

The isomer ratios for the (p,p4n) reaction show a sharp decrease near the threshold and then become almost constant at higher energies. It is to be mentioned that these ratios are affected by the decay of the unknown short-lived Zr^{85} nuclide. It is not known whether Zr^{85} decays to Y^{85m} or Y^{85g}, or branches between the two states. However, on scrutinising the output of the cascade-evaporation calculation, it has been found that the probability of formation of Zr^{85} is only about 15-20% that of Y^{85}. The contribution from Zr^{85} will consequently affect the isomer ratios for Y^{85} to only a small extent.

The sharp decrease near the threshold is, as already mentioned, probably due to the fact that the ground state is favourably formed near the threshold in spite of its large spin (9/2+) compared to that of the metastable state (1/2-). At energies above the threshold the isomer

ratios should have increased if the compound nucleus mechanism were valid at these energies. Thus the constant isomer ratios substantiate the fact that the spin distribution of the residual nuclei resulting from the cascade process is nearly independent of the bombarding energy.

IV-4B. An Approximate Analysis

Qualitative calculations have been performed by several authors for the prediction of the isomer ratios. Katz et al (93) calculated the isomer ratios from an initial angular momentum distribution of the compound nuclei. They assumed that all compound nuclei with total angular momentum below a certain cut-off value decay to the low spin state and the remainder feed the high spin state. Their calculation predicted fairly well the isomer ratios for a number of low energy reactions producing Br^{80}. Meadows et al (42) also calculated the isomer ratios for various (p,pn) reactions from an initial angular momentum distribution of the compound nuclei.

A similar approach has been adopted for an approximate calculation of the isomer ratios presented here. The spins of the target and the projectile have been assumed to be zero in this calculation. Under this assumption, the partial cross-section for compound nucleus formation is given by

$$\sigma_\ell(E) = \pi \lambda\!\!\!^{-2} (2\ell + 1)\, T_\ell(E) \quad \ldots\ldots \text{(IV-26)}$$

where $\lambda\!\!\!^{-}$ is the wavelength of the incident particle with an orbital angular momentum ℓ at an energy E and T_ℓ is the transmission coefficient. Values of T_ℓ (E) for the present system are not available in the energy range of

our interest. As an alternative, we have assumed the sharp cut-off approximation for the transmission coefficients as suggested by Ericson (94). This approximation implies that T_ℓ is unity for all angular momenta up to the maximum ℓ (ℓ_{max}) and zero above ℓ_{max}. Thus for each value of ℓ up to ℓ_{max}, the partial cross-section for compound nucleus formation reduces to

$$\sigma_\ell(E) = \pi\lambda\!\!\!^{-2} (2\ell + 1) \qquad \ldots\ldots \text{(IV-27)}$$

The quantity ℓ_{max} is given in the sharp cut-off approximation as

$$\ell_{max} = 2\bar{\ell} = 2\sqrt{\frac{\mu(E_{c.m.} - V)R^2}{\hbar^2}} \qquad \ldots\ldots \text{(IV-28)}$$

Here $\bar{\ell}$ is the average angular momentum brought in by the incident particle. μ is the reduced mass and $E_{c.m.}$ is the centre of mass kinetic energy of the incident particle. V is the Coulomb barrier and R is the interaction radius (taken as $1.5 \times A^{1/3}$ fermi in this calculation). ℓ_{max} has been calculated according to Eqn. IV-28 for different energies and the corresponding σ_ℓ has been calculated for all ℓ values according to Eqn. IV-27. σ_ℓ has been plotted against ℓ in Fig. 39, thus showing the angular momentum distribution of the compound nuclei for different energies.

We now assume that there exists some sharp cut-off point in the angular momentum distribution such that all compound nuclei with angular momentum equal to or less than a chosen ℓ yield the low spin isomer, whereas all compound nuclei with angular momentum greater than the cut-off ℓ yield the high spin isomer. Then the isomer ratio is calculated as

$$\frac{\sigma_H}{\sigma_L} = \sum_{\ell=K+1}^{\ell_{max}} \sigma_\ell \Big/ \sum_{\ell=0}^{K} \sigma_\ell \qquad \ldots\ldots \text{(IV-29)}$$

where K is the cut-off point. Isomer ratios were obtained using Eqn. IV-29 with different values of K over the energy range of 25-85 Mev. These ratios have been plotted against proton energy in Fig. 40. The experimental isomer ratios for Y^{87}, Y^{86} and Y^{85} have been superimposed on this plot. It is seen that between the threshold and peak energies, the experimental isomer ratios for Y^{87} lie between the calculated ratios for cut-off values of $\ell = 5$ and $\ell = 6$, whereas those for Y^{86} lie between the calculated ratios for cut-off values of $\ell = 9$ and $\ell = 10$. Beyond the peak energies, direct interactions become predominant and hence deviation of the ratios from a prediction based on compound nucleus formation is expected. The low cut-off value for Y^{87} and the high cut-off value for Y^{86} are understandable from a consideration of the spins of the two metastable states of these nuclides. The spin of $Y^{86m}(8+)$ is much larger than that of $Y^{87m}(9/2+)$. Y^{86m} will hence only be formed in the decay of the compound nuclei having high spin values. Since, as indicated in Fig. 39, the probability for forming compound nuclei with $\ell > 9$ in the energy range of interest is fairly small, the isomer ratios for Y^{86} are smaller than those for Y^{87}. However, no such conclusions can be made for the isomer ratios for Y^{85} because of the direct processes occurring in the energy range in question.

The assumption that all compound nuclei having angular momentum less than or equal to a particular cut-off value populate the low spin state and those with angular momentum above the cut-off value populate the high spin state is certainly a crude approximation. The high spin state is surely formed by the compound nuclei with angular momentum less than the cut-off value and the reverse is true for the low spin state.

Moreover, the target and projectile spins will broaden the spin distribution of the compound nuclei. The initial spin distribution of the compound nuclei will also be changed as a result of the emission of particles and photons which in general carry away a range of angular momenta. The isomer ratio will thus be determined by the spin distribution of the residual nuclei in the final de-excitation step instead of by the distribution of ℓ values in the compound nuclei. However as a first indication, it is reasonable to conclude that a cut-off value of ℓ = 5-6 in the angular momentum distribution of the compound nuclei determines the isomer ratios for Y^{87} between the threshold and peak energies. A value of ℓ = 9-10 determines the isomer ratios for Y^{86}.

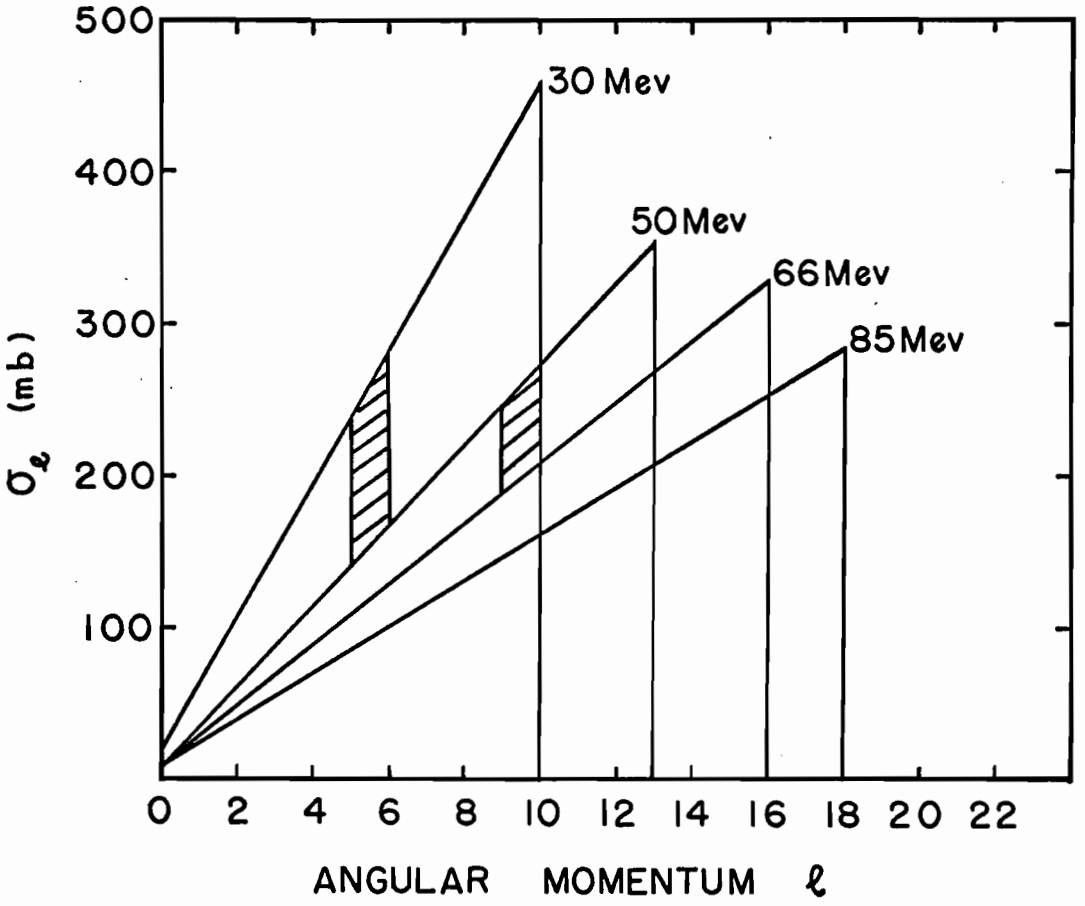

FIG. 39. Angular momentum distribution of the compound nuclei produced at different energies. The shaded areas between $\ell = 5$ and $\ell = 6$ and that between $\ell = 9$ and $\ell = 10$ represent the angular momentum cut-off values that give the reasonable agreement between the calculated and experimental isomer ratios for the (p, p2n) and (p, p3n) reactions respectively between the threshold and peak energies.

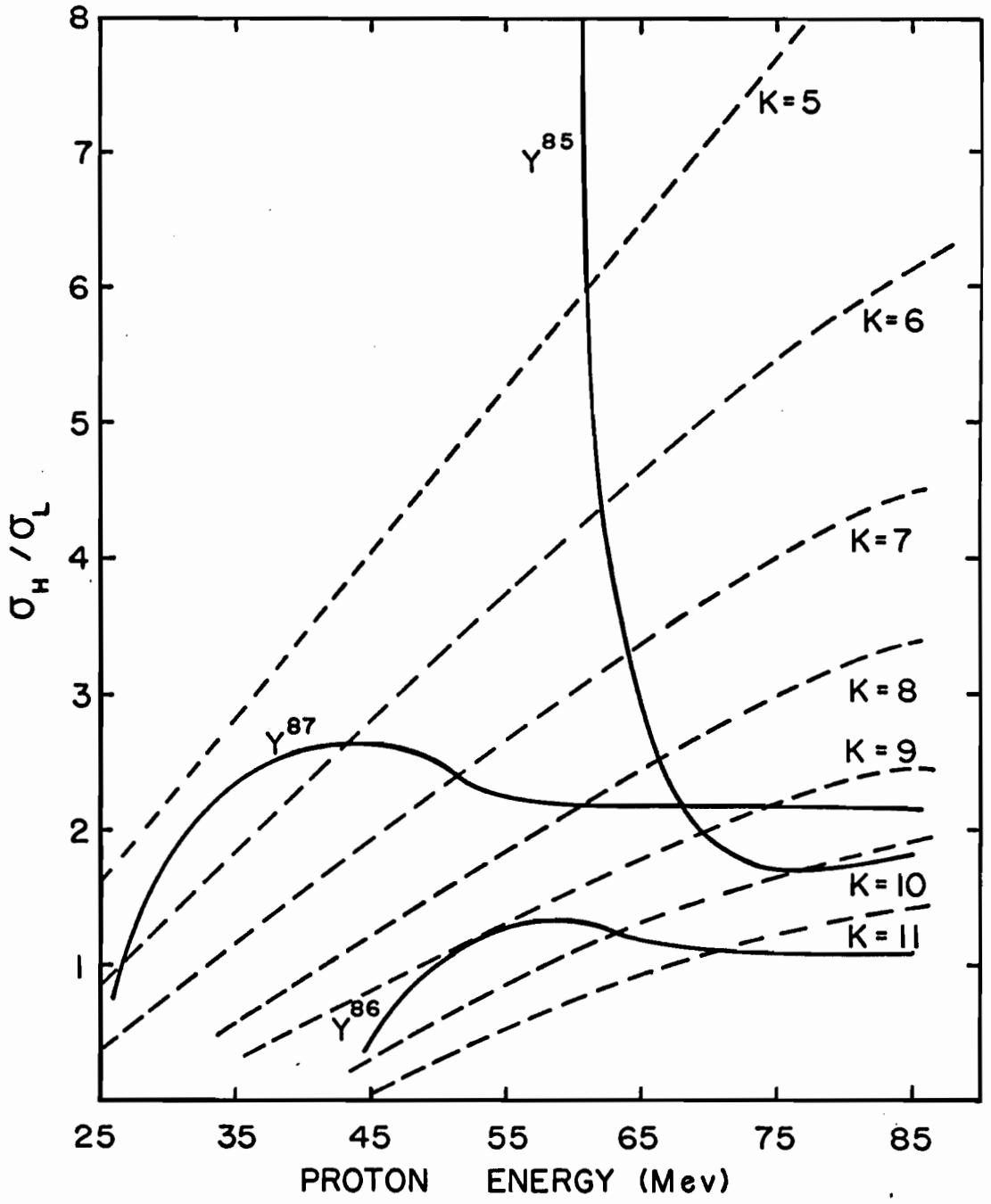

Fig. 40. A comparison of the experimental and calculated isomer ratios for the products of the (p, p2n), (p, p3n) and (p, p4n) reactions. The dashed curves represent the calculated isomer ratios for cut-off values at different angular momenta (indicated by K on each curve). The solid curves represent the experimental isomer ratios for Y^{87}, Y^{86} and Y^{85} nuclides as indicated on the curves.

V. SUMMARY

Excitation functions for the (p,xn) and (p,pxn) reactions induced in Y^{89} by 5-85 Mev protons have been measured by radiochemical techniques. All the excitation functions have the expected shapes and magnitudes. They exhibit several features which can be attributed to a compound nucleus mechanism at low energies and a cascade-evaporation mechanism at higher energies.

An approximate analysis has been made in order to understand the observed constancy of the isobaric ratios $\sigma(p,2n)/\sigma(p,pn)$, $\sigma(p,3n)/\sigma(p,p2n)$ and $\sigma(p,4n)/\sigma(p,p3n)$ at higher energies. The analysis indicates that the cascade process is the decisive phase in giving the same values for all the ratios.

The measured excitation functions have been compared with the statistical theory and cascade-evaporation calculations. Both calculations agree fairly well with the experimental values at energies up to the peak of the simple (p,n), (p,2n), (p,pn), (p,p2n) excitation functions. The statistical theory predicts too large peak cross-sections for the complex (p,3n), (p,4n), (p,p3n), (p,p4n) and (p,p5n) reactions. The cascade-evaporation calculation, on the other hand, matches the shapes of all excitation functions. However, at higher energies, this calculation also gives too low cross-sections for the simple reactions and too large cross-sections for the complex reactions.

The analysis shows that compound nucleus formation is the principal reaction mechanism at energies up to 25-30 Mev. At higher energies compound nucleus formation decreases and direct interactions predominate. The high energy tails of the excitation functions for the simple reactions

have been interpreted in terms of knock-on processes occurring at the diffuse surface of the nucleus.

The isomer ratios for Y^{87}, Y^{86} and Y^{85} have been measured. These ratios indicate that between the threshold and peak energies, compound nucleus formation is the main reaction mechanism. However, beyond the peak energies direct interactions become predominant. An approximate calculation has been performed for the isomer ratios for Y^{87} and Y^{86} using the sharp cut-off approximation. The calculation indicates that all compound nuclei with angular momentum less than or equal to ℓ = 5-6 populate the low spin isomer of Y^{87} and those with angular momentum above ℓ = 5-6 populate the high spin isomer of Y^{87}. A similar cut-off value of ℓ = 9-10 in the angular momentum distribution of the compound nuclei is consistent with the experimental isomer ratios for Y^{86} between the threshold and peak energies.

APPENDIX

I. Radioactive Decay Equations

Let us consider the decay chain

$$A \longrightarrow B \longrightarrow C \longrightarrow$$

where A, B and C are the radioactive species.

The disintegration rate of C at any separation time is composed of:

(a) the disintegration rate due to growth of C through the chain $A \longrightarrow B \longrightarrow C \longrightarrow$ during the bombardment, multiplied by $e^{-\lambda_3 t}$.

(b) the disintegration rate due to growth of C from the chain $B \longrightarrow C \longrightarrow$ during the bombardment, multiplied by $e^{-\lambda_3 t}$.

(c) the disintegration rate due to growth of C through the chain $A \longrightarrow B \longrightarrow C \longrightarrow$, during separation time.

(d) the disintegration rate due to growth from the chain $B \longrightarrow C \longrightarrow$ during separation time.

(e) the disintegration rate due to independently formed C during the bombardment, multiplied by $e^{-\lambda_3 t}$.

Before we calculate these contributions individually, we define the following symbols to be used in the derivation.

D_1, D_2, D_3 = disintegration rates of A, B and C respectively.

λ_1, λ_2, λ_3 = decay constants of A, B, and C respectively.

N_1, N_2, N_3 = number of atoms of A, B and C respectively.

t_1 and t_2 = duration of bombardment and time between end of bombardment and separation of C from A and B.

Now we shall calculate the contributions (a), (b), (c), (d) and

(e) as follows:-

(a) We know that at the end of bombardment t the disintegration rate of independently formed species A is given by

$$D_1 = In\,\sigma_1(1 - e^{-\lambda_1 t})$$
$$= R_1(1 - e^{-\lambda_1 t}) \qquad \ldots\ldots (I\text{-}1)$$

where $R_1 = In\sigma_1$

I = incident proton intensity per unit time.

n = number of target nuclei per cm^2.

σ_1 = formation cross-section of species A.

Now the species B is formed at the rate at which species A decays, $\lambda_1 N_1$ and itself decays at the rate, $\lambda_2 N_2$. Thus,

$$\frac{dN_2}{dt} = \lambda_1 N_1 - \lambda_2 N_2 \qquad \ldots\ldots (I\text{-}2)$$

From Eq. (I-1) we have

$$\lambda_1 N_1 = D_1 = R_1(1 - e^{-\lambda_1 t})$$

Therefore,

$$\frac{dN_2}{dt} + \lambda_2 N_2 = R_1(1 - e^{-\lambda_1 t})$$

On integration, one gets

$$N_2 e^{\lambda_2 t} = R_1 \int \left[1 - e^{-\lambda_1 t}\right] e^{\lambda_2 t}\, dt + A$$

$$= R_1\left[\frac{e^{\lambda_2 t}}{\lambda_2} - \frac{e^{(\lambda_2-\lambda_1)t}}{(\lambda_2-\lambda_1)}\right] + A \qquad \ldots\ldots (I\text{-}3)$$

where A is the integration constant.

When $t = 0$, $N_2 = 0$, and therefore,

$$A = -R_1\left[\frac{1}{\lambda_2} - \frac{1}{(\lambda_2-\lambda_1)}\right]$$

Inserting the value of A in Eqn. I-3 and dividing throughout by $e^{\lambda_2 t}$, one gets

$$N_2 = R_1\left[\frac{1}{\lambda_2} - \frac{e^{-\lambda_1 t}}{(\lambda_2-\lambda_1)} - \frac{e^{-\lambda_2 t}}{\lambda_2} + \frac{e^{-\lambda_2 t}}{(\lambda_2-\lambda_1)}\right]$$

$$= \frac{R_1}{\lambda_2}\left[1 - \frac{\lambda_2 e^{-\lambda_1 t} - \lambda_1 e^{-\lambda_2 t}}{(\lambda_2-\lambda_1)}\right]$$

$$\lambda_2 N_2 = R_1\left[1 - \frac{\lambda_2 e^{-\lambda_1 t} - \lambda_1 e^{-\lambda_2 t}}{(\lambda_2-\lambda_1)}\right] \qquad \ldots\ldots (I\text{-}4)$$

where $R_1 = \dfrac{D_1}{(1-e^{-\lambda_1 t})}$, as one can see from Eqn. I-1.

Now if the time of bombardment is t_1, and if one represents the disintegration rate of A at the end of bombardment by D_1^o and that of B as $D_2^{(a)}$ due to growth from A during bombardment, then

$$D_2^{(a)} = \frac{D_1^o}{(1-e^{-\lambda_1 t_1})}\left[1 - \frac{\lambda_2 e^{-\lambda_1 t_1} - \lambda_1 e^{-\lambda_2 t_1}}{(\lambda_2-\lambda_1)}\right] \ldots\ldots (I\text{-}5)$$

From $D_2^{(a)}$ we can calculate the disintegration rate of C, $D_3^{(a)}$, at the end of bombardment due to growth from A through the chain, as follows:

$$\frac{dN_3}{dt} = \lambda_2 N_2 - \lambda_3 N_3$$

Using Eqn. I-4 for $\lambda_2 N_2$ in the above relation, we get

$$\frac{dN_3}{dt} + \lambda_3 N_3 = R_1 \left[1 - \frac{\lambda_2 e^{-\lambda_1 t} - \lambda_1 e^{-\lambda_2 t}}{(\lambda_2 - \lambda_1)} \right]$$

Integration of the above equation and then evaluation of the integration constant at t = 0 leads to the following form for a duration of bombardment t_1

$$N_3 = \left[\frac{1}{\lambda_3} - \frac{\lambda_2 e^{-\lambda_1 t_1}}{(\lambda_3 - \lambda_1)(\lambda_2 - \lambda_1)} + \frac{\lambda_1 e^{-\lambda_2 t_1}}{(\lambda_3 - \lambda_2)(\lambda_2 - \lambda_1)} - \frac{e^{-\lambda_3 t_1}}{\lambda_3} + \frac{\lambda_2 e^{-\lambda_3 t_1}}{(\lambda_3 - \lambda_1)(\lambda_2 - \lambda_1)} - \frac{\lambda_1 e^{-\lambda_3 t_1}}{(\lambda_3 - \lambda_2)(\lambda_2 - \lambda_1)} \right]$$

Multiplying throughout by λ_3 and simplifying and also considering the decay during the separation time t_2, one gets for the disintegration rate of C at the end of separation from this contribution,

$$\left[D_3^{(a)} \right]_{t_2} = \frac{D_1^o}{(1 - e^{-\lambda_1 t_1})} \left[(1 - e^{-\lambda_3 t_1}) - \frac{\lambda_2 \lambda_3 \left[e^{-\lambda_1 t_1} - e^{-\lambda_3 t_1} \right]}{(\lambda_3 - \lambda_1)(\lambda_2 - \lambda_1)} + \frac{\lambda_1 \lambda_3 \left[e^{-\lambda_2 t_1} - e^{-\lambda_3 t_1} \right]}{(\lambda_3 - \lambda_2)(\lambda_2 - \lambda_1)} \right] e^{-\lambda_3 t_2} \quad \ldots\ldots (I\text{-}6)$$

(b) The disintegration rate of C at the end of bombardment due to growth during bombardment from the independently formed B is given by Eqn. I-5 with replacement of λ_1 by λ_2, λ_2 by λ_3, D_1^o by D_2^o and $D_2^{(a)}$ by $D_3^{(b)}$. Therefore, considering its decay during separation time t_2, one obtains this disintegration rate of C at the end of separation as

$$\left[D_3^{(b)}\right]_{t_2} = \frac{D_2^o}{(1-e^{-\lambda_2 t_1})}\left[1 - \frac{\lambda_3 e^{-\lambda_2 t_1} - \lambda_2 e^{-\lambda_3 t_1}}{(\lambda_3-\lambda_2)}\right] e^{-\lambda_3 t_2} \quad \ldots\ldots (I-7)$$

(c) The disintegration rate of C due to growth from A through the chain A ---> B ---> C ---> during separation time t is obtained as follows. The rate of growth of B from A is given by

$$\frac{dN_2}{dt} = \lambda_1 N_1 - \lambda_2 N_2$$

$$\frac{dN_2}{dt} + \lambda_2 N_2 = \lambda_1 N_1^o e^{-\lambda_1 t}$$

On integration,

$$N_2 e^{\lambda_2 t} = \int \lambda_1 N_1^o e^{(\lambda_2-\lambda_1)t}\, dt + A$$

$$= \frac{\lambda_1 N_1^o}{(\lambda_2-\lambda_1)} e^{(\lambda_2-\lambda_1)t} + A \quad \ldots\ldots (I-8)$$

When $t = 0$, $N_2 = 0$, therefore,

$$A = -\frac{\lambda_1 N_1^o}{(\lambda_2-\lambda_1)}$$

Putting the value of A in (I-8) and dividing throughout by $e^{\lambda_2 t}$ one finds

$$N_2 = \frac{\lambda_1 N_1^o}{(\lambda_2-\lambda_1)} e^{-\lambda_1 t} - \frac{\lambda_1 N_1^o}{(\lambda_2-\lambda_1)} e^{-\lambda_2 t}$$

$$= \frac{\lambda_1 N_1^o}{(\lambda_2-\lambda_1)} \left[e^{-\lambda_1 t} - e^{-\lambda_2 t} \right]$$

$$\left[D_2^{(c)} \right]_{t_2} = \lambda_2 N_2$$

$$= \frac{\lambda_2 D_1^o}{(\lambda_2-\lambda_1)} \left[e^{-\lambda_1 t_2} - e^{-\lambda_2 t_2} \right] \qquad \ldots\ldots (I\text{-}9)$$

where $D_2^{(c)}$ represents the disintegration rate of B at the end of separation due to growth from A.

Similarly the rate of growth of C from B which is formed from A during the separation time can be obtained by

$$\frac{dN_3}{dt} = \lambda_2 N_2 - \lambda_3 N_3$$

Putting Eqn. I-9 for $\lambda_2 N_2$ in the above relation and simplifying after integration one gets the disintegration rate of C at the end of separation t_2 as

$$\left[D_3^{(c)} \right]_{t_2} = \lambda_3 \lambda_2 D_1^o \left[\frac{e^{-\lambda_1 t_2}}{(\lambda_3-\lambda_1)(\lambda_2-\lambda_1)} - \frac{e^{-\lambda_2 t_2}}{(\lambda_3-\lambda_2)(\lambda_2-\lambda_1)} + \frac{e^{-\lambda_3 t_2}}{(\lambda_3-\lambda_1)(\lambda_3-\lambda_2)} \right] \qquad \ldots\ldots (I\text{-}10)$$

(d) The disintegration rate of C due to growth from the independently formed B during separation time is given by Eqn. I-9, with the replacement of λ_1 by λ_2, λ_2 by λ_3, D_1^o by D_2^o and $D_2^{(c)}$ by $D_3^{(d)}$. Therefore,

$$\left[D_3^{(d)}\right]_{t_2} = \lambda_3 N_3 = \frac{\lambda_3 D_2^o}{(\lambda_3-\lambda_2)}\left[e^{-\lambda_2 t_2} - e^{-\lambda_3 t_2}\right] \quad \ldots\ldots \text{(I-11)}$$

(e) The disintegration rate of independently formed C at the end of separation t_2 is given by

$$\left[D_3^{(3)}\right]_{t_2} = D_3^o\, e^{-\lambda_3 t_2} \quad \ldots\ldots \text{(I-12)}$$

where D_3^o is the disintegration rate of independently formed C at the end of bombardment. This is the quantity we wish to determine.

Therefore, the total disintegration rates D_2 and D_3 of B and C respectively at the end of separation are given as

$$D_2 = \left[D_2^{(a)}\right]_{t_2} + \left[D_2^{(c)}\right]_{t_2} + \left[D_2^{(e)}\right]_{t_2} \quad \ldots\ldots \text{(I-13)}$$

$$D_3 = \left[D_3^{(a)}\right]_{t_2} + \left[D_3^{(b)}\right]_{t_2} + \left[D_3^{(c)}\right]_{t_2} + \left[D_3^{(d)}\right]_{t_2} + \left[D_3^{(e)}\right]_{t_2} \quad \ldots\ldots \text{(I-14)}$$

The first term in Eqn. I-13 is given by Eqn. I-5 multiplied by $e^{-\lambda_2 t_2}$. The second term is given by Eqn. I-9 and the third term by $D_2^o\, e^{-\lambda_2 t_2}$. Therefore, putting all these values in Eqn. I-13 we get

$$D_2 = \frac{D_1^o}{(1-e^{-\lambda_1 t_1})}\left[1 - \frac{\lambda_2 e^{-\lambda_1 t_1} - \lambda_1 e^{-\lambda_2 t_1}}{(\lambda_2-\lambda_1)}\right] e^{-\lambda_2 t_2} + \frac{\lambda_2 D_1^o}{(\lambda_2-\lambda_1)}\left[e^{-\lambda_1 t_2} - e^{-\lambda_2 t_2}\right] + D_2^o\, e^{-\lambda_2 t_2} \quad \ldots\ldots \text{(I-15)}$$

Similarly, putting the values of all the terms in Eqn. I-14, the following expression is obtained

$$D_3 = \frac{D_1^o}{(1-e^{-\lambda_1 t_1})}\left[(1-e^{-\lambda_3 t_1}) - \frac{\lambda_2\lambda_3\,(e^{-\lambda_1 t_1} - e^{-\lambda_3 t_1})}{(\lambda_3-\lambda_1)(\lambda_2-\lambda_1)} + \frac{\lambda_1\lambda_3(e^{-\lambda_2 t_1} - e^{-\lambda_3 t_1})}{(\lambda_3-\lambda_2)(\lambda_2-\lambda_1)}\right] e^{-\lambda_3 t_2}$$

$$+ \frac{D_2^o}{(1-e^{-\lambda_2 t_1})}\left[1 - \frac{\lambda_3 e^{-\lambda_2 t_1} - \lambda_2 e^{-\lambda_3 t_1}}{(\lambda_3-\lambda_2)}\right] e^{-\lambda_3 t_2}$$

$$+ \lambda_3\lambda_2 D_1^o\left[\frac{e^{-\lambda_1 t_2}}{(\lambda_3-\lambda_1)(\lambda_2-\lambda_1)} - \frac{e^{-\lambda_2 t_2}}{(\lambda_3-\lambda_2)(\lambda_2-\lambda_1)} + \frac{e^{-\lambda_3 t_2}}{(\lambda_3-\lambda_1)(\lambda_3-\lambda_2)}\right]$$

$$+ \frac{\lambda_3 D_2^o}{(\lambda_3-\lambda_2)}\left[e^{-\lambda_2 t_2} - e^{-\lambda_3 t_2}\right] + D_3^o\, e^{-\lambda_3 t_2} \quad \ldots\ldots \text{(I-16)}$$

From a knowledge of D_1^o, D_2 and D_3, D_2^o and D_3^o can be calculated from Eqns. I-15 and I-16. For the decay chain $Zr^{87} \longrightarrow Y^{87m} \longrightarrow Y^{87g} \longrightarrow$, D_2^o of Y^{87m} was calculated by Eqn. I-15 and D_3^o of Y^{87g} was calculated by Eqn. I-16. D_1^o, D_2 and D_3 were obtained from the measured decay curves. D_3 was however obtained by applying correction for the decay of Y^{87m} to Y^{87g} after the separation according to the following relation

$$D_3 = D_{3(extra)} + \frac{\lambda_3}{\lambda_3-\lambda_2} D_2$$

where $D_{3(extra)}$ and D_2 are the extrapolated disintegration rates of Y^{87m}

and Y^{87g} at the end of separation respectively.

Eqn. I-15 was used in finding D_2^o of Y^{86g} and correcting for the growth of Y^{86g} from Y^{86m} and Zr^{86}. All the calculations were made by a simple computer program.

REFERENCES

1. N. Bohr, Nature 137, 344 (1936).
2. V.F. Weisskopf, Phys. Rev. 52, 295 (1937).
3. S.N. Ghoshal, Phys. Rev. 80, 939 (1950).
4. W. John, Phys. Rev. 103, 704 (1956).
5. J.R. Grover, Phys. Rev. 123, 267 (1961).
6. N.T. Porile, S. Tanaka, H. Amano, M. Furukawa, S. Iwata and M. Yagi, Nucl. Phys. 43, 500 (1963).
7. J.R. Grover and R.J. Nagle, Phys. Rev. 134, B1248 (1964).
8. L. Wolfenstein, Phys. Rev. 82, 690 (1951).
9. R.N. Glover and K.H. Purser, Nucl. Phys. 24, 431 (1961).
10. A.H. Armstrong and L. Rosen, Nucl. Phys. 19, 40 (1960).
11. R. Sherr and F. Brady, Phys. Rev. 124, 1928 (1961).
12. N.O. Lassen and N.O. Roy Poulsen, International Conference on Low Energy Physics, Paris, July (1958).
13. N.T. Porile, A.M. Poskanzer and M. Rho, Phys. Rev. 128, 242 (1962).
14. M. Blann and A. Ewart, Phys. Rev. 134, B783 (1964).
15. N.T. Porile, Phys. Rev. 115, 939 (1959).
16. F.S. Houck and J.M. Miller, Phys. Rev. 123, 231 (1961).
17. R.L. Hahn and J.M. Miller, Phys. Rev. 124, 1879 (1961).
18. R.M. Eisberg and G. Igo, Phys. Rev. 93, 1039 (1954).
19. P.C. Gugelot, Phys. Rev. 93, 425 (1954).
20. B.L. Cohen, Phys. Rev. 105, 1549 (1957).
21. V.F. Weisskopf, Physics Today 14, No. 7, 18 (1961).
22. D.C. Peaslee, Ann. Rev. Nucl. Sci. 5, 99 (1955).
23. P.E. Hodgson, "The Optical Model of Elastic Scattering", published by Oxford at the Clarendon Press (1963).

24. R. Serber, Phys. Rev. 72, 1114 (1947).

25. P.E. Hodgson, Phil. Mag. 45, 190 (1954).

26. P.E. Hodgson, Nucl. Phys. 8, 1 (1958).

27. M.L. Goldberger, Phys. Rev. 74, 1268 (1948).

28. G. Bernardini, E.T. Booth and S.J. Lindenbaum, Phys. Rev. 88, 1017 (1952).

29. H. McManus, W.T. Sharp and H. Gellman, Phys. Rev. 93, 924A (1954).

30. G. Rudstam, "Spallation of Medium Weight Elements", Ph.D. Thesis, University of Uppsala, Uppsala, Sweden (1956).

31. N. Metropolis, R. Bivins, M. Storm, A. Turkevich, J.M. Miller and G. Friedlander, Phys. Rev. 110, 185 (1958).

32. N. Metropolis, R. Bivins, M. Storm, A. Turkevich, J.M. Miller and G. Friedlander, Phys. Rev. 110, 204 (1958).

33. I. Dostrovsky, R. Bivins and P. Rabinowitz, Phys. Rev. 111, 1659 (1958).

34. I. Dostrovsky, Z. Frankel and G. Friedlander, Phys. Rev. 116, 683 (1959).

35. J.W. Meadows, Phys. Rev. 91, 885 (1953).

36. R.A. Sharp, R.M. Diamond and G. Wilkinson, Phys. Rev. 101, 1493 (1956).

37. K. Strauch and F. Titus, Phys. Rev. 104, 191 (1956).

38. J. Hadley and H. York, Phys. Rev. 80, 345 (1950).

39. H.W. Bertini, ORNL-3383 (1963).

40. Chen, Fraenkel, Friedlander, Grover, Miller, Shimamoto (to be published).

41. James Wing, "Isomeric-Yield Ratios in Nuclear Reactions", Argonne National Laboratory Report ANL-6598, Sept. 1962 (unpublished).

42. J.W. Meadows, R.M. Diamond and R.A. Sharp, Phys. Rev. 102, 190 (1956).

43. R. Vandenbosch and J.R. Huizenga, Phys. Rev. 120, 1313 (1960).

44. J.L. Need and B. Linder, Phys. Rev. 129, 1298 (1963).

45. J.L. Need, Phys. Rev. 129, 1302 (1963).

46. D.W. Seegmiller, Ph.D. Thesis, UCRL-10850, Aug. 1963 (unpublished).

47. R.L. Kiefer, Ph.D. Thesis, UCRL-11049, Oct. 1963 (unpublished).

48. A.A. Caretto and E.O. Wiig, Phys. Rev. 115, 1238 (1959).

49. T.M. Kavanagh and R.E. Bell, Can. J. Phys. 39, 1172 (1961).

50. S. Hontzeas and L. Yaffe, Can. J. Chem. 41, 2194 (1963).

51. T.D. Price and R.E. Telford, in "The Analytical Chemistry of the Manhattan Project", edited by C.J. Rodden, N.N.E. Series (McGraw-Hill Book Co., Inc., 1950).

52. K.A. Kraus and G.E. Moore, J. Am. Chem. Soc. 75, 1460 (1953).

53. A.D. Horton, Anal. Chem. 25, 1331 (1953).

54. E.B. Sandell, "Colorimetric Determination of Traces of Metals", p. 748, Third Edition (Revised) (published by Interscience Publishers Inc., New York, 1959).

55. F.J. Welcher, "The Analytical Uses of Ethylene-diaminetetra-acetic Acid", published by D. Van Nostrand Company Inc., Princeton, New Jersey (Reprinted 1958).

56. G.R. Grant, Ph.D. Thesis, McGill University (1961).

57. N.H. Lazar, IRE Transactions of the Professional Group on Nuclear Science NS-5, 138 (1958).

58. R.L. Heath, "Scintillation Spectrometry Gamma-ray Spectrum Catalogue", IDO-16408 (1957).

59. Nuclear Data Sheets - (National Academy of Sciences, National Research Council, Washington, D.C. 1959, 1960 etc.).

60. J.B. Cumming, "Application of Computers to Nuclear and Radiochemistry", National Academy of Sciences, National Research Council, Nuclear Science Series, NAS-NS-3107, p. 25 (1962).

61. S. Mehgir and L. Yaffe - to be published.

62. S. Monaro, G.B. Vingiani and R. Van Lieshout, Physica 27, 985 (1961).

63. D.M. Van Patter and S.M. Shafroth, Nucl. Phys. 50, 113 (1964).

64. E.K. Hyde, M.G. Florence and A.E. Larsh, Phys. Rev. 97, 1255 (1955).

65. F.D.S. Butement and G.B. Briscoe, J. Inorg. Nucl. Chem. 25, 151 (1963).

66. E.K. Hyde, M.G. Florence and F.S. Stephens, UCRL-2813 (1954).

67. J.I. Rode, O.E. Johnson and W.G. Smith, Phys. Rev. 129, 815 (1963).

68. T. Yamazaki, H. Ikegami and M. Sakai, Nucl. Phys. 30, 68 (1962).

69. L. Haskin and R. Vandenbosch, Phys. Rev. 123, 184 (1961).

70. Y.E. Kim, D.J. Horen and J.M. Hollander, Nucl. Phys. 31, 447 (1962).

71. D.J. Horen and W.H. Kelley, Bull. Am. Phys. Soc. 7, 341 (1962).

72. I. Dostrovsky, S. Katcoff and R.W. Stoenner, Phys. Rev. 132, 2600 (1963).

73. V. Maxia, W.H. Kelley and D.J. Horen, J. Inorg. Nucl. Chem. 24, 1175 (1962).

74. J.B. Cumming and N.T. Porile, Phys. Rev. 122, 1267 (1961).

75. J. Delaunay-Olkowsky, P. Strohal and N. Cindro, Nucl. Phys. 47, 266 (1963).

76. Mark Gusakow, Ph.D. Thesis, Paris University (1962).

77. J.M. Miller and J. Hudis, Ann. Rev. Nucl. Sci. 9, 159 (1959).

78. R.D. Evans, "The Atomic Nucleus", published by McGraw-Hill Book Company, (1955), page 835.

79. W.N. Hess, Rev. Mod. Phys. 30, 368 (1958).

80. F. Everling, L.A. König, J.H.E. Mattauch and A.H. Wapstra, Nucl. Phys. 18, 529 (1960).

81. J. Blatt and V.F. Weisskopf, "Theoretical Nuclear Physics", published by John Wiley and Sons, Inc., New York, (1952).

82. M.M. Shapiro, Phys. Rev. 90, 171 (1953).

83. H. Hurwitz and H.A. Bethe, Phys. Rev. 81, 898 (1951).

84. T.D. Newton, Can. J. Phys. 34, 804 (1956).

85. A.G.W. Cameron, Can. J. Phys. 36, 1040 (1958).

86. B.L. Cohen and A.G. Rubin, Phys. Rev. 113, 579 (1959).

87. D. Bodansky, Ann. Rev. Nucl. Sci. 12, 79 (1962).

88. S. Hayakawa, M. Kawai and K. Kikuchi, Progr. Theor. Phys. (Japan) 13, 415 (1955).

89. S.T. Butler, N. Austern and C. Pearson, Phys. Rev. 112, 1227 (1958).

90. K. Kikuchi, Nucl. Phys. 20, 590 (1960).

91. B.L. Cohen and A.G. Rubin, Phys. Rev. 111, 1568 (1958).

92. L.R.B. Elton and L.C. Gomes, Phys. Rev. 105, 1027 (1957).

93. L. Katz, L. Pease and H. Moody, Can. J. Phys. 30, 476 (1952).

94. T. Ericson, Phil. Mag. Supplement 9, 425 (1960).